# TRANSPARENT AND CONDUCTING COPPER NANOWIRE NETWORKS WITH IMPROVED OXIDATION STABILITY

A THESIS SUBMITTED TO
THE GRADUATE SCHOOL OF NATURAL AND APPLIED SCIENCES
OF
MIDDLE EAST TECHNICAL UNIVERSITY

BY

SEVİM POLAT GENLİK

IN PARTIAL FULFILLMENT OF THE REQUIREMENTS
FOR
THE DEGREE OF MASTER OF SCIENCE
IN
METALLURGICAL AND MATERIALS ENGINEERING

JULY 2018

Approval of the thesis

**TRANSPARENT AND CONDUCTING COPPER NANOWIRE NETWORKS WITH IMPROVED OXIDATION STABILITY**

Submitted by **SEVİM POLAT GENLİK** in partial fulfillment of the requirements for the degree of **Master of Science in Department of Metallurgical and Materials Engineering, Middle East Technical University** by,

Prof. Dr. Halil Kalıpçılar _____
Dean, Graduate School of **Natural and Applied Sciences, METU**

Prof. Dr. Cemil Hakan Gür _____
Head of Department, **Metallurgical and Mat. Eng. Dept., METU**

Assoc. Prof. Dr. Hüsnü Emrah Ünalan _____
Supervisor, **Metallurgical and Materials Eng. Dept., METU**

**Examining Committee Members:**

Assoc. Prof. Dr. E. Görkem Günbaş _____
Chemistry Dept., METU

Assoc. Prof. Dr. H. Emrah Ünalan _____
Metallurgical and Materials Engineering Dept., METU

Assoc. Prof. Dr. Emrah Özensoy _____
Chemistry Dept., Bilkent University

Assist. Prof. Dr. Simge Çınar _____
Metallurgical and Materials Engineering Dept., METU

Assist. Prof. Dr. Selçuk Yerci _____
Micro and Nanotechnology Dept., METU

**Date:** 11.07.2018

**I hereby declare that all information in this document has been obtained and presented in accordance with academic rules and ethical conduct. I also declare that, as required by these rules and conduct, I have fully cited and referenced all material and results that are not original to this work**.

Name, Last name: Sevim Polat Genlik

Signature :

## ABSTRACT

### TRANSPARENT AND CONDUCTING COPPER NANOWIRE NETWORKS WITH IMPROVED OXIDATION STABILITY

Polat Genlik, Sevim

M.S., Department of Metallurgical and Materials Engineering

Supervisor: Assoc. Prof. Dr. H. Emrah Ünalan

July 2018, 125 pages

Among all scalably synthesized metal nanowires, silver nanowires are the most widely studied and the first commercialized nanowire type. On the other hand, copper nanowires (Cu NWs) are not far behind the silver nanowires and hold great promise due to their lower cost in combination with comparable electrical conductivity in the network form. However, oxidation is the prominent barrier in front of the large scale utilization of Cu NWs. It is well known that bulk copper itself is also prone to oxidation, and numerous methods have been proposed to increase its resistance against oxidation. Inspired from bulk copper, in this thesis, benzotriazole (BTA) was utilized as an organic corrosion inhibitor to enhance the stability of Cu NW networks. High aspect ratio Cu NWs were synthesized by an environmentally benign hydrothermal method and highly transparent and conducting Cu NW networks (20 ohm/sq sheet resistance with a transmittance of 88% at a wavelength of 550 nm) were fabricated through spray deposition. The parameters affecting optoelectronic performance such as nanowire density, annealing temperature and time were studied in detail. Subsequent to the deposition of Cu NW networks, they were spin coated with a solution of BTA for passivation. Long term stability of the

passivated networks under ambient and severe humidity conditions were systematically studied in comparison to that of bare control samples. It was found that BTA inhibits the formation of an oxide layer on Cu NWs for at least one year of storage under ambient atmospheric conditions. No significant change in sheet resistance of passivated Cu NW networks was observed ($R/R_0 < 1.1$). High humidity conditions accelerated the degradation of bare Cu NW networks and they became insulating after 2 days under 75% RH condition, while they became insulating after a day under 90% RH. On the other hand, initial sheet resistance of BTA passivated networks was maintained up to 10 days under 75% RH condition, while it was maintained for 7 days under 90% RH. Moreover, attenuated total reflectance infrared spectroscopy (ATR-IR) was used to monitor the thermal stability of BTA for the protection of Cu NW networks and BTA was found to be thermally stable up to 125 °C. All in all, this highly effective and simple strategy to improve the stability of Cu NW networks without deteriorating the optoelectronic performance will certainly open new avenues for their large scale utilization in various optoelectronic devices.

**Keywords:** nanowires, transparent electrodes, copper nanowires, oxidation stability, benzotriazole

# ÖZ

## OKSİDASYON KARARLILIĞI ARTTIRILMIŞ ŞEFFAF VE İLETKEN BAKIR NANOTEL AĞLARI

Polat Genlik, Sevim

Yüksek Lisans, Metalurji ve Malzeme Mühendisliği Bölümü

Tez Yöneticisi : Doç. Dr. H. Emrah Ünalan

Temmuz 2018, 125 sayfa

Tüm ölçeklenebilir sentezlenmiş metal nanoteller arasında, gümüş nanoteller en çok incelenen ve ilk ticarileşmiş nanotel tipidir. Öte yandan, bakır nanoteller gümüş nanotellerin çok gerisinde değildir ve karşılaştırılabilir elektriksel iletkenliği ile birlikte düşük maliyetlerinden dolayı umut vericidir. Ancak oksidasyon, bakır nanotellerin büyük ölçekli kullanımının önündeki en büyük engeldir. Yığın bakırın kendisinin de oksidasyona eğilimli olduğu iyi bilinmektedir ve oksidasyona karşı direncini arttırmak için çeşitli yöntemler önerilmiştir. Bu tezde, dökme bakırdan esinlenerek, bakır nanotellerin stabilitesini arttırmak için bir organik korozyon inhibitörü olarak benzotriazol (BTA) kullanılmıştır. Yüksek boy-en oranlı bakır nanoteller, çevresel olarak zararsız hidrotermal yöntemle sentezlenmiş ve oldukça saydam ve iletken bakır nanotel ağları (% 88 şeffaflık ve 20 ohm/sq levha direnci) sprey biriktirme yöntemi ile üretilmiştir. Nanotel yoğunluğu, tavlama sıcaklığı ve

zamanı gibi optoelektronik performansı etkileyen parametreler detaylı olarak incelenmiştir. Bakır nanotel ağlarının biriktirilmesinden sonra, üretilen ağlar pasivasyon için BTA çözeltisi ile kaplanmıştır. Atmosferik ortamda ve şiddetli nem koşulları altında, pasifleştirilmiş elektrotların uzun süreli stabilitesi pasifleştirilmemiş kontrol örneklerine kıyasla sistematik olarak incelenmiştir. BTA'nın, atmosferik koşullar altında en az bir yıllık depolama için bakır nanoteller üzerinde oksit tabakası oluşumunu inhibe ettiği bulunmuştur. Aynı koşullarda, pasifleştirilmiş bakır nanotel ağlarının tabaka direncinde önemli bir değişiklik gözlenmemiştir ($R / R_0 < 1.1$). Yüksek nem koşulları pasifleştirilmemiş bakır nanotel ağlarının bozulmasını hızlandırdı. % 70 bağıl nem koşullarında 2 gün sonra yalıtkan olan ağlar, %90 bağıl nem altında bir gün sonra yalıtkan hale gelmiştir. Öte yandan, BTA korumalı numunelerin ilk tabaka direncinin, % 70 bağıl nem koşulunda 10 güne kadar muhafaza edilirken, % 90 bağıl nem altında 7 güne kadar muhafaza edildiği gösterilmiştir. Ayrıca, bakır nanotel ağlarının korunmasını sağlayan BTA'nın termal stabilitesini izlemek için zayıflatılmış toplam yansıma kızılötesi spektroskopisi (ATR-IR) kullanılmıştır ve BTA'nın 125 ° C'ye kadar termal olarak kararlı olduğu tespit edilmiştir. Sonuç olarak, bakır nanotel ağlarının optoelektronik performansı bozmadan stabilitesini artıran bu son derece etkili ve basit strateji, bakır nanotellerin çeşitli optoelektronik cihazlarda büyük ölçekli kullanımları için yeni imkanlar yaratacaktır.

**Anahtar Kelimeler:** nanoteller, şeffaf elektrotlar, bakır nanoteller, oksidasyon kararlılığı, benzotriazol

***To my Family***

## ACKNOWLEDGEMENTS

Firstly, I would like to express my deepest appreciation to my advisor Assoc. Prof. Dr. H. Emrah Ünalan for his patience and guidance that broaden my vision throughout this research. He has been highly supportive and has given me lots of opportunities as well as the freedom to pursue various projects without objection. I would not have the courage to complete my work without his guidance and persistent help. It is a great honor to study under his supervision.

This work was financially supported by Middle East Technical University, Scientific Research Projects Programme under project numbers BAP-07-02-2016-003, BAP-07-02-2017-011 and BAP-07-02-2017-004-265.

I am also thankful to my research partner Doğancan Tigan for his intimate friendship, support, assistance and insightful discussions which helped me to clarify my understanding of some points of the research. I would also like to express my special thanks to Ece Alpuğan, Mete Batuhan Durukan, Doğa Doğanay and Selin Özkul for their true friendship and support throughout my study. I would like to thank my lab mates Recep Yüksel, Alptekin Aydınlı, Şahin Coşkun, Yusuf Tütel, Onur Türel, İpek Bayraktar, Serkan Koylan, Efe Boyacıgiller, Elif Özlem Güner and Özlem Ünal. I always feel lucky to be a part of this productive research group.

I would also like to thank Assoc. Prof. Dr. Emrah Özensoy from Bilkent University and his students Kerem Emre Ercan and Yusuf Kocak for their collobaration.

I am also thankful to Assist. Prof. Dr. Simge Çınar and Prof. Dr. Müfit Akınç for their support which kept me motivated in the last years of my research. In addition to my advisor, they are the best role model and the main reason why I decided to pursue a doctoral study.

I would like to thank you Serkan Yılmaz for his help with TEM analysis. I am also thankful to Assist. Prof. Meltem Sezen from Sabancı University for cross-sectional

TEM sample preparation by focused ion beam. In addition, I am thankful to Bersu Baştuğ and Özlem Ünal for their help in UV-VIS analysis.

Lastly, I would like to express my gratitude to my family, Ayşe Civan, Şirin Polat and Deniz Genlik for their endless support and faith on me. Every achievement I made is a result of their effort. I love you.

## TABLE OF CONTENTS

## LIST OF TABLES

TABLES

## LIST OF FIGURES

FIGURES

## LIST OF ABBREVIATIONS

| | |
|---|---|
| **AMD** | Areal Mass Density |
| **ATR-IR** | Attenuated Total Reflectance Infrared |
| **AZO** | Aluminum doped Zinc Oxide |
| **AAO** | Anodized Aluminum Oxide |
| **BTA** | Benzotriazole |
| **CNT** | Carbon Nanotube |
| **CVD** | Chemical Vapor Deposition |
| **EDA** | Ethylenediamine |
| **FCC** | Face Centered Cubic |
| **FTO** | Fluorine Doped Indium Tin Oxide |
| **HDA** | Hexadecylamine |
| **HRSEM** | High Resolution Scanning Electron Microscopy |
| **FIB** | Focused Ion Beam |
| **HRTEM** | High Resolution Transmission Electron Microscope |
| **ITO** | Indium Tin Oxide |
| **LCD** | Liquid Crystal Display |
| **LED** | Light Emitting Diode |
| **MWCNT** | Multi Walled Carbon Nanotube |
| **NP** | Nanoparticle |
| **NW** | Nanowire |
| **OLED** | Organic Light Emitting Diode |
| **OAG** | Oxide Assisted Growth |
| **ODA** | Octadecylamine |
| **PECVD** | Plasma Enhanced Chemical Vapour Deposition |
| **PEDOT: PSS** | Poly(3,4-ethylenedioxythiophene) polystyrene |
| **PET** | Polyethylene terephthalate |
| **PVP** | Polyvinylpolypyrrodilone |
| **R** | Resistance |

| | |
|---|---|
| **RH** | Relative Humidity |
| **$R_{sh}$** | Sheet resistance |
| **SEM** | Scanning Electron Microscope |
| **SWCNT** | Single-Walled Carbon Nanotubes |
| **SLS** | Solution-Liquid-Solid |
| **SCG** | Self-catalytic Growth |
| **TCE** | Transparent Conducting Electrode |
| **TV** | Television |
| **TCO** | Transparent Conducting Oxide |
| **TEM** | Transmission Electron Microscope |
| **VVD** | Vacuum Vapor Deposition |
| **VSS** | Vapor-Solid-Solid |
| **VLS** | Vapor-Liquid-Solid |
| **XRD** | X-ray DiffractionXPS X-ray Photoelectron Spectroscopy |

# CHAPTER 1

## INTRODUCTION

Over the last 20 years, high technology devices started to appear in every moment of people's life. Therefore, high penetration rate of technology along with the increase in the world population is boosting the growth of markets related with electronics and optoelectronics. Optoelectronics is a branch of technology concerned with the electronic systems that are detecting, controlling and sourcing light. Nowadays, most popular optoelectronic products dominating the market are organic light emitting diode (OLED) displays, liquid crystal displays (LCDs), and touch screen monitors/displays. These devices are integrated in end-user products such as smart phones, smart watches, tablets and TVs. Along with the growing demand, desire to achieve cost effective, scalable and safe methods to fabricate high quality products is accelerating the studies related with optoelectronics. In addition to OLEDs and LEDs, there exist significant number of studies on photovoltaics (PVs), thanks to people's awareness on environmental pollution and necessity for renewable energy sources. Moreover, smart windows are another trending optoelectronic device that are utilized mainly in automotive industry and commercial buildings. The common point of all these aforementioned optoelectronic devices is transparent and conducting electrodes (TCEs). This is because all these devices require one or more transparent electrodes in their device structure. TCEs are thin films of materials that are electrically conducting and transparent to light of visible wavelengths. TCEs have two possible functions in optoelectronic devices. First is providing charge carriers to the device without hindering either entrance or exit of light. The second one is the collection of charges from the adjacent device layers again without blockage of light.

The most extensively investigated and commercially dominating TE material is a transparent conducting oxide called indium tin oxide (ITO). Integration of ITO based TCEs into photovoltaics, OLEDs, touch screens and smart windows have been successfully demonstrated and majority of commercial products rely on this material. However, emerging new device architectures and new application fields for these devices require three main physical properties that cannot be met by ITO based TCEs. These are high optical transparency, high electrical conductivity and high mechanical flexibility. Due to its ceramic nature, ITO's flexibility is very limited and so ITO based TCEs are not mechanically durable. In addition to lack of flexibility, ITO has other drawbacks such as high cost raw materials and high cost deposition systems. Indium -raw material of ITO- sources are very limited and therefore its price is rising gradually. In addition, in order to fabricate ITO based TCEs with high electrical conductivity and transparency, a high cost vacuum process such as radio frequency-sputtering (RF sputtering) is required.

For these reasons, significant number of studies have been devoted to develop an alternative TCE material for the replacement of ITO. Firstly, other transparent conducting oxides were investigated. Fluorine doped tin oxide (FTO), aluminum doped zinc oxide (AZO) are a few examples to these oxides. However, their mechanical flexibility was not far good from that of ITO. Then carbon nanotubes, in particular single walled carbon nanotube (SWCNTs) thin films were proposed as an alternative material. However, these films suffered from high contact resistance created at the junction points of the adjacent tubes. Recently, graphene based transparent electrodes with promising results have been demonstrated. However, synthesis of defect free, single grain graphene involves high cost production methods. On the other hand, low cost and solution based methods to synthesize graphene was demonstrated; but, electrodes fabricated using solution based methods failed to show high performance due to the low quality of graphene. Besides these alternatives, most promising alternative material to replace ITO is random networks of metallic nanowires. Networks of metal nanowires can be deposited using cost-

effective solution based approaches and thus are suitable for large area deposition. Having high intrinsic electrical conductivity, copper nanowires (Cu NWs) and silver nanowires (Ag NWs) are the two mostly investigated metal nanowire types. Fabricated electrodes based on these nanowires exhibited performances equivalent to or even better than that of ITO.

Bulk copper is 1000 times more abundant and only 6% less conductive than silver [1]. The advantage of the low cost raw material is what makes Cu NWs more appealing than Ag NWs although Ag NWs are available since the beginning of 2010's, while Cu NWs only started to appear in the last 4-5 years. Moreover, many research groups demonstrated high performance transparent electrodes based on Cu NW networks [2][3][4][5]. However, oxidation is the biggest challenge that should be overcome for the large scale utilization of Cu NW networks. Although limited number of studies to stabilize Cu NWs against oxidation have been demonstrated, these proposed methods are complex, expensive and not suitable for long term protection.

In this thesis, Cu NWs were synthesized via hydrothermal method in a reproducible way and characterized in order to determine their uniformity, morphology, dimensions, purity and crystallinity (Chapter 2). Then, fabrication of TCEs using as-synthesized Cu NWs via spray deposition method were demonstrated. The effect of thermal annealing temperature and time were investigated to improve the performance of the fabricated Cu NW networks. Moreover, the effect of network density (amount of NWs per unit area) on the optoelectronic properties of fabricated electrodes were investigated (Chapter 3). In the final part of the thesis, a novel, simple and effective method to stabilize Cu NWs against oxidation was demonstrated. In this method, bulk Cu organic corrosion inhibitor benzotriazole (BTA) was used for the protection of Cu NWs. The stability of BTA passivated samples under ambient and severe (high temperatures (75°C, 125°C, 150°C ), high relative humidity (70% RH and 90% RH) conditions were investigated and compared to that of bare control samples. Moreover, the stability of both BTA passivated and

bare networks were also investigated under the conditions that are going to be faced when Cu NW networks are utilized in optoelectronic devices such as extended voltage biasing and deposition of an acidic PEDOT: PSS over layer (Chapter 4).

# CHAPTER 2

# SYNTHESIS OF COPPER NANOWIRES

## 2.1 Introduction

A variety of shape controlled synthesis methods have been reported and extensively investigated to create one dimensional metallic nanostructures [6]. All these various proposed methods have been developed to achieve four important characteristics; *(i)* precise control over uniformity, dimensions and morphology of the products, *(ii)* scalability, *(iii)* cost effectiveness and *(iv)* reproducibility. In this chapter, different synthetic strategies developed for the synthesis of nanowires under three topics as "vapor phase synthesis", "template assisted synthesis" and "solution phase synthesis" will be discussed in terms of four important characteristics stated above. Moreover, some reported methods that are specific to Cu NW synthesis will be mentioned in detail. Firstly, vapor phase synthesis methods were used for the synthesis of one dimensional (1D) nanostructures such as nanorods, nanowires and whiskers. Although this method has an obvious advantage in terms of product quality, it is expensive since whole process requires controlled atmosphere environment necessitating a high cost equipment. Another general approach for the formation of 1D nanostructures is the template assisted synthesis based on the electrochemical reduction of metal ions inside the templates with desired morphology. This method is very straightforward; but, synthesized NWs are generally polycrystalline and the yield is very limited [7]. Last approach is the solution phase synthesis. This approach is recently emerged when compared to others and it is now accepted as the mainstream strategy for the synthesis of metallic nanowires. This is because it is scalable, cost-effective and can be controlled precisely.

### 2.1.1 Vapor Phase Synthesis

Vapor phase method is most widely used for the synthesis of semiconducting and oxide based nanowires [2][8][9]. However, vapor phase synthesis for various metallic nanowires have also been demonstrated [10][11][12]. This method involves transportation of the vapor of a specific precursor down the temperature gradient and final condensation over a certain liquid/solid phase catalysts. Among all vapor phase synthesis methods ( i.e. oxide assisted growth (OAG), self-catalytic growth (SCG), solution-liquid-solid (SLS) approach, vapor-solid-solid (VSS) approach, vapor-liquid-solid (VLS) ) is the most successful one in terms of quality of the product [13]. First explanation of the mechanism for the growth of 1D nanostructures by VLS method was given by Wagner *et al*. In their study, growth of silicon whiskers from the gas phase were reported on a silicon substrate with gold droplets as the catalyst [14]. This mechanism composed of three distinct stages, which are metal alloying, nucleation and growth. In alloying stage, liquid metal catalysts make an alloy with the components in the vapor through adsorption. With a controlled supply of the vapor precursor, alloy is supersaturated. Therefore, the nucleation at the liquid-solid interface takes place in the second stage. As the process proceeds, 1D crystal growth initiates. Schematic illustration of 1D growth by VLS mechanism is provided in Figure 2.1. In this method, diameters of the nanowires depend on the size of the catalyst particles. Therefore, this method is capable of synthesizing NWs with different aspect ratios.

VLS method is highly advantageous since it allows the synthesis of NWs that are vertically aligned on the growth substrates. However, catalyst contamination is almost unavoidable in this method. Moreover, whole procedure need to take place under controlled atmosphere conditions. Therefore, a high cost equipment is necessary, which makes this method impractical for the large scale production of NWs.

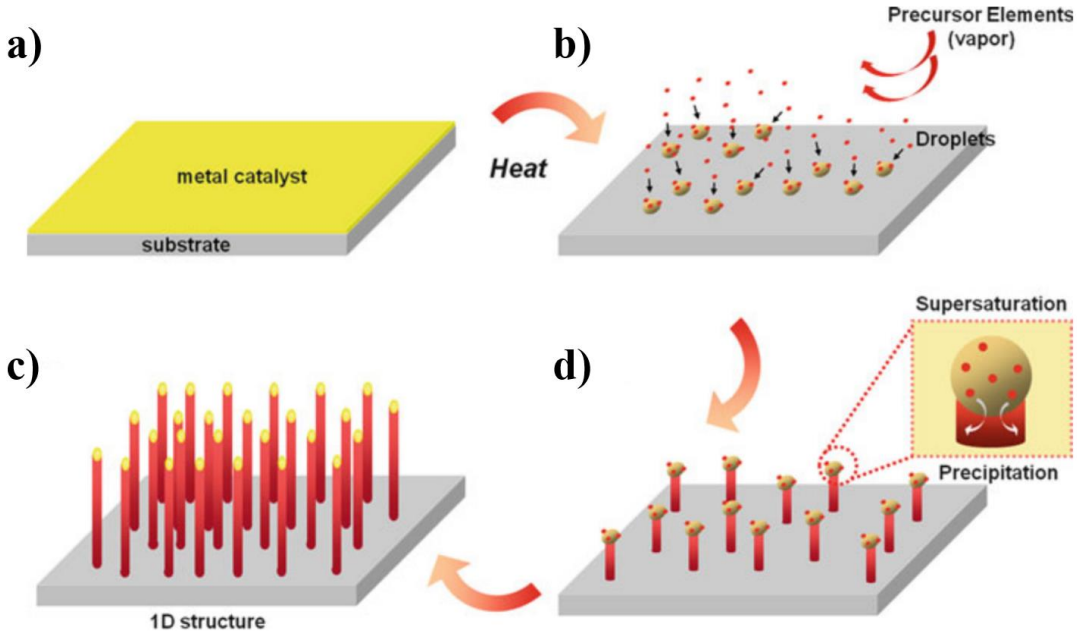


**Figure 2. 1** Schematic illustration for 1D growth by VLS mechanism [15].

Vapor phase synthesis of Cu NWs include chemical vapor deposition (CVD) [16][17], thermal assisted photo-reduction [18], vacuum thermal decomposition [19] and vacuum vapor deposition [20] methods.

Kim *et al.* demonstrated CVD growth of Cu NWs on metal, metal oxide, glass and polymer substrates using $Cu(etac)[P(OEt)_3]_2$ precursor without using a catalyst [17]. The diameter of the CVD grown Cu NWs in this study was in the range of 70-250 nm. The NWs had a fivefold twinned structure with {100} side facets and {111} end facets. This study demonstrated that vapor phase synthesis of crystalline pentatwinned Cu NWs is possible in addition to solution phase synthesis methods. Figure 2.2 shows SEM images of CVD grown Cu NWs on silicon substrates.

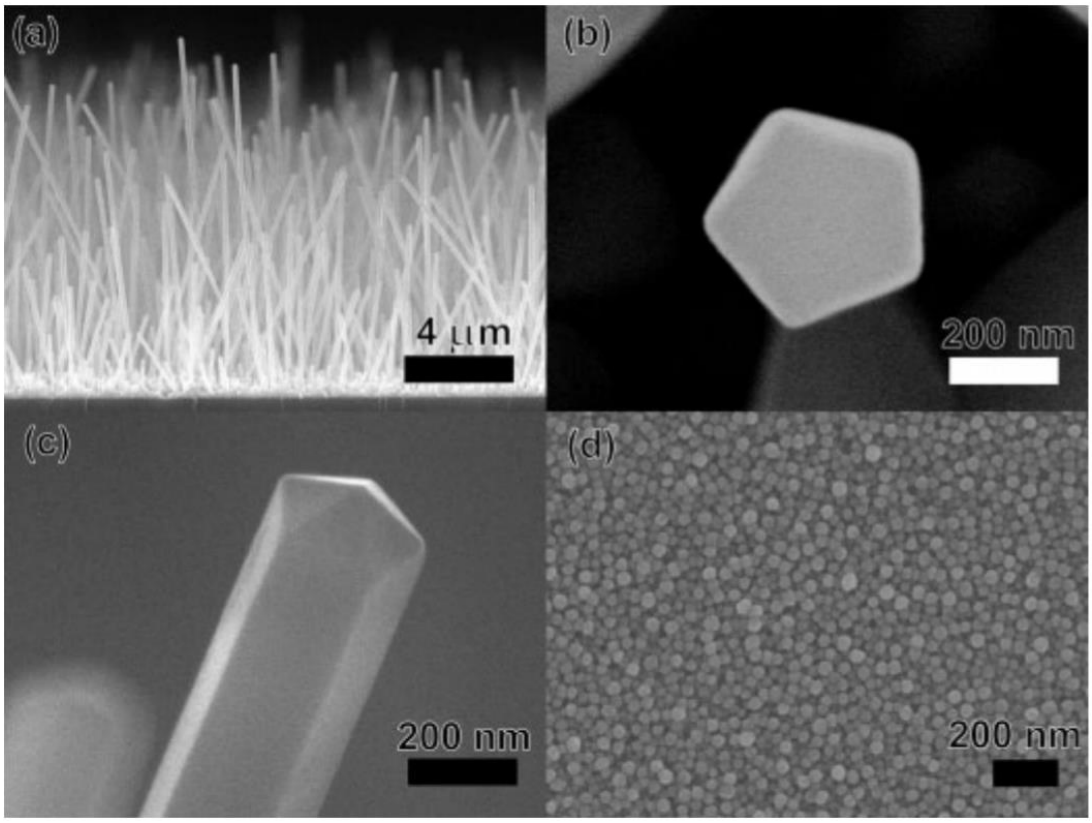


**Figure 2. 2** SEM images of CVD grown Cu NWs on Si substrate in (a) Low-magnification side-view, (b) high-magnification top-view, (c) high-magnification side-view. (d) Cu seeds formed at an early stage of Cu NW growth[17].

Another CVD based growth of Cu NWs was published by Choi and his coworkers [16]. Various volatile liquid precursors having different thermal stabilities have been used for the synthesis of free-standing Cu NWs by CVD.

Amongst the precursors studied, $Cu(etac)[P(OEt)_3]_2$ precursor demonstrated best thermal stability and allowed the synthesis of NWs with an average diameter of 70-100 nm. Nanowires grown through [111] directions were highly crystalline as shown by the XRD analysis.

Liu *et al*. demonstrated the synthesis of high aspect ratio, uniform diameter, defect free Cu NWs through a novel vacuum vapor deposition [20]. This is a one-step

method and involves generation of copper vapor and its redeposition onto molybdenum grid substrate at a pressure of 2 x $10^{-5}$ Pa. Diameters and lengths of these Cu NWs were in the range of 50 to 100 nm and around 20 μm, respectively.

### 2.1.2 Template-Assisted Synthesis

Template-assisted synthesis is a straightforward route to form 1 D nanostructures with the assistance of templates that are directing nucleation and growth of materials. These templates are classified into two as "hard templates" such as nano porous alumina, carbon nanotubes, polymeric templates and "soft templates" such as bacteria, DNA strains, rod-shaped viruses [21][22][23]. At the end of the synthesis these templates can be easily moved away via chemical etching or calcination depending on the type of the template. Therefore, free-standing nanostructures can be obtained with this synthesis method since templates are only sacrificial materials that are manipulating the shape. Keeping the templates as a composite structure is also possible depending on the application; but in general, nanostructures to be used in optoelectronic devices are freed from the template. Schematic representation for the template assisted synthesis of 1D structures is provided in Figure 2.3.

One disadvantage of template- assisted synthesis is that synthesized nanostructures are generally polycrystalline and very high control over the processing parameters is required to obtain single crystal and morphologically uniform products. Therefore, synthesized NWs with this method are not suitable to be used in optoelectronic devices. Another disadvantage comes from the additional cost of the template preparation and irreversible removal of the templates. Thus, template assisted synthesis is time consuming and costly due to the single use templates.

Growth of 1 D nanostructures through electrochemical deposition within the channels or pores of the templates is the most extensively studied approach amongst all other template assisted methods. The use of both polymer templates prepared by ion etching and porous alumina templates prepared by anodic oxidation of aluminum

substrates in acidic solutions were investigated for the synthesis of Cu NWs [22][24][25][26][27].

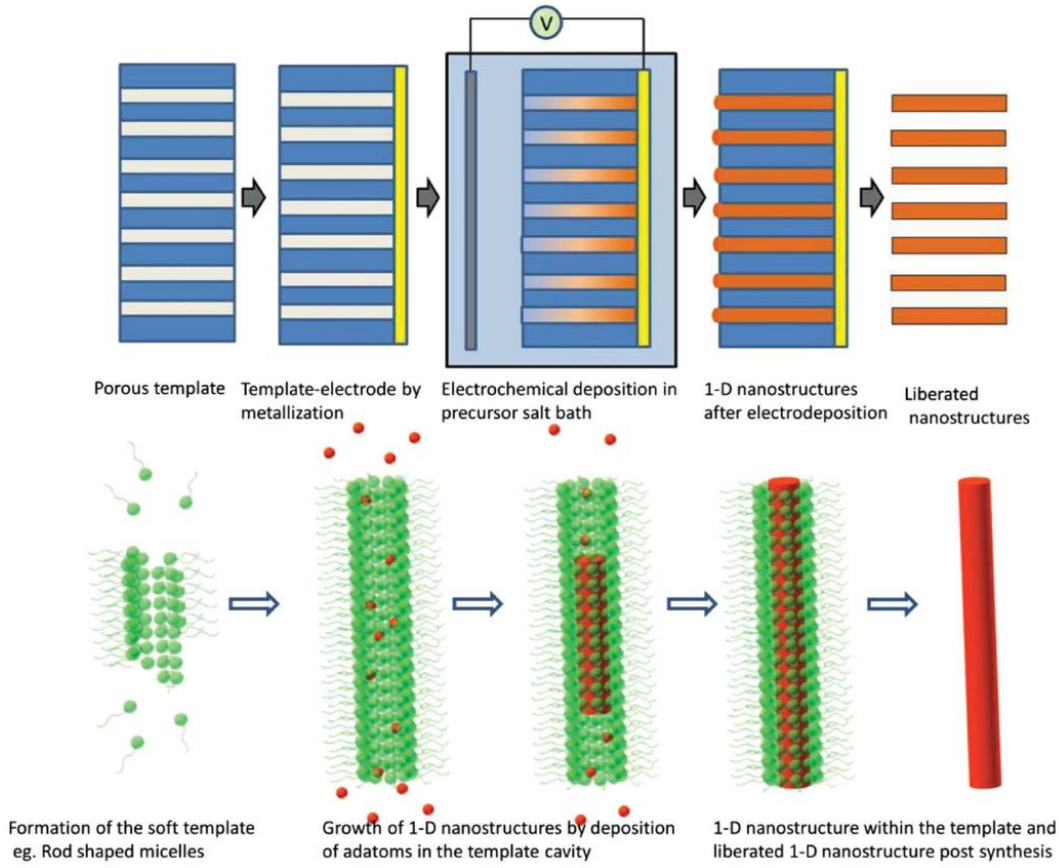


**Figure 2. 3** Schematics of the template assisted synthesis route for 1D nanostructures [2].

Gao *et al.* showed synthesis of both single-crystal and polycrystalline Cu NWs (60 nm diameter and 30 μm length) within the nano cylindrical channels of anodized aluminum oxide (AAO) [28]. Crystallinity of NWs were found to be strongly dependent on the applied deposition potential. It must also be noted that not only deposition potential; but also, the deposition electrolyte, deposition time, deposition temperature affects the quality of products. For example, Shin *et al.* reported high deposition temperatures in electrodeposition via AAO templates resulted with NWs

with rough and irregular shapes, whereas NWs became smooth and uniform as the temperature was decreased [26]. Figure 2.4 shows the schematic of procedure followed for the synthesis of Cu NWs via electrodeposition within AAO templates along with the SEM and TEM images of the synthesized Cu NWs.

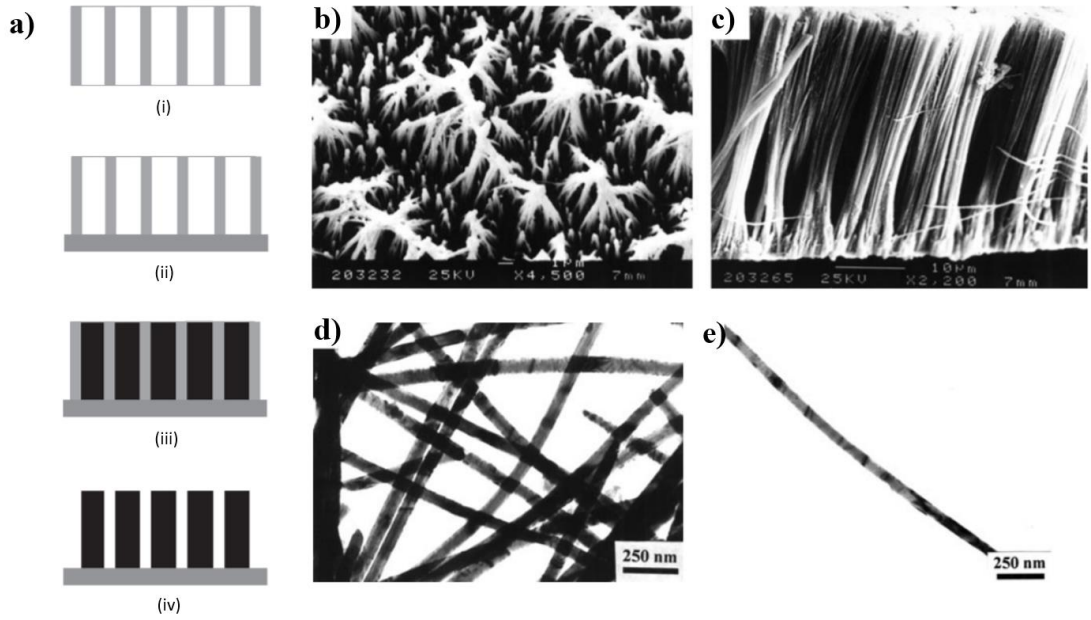


**Figure 2. 4** (a) Schematic presentation of the template assisted synthesis process: (a,i) the AAO template (a,ii) evaporation of conductor layers on one side of the AAO template (a,iii) the metal electrodeposition process and (a,iv) metal nanowires after removing the template. (b) Top-view and (c) cross-section view SEM images of Cu NWs formed at 0.15V. TEM images of (d) Cu NWs (e) an individual wire formed at 0.15V [26].

Toimil Molares *et al.* prepared polymer porous membranes based on polycarbonate foils irradiated with Au ions to synthesize high aspect ratio (L/D = 500) Cu NWs via electrodeposition of copper [25]. The procedure followed in the electrodeposition in polymer templates does not differ from that for porous alumina templates. However, AAO templates have the advantage of tunable channel diameter and length via

controlling anodization parameters such as time of anodic oxidation and concentration of the electrolytes. On the other hand, electrodeposition within both templates have lots of experimental parameters that need to be precisely controlled for reproducibility increasing complexity.

### 2.1.3 Solution Phase Synthesis

Solution phase synthesis method in which metal NWs synthesized in a colloidal solution is an important method due to its scalability, cost-effectiveness and precise control over the processing parameters. Although, this method has only ten years of history, hundreds of different studies investigating the growth mechanism, optimization of reaction parameters, such as chemical concentration, rate of mixing, reaction time and temperature as well as the utilization of the synthesized products have been reported [6].

Some solution phase synthesis methods of metallic nanowires are based on special capping agents. Generally, methods based on capping agents involve a metal source providing metal ions to the solution, reducing agent converting metal ions into metal atoms and a capping agent providing anisotropic crystal growth. According to Wulff facets theorem, shape of a crystal is determined by the relative surface energies of different facets since the crystal is bounded by the facets thermodynamically providing minimum total surface energy [2]. Another factor determining the shape of a crystal is the growth kinetics of planes. Slowly growing planes enclose the crystal since fastest growing ones should disappear [13]. As a result, thanks to these two confinements, suitable capping agents provide anisotropic growth by changing the growth kinetics and surface energies of certain planes. A schematic illustrating the solution phase synthesis method based on capping agent is provided in Figure 2.5.

General solution phase synthesis method for Ag NWs is polyol process that is effective and suitable for the large scale production of high-quality products. However, anisotropic growth of copper is not trivial to be developed when the same

polyol method is utilized to synthesize Cu NWs. Only irregular nanoparticles is obtained since polyol solvents are weak reducing agents for the copper ions [6].

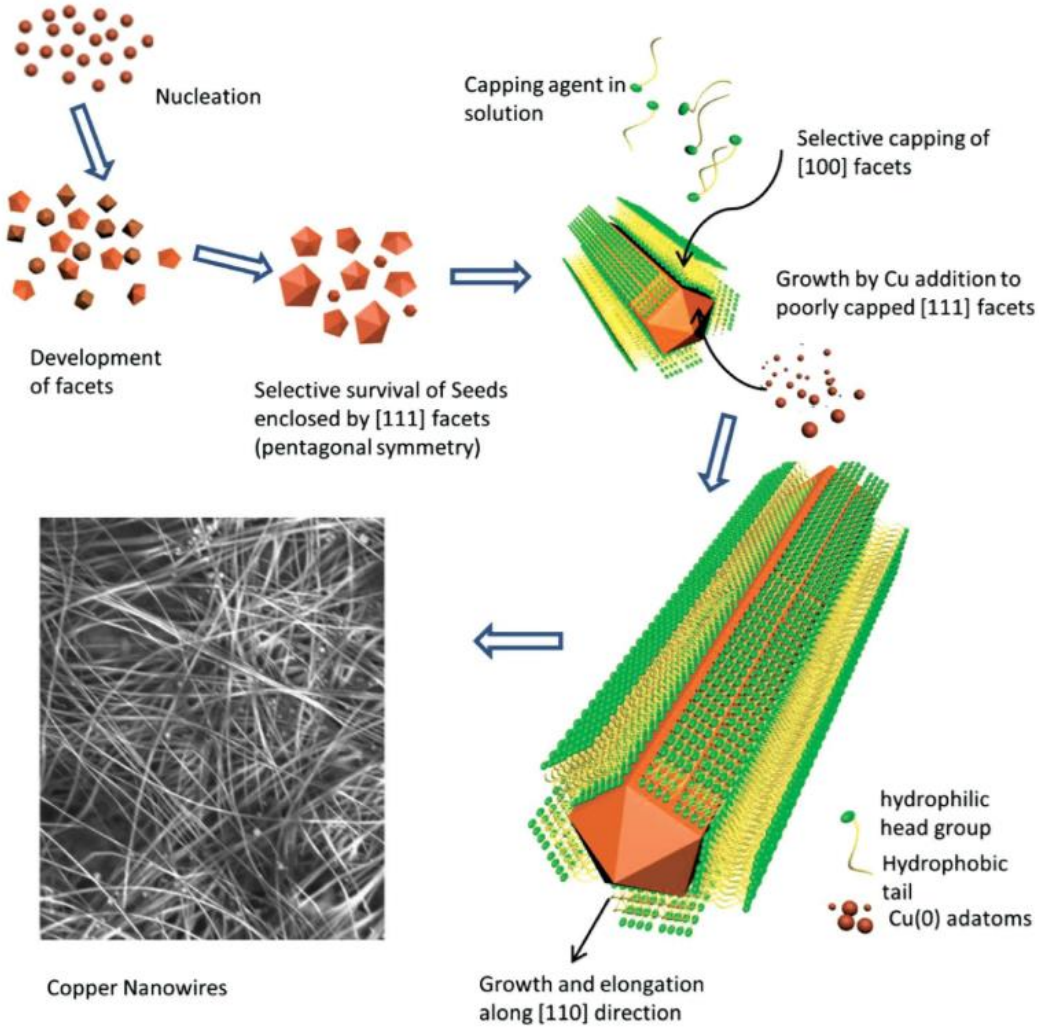


**Figure 2. 5** Schematics for solution phase synthesis of Cu NWs [2].

Among several proposed solution phase synthesis routes for Cu NWs, two general approaches have attracted much more attention compared to others, which are ethylenediamie (EDA)-mediated synthesis and alkylamine-mediated synthesis.

#### 2.1.3.1 Ethylenediamine (EDA)-mediated Synthesis

Solution phase method for the synthesis of Cu NWs was proposed by Chang *et al.* in 2005 for the first time [29]. In this method, copper ions were reduced by hydrazine ($N_2H_4$) in aqueous solution containing EDA as the capping agent at a relatively low temperature of 60°C. Synthesis reaction for EDA-mediated synthesis is given in Figure 2.6 (a). Synthesized Cu NWs had aspect ratios larger than 350 (diameter in the range of 90-120 nm and length in the range of 40-50 μm). Then Rathmell *et al.* reported a modified version of Chang's method [30]. It was demonstrated that the reaction can be scaled up 200 times (from 0.006 g to 1.2 g Cu NWs) and so confirmed the scalability of this method (see Figure 2.6 (b)). However, resulting Cu NWs in this scaled up method had lower aspect ratio due to limited length in the range 7-13 μm. Moreover, NWs had spherical nanoparticles attached to one end. Then, it was found that this spherical particles are the aggregates of copper (I) oxide ($Cu_2O$) formed at the early stages of the synthesis route acting as a seed for the Cu NW growth. By considering this growth mechanism, they increased the aspect ratio of NWs up to 2300 by introducing $Cu_2O$ seeds to the synthesis solution prior to the start of the reaction [31]. Figure 2.6 (c) shows an SEM image of high aspect ratio Cu NWs synthesized via EDA-mediated method.

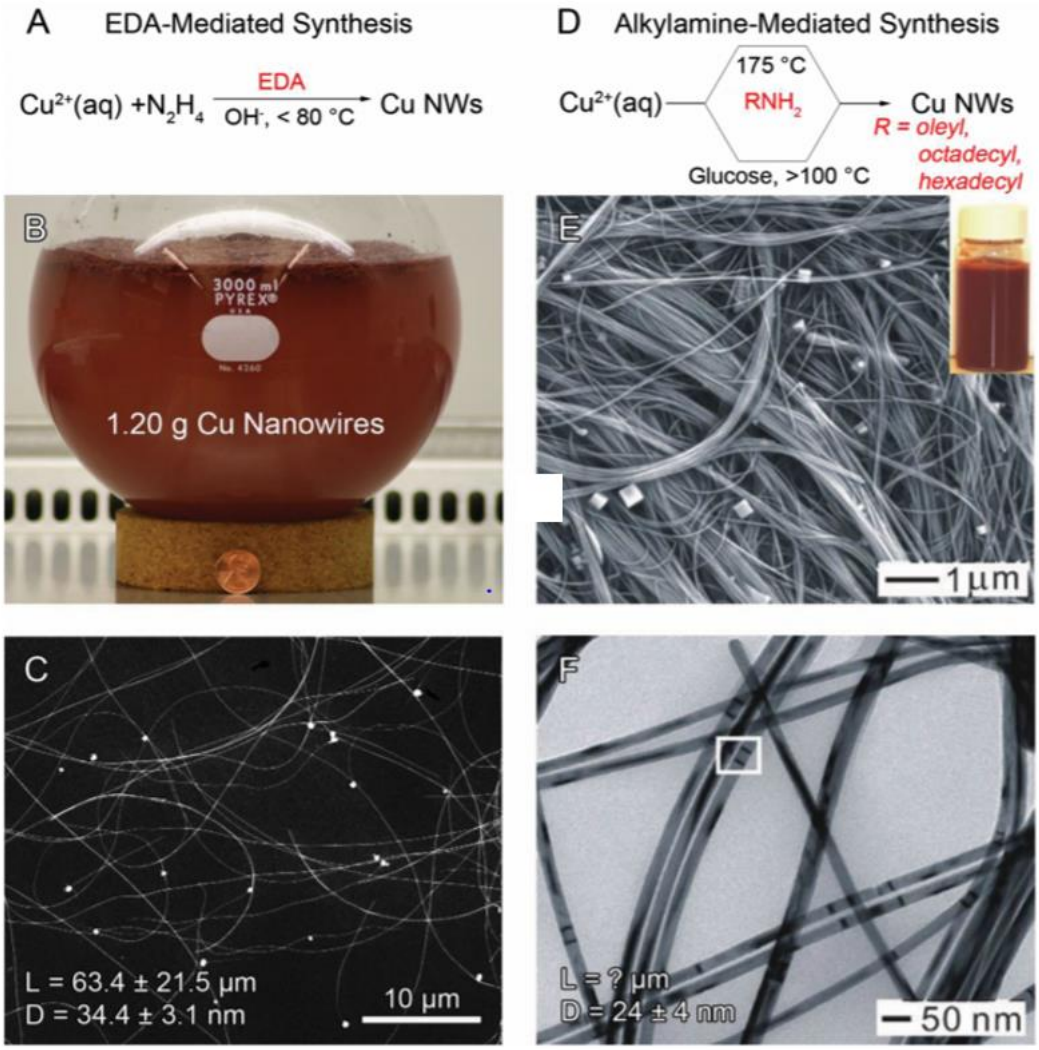


**Figure 2. 6** (a) Reaction scheme of EDA-mediated synthesis. (b) Photograph of the reaction flask after the growth of Cu NWs at 80°C for 1 hr. (c) SEM image of Cu NWs. (d) Reaction scheme of alkylamine-mediated synthesis. (e) SEM and (f) TEM images of Cu NWs prepared with hexadecylamine as capping agent [1].

### 2.1.3.2 Alkylamine-mediated Synthesis

Alkylamine-mediated synthesis methods seem to be one of the best option for large scale synthesis of high quality Cu NWs if the EDA-mediated synthesis methods involving toxic hydrazine is ignored. However, temperatures for the reaction to take

place is higher with respect to EDA-mediated synthesis methods. Synthesis reaction governing the alkylamine-mediated synthesis of Cu NWs is provided in Figure 2.6 (d).

Firstly, Shi *et al.* reported a hydrothermal route to synthesize Cu NWs via reducing copper chloride ($CuCl_2$) by octadecylamine (ODA) in an aqueous solution at 180°C [32]. In this method, ODA was not only the reducing agent but also acted as a capping agent. The synthesized Cu NWs had diameters in the range of 30-100 nm and lengths up to millimeters. Then Mohl *et al.* reported a new reducing agent, glucose, for the alkylamine-mediated synthesis of Cu NWs via hydrothermal route at low temperatures (120°C) [33]. With this method, Cu NWs with a uniform diameter of 65 nm and length in order of micrometers were obtained. Then Xia's group reported slightly modified version of the synthesis method developed by Mohl *et al.* by decreasing the reduction temperature down to 100°C [34]. Figure 2.6 (d) and (e) show the SEM and TEM images of Cu NWs synthesized by Xia and his coworkers. As seen in figure, high aspect ratio, highly crystalline and pure Cu NWs with a uniform diameter of 25 nm were obtained.

The major advantage of this method is that all the chemicals used in the synthesis are environmentally friendly. Moreover, the reaction temperature is relatively lower than the other synthesis methods. Very high aspect ratio Cu NWs can be synthesized in one pot without the introduction of any type of seed into the solution.

## 2.2 Experimental Details

All glassware, Teflon liner and magnetic stir bars used in the experiment were cleaned via Alconox detergent and rinsed with deionized (DI) water. Then ultrasonic cleaning is performed in acetone (99.8%), isopropyl alcohol (99.8%) and deionized water (18.3 MΩ), respectively through 20 minutes for each. All chemicals including detergent were purchased from Sigma-Aldrich and used without further purification. Hexadecylamine (HDA) ($C_{16}H_{35}N$) (≥ 94.0 % (a/a)), copper (II) chloride dihydrate ($CuCl_2.2H_2O$) (≥ 99.0 %), D-(+)-glucose monohydrate (anhydrous, 97.5-102.0%),

polyvinylpyrrolidone (PVP) (MW = 55000, monomer-based calculation) and chloroform (99.8%) were used for the synthesis and purification of Cu NWs.

### 2.2.1 Synthesis of Copper Nanowires

Cu NWs were synthesized according to the published procedure developed by Mohl *et al.* with slight modifications [33]. In a typical synthesis, 147 mg $CuCl_2.2H_2O$, 350 mg glucose, 1260 mg HDA and 70 mL DI water (the solvent) were mixed in a glass beaker and stirred for 12 hours via vigorous magnetic stirring at room temperature to obtain a homogeneous mixture. Then the obtained light blue emulsion was transferred into a Teflon-lined autoclave with 100 mL capacity. The reactor was sealed and heated at 105°C for 12 hours without further stirring. At the end of the synthesis, the reactor was left to cool down to room temperature. After complete cooling, the reactor was opened and final red-brown solution was collected.


**Figure 2. 7** Cu NW synthesis route via hydrothermal method used in this work.

In this solution phase synthesis method, $CuCl_2.2H_2O$ serves as the copper source which provides $Cu^{2+}$ ions to the initial solution. Glucose is a reducing agent which reduces the $Cu^{2+}$ ions to $Cu^0$ atoms. HDA is a capping agent, which provides anisotropic growth by selective adsorption on certain facets of copper seeds. As the temperature starts to increase, the formation of Cu species in various forms (bipyramids, cubes, pentatwinned particles) occur via the reduction of $Cu^{2+}$ ions as

well as the oxidation of glucose to gluconic acid according to reaction provided in Figure 2.8 [35].

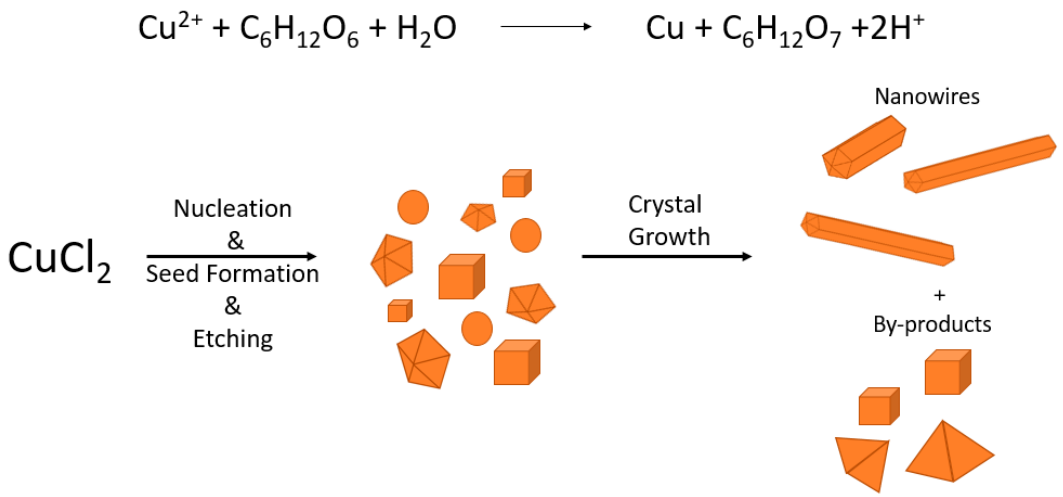


**Figure 2. 8** Schematic representation for the formation of Cu NWs via hydrothermal method.

As already demonstrated for Ag NWs, the final shape of nanocrystals are completely correlated with the shape of the seeds formed in the solution [36]. For example, growth from a single crystal seed results in the formation of nanocubes and growth from a multiply twinned decahedral seed results in the formation of pentatwinned NWs [34].

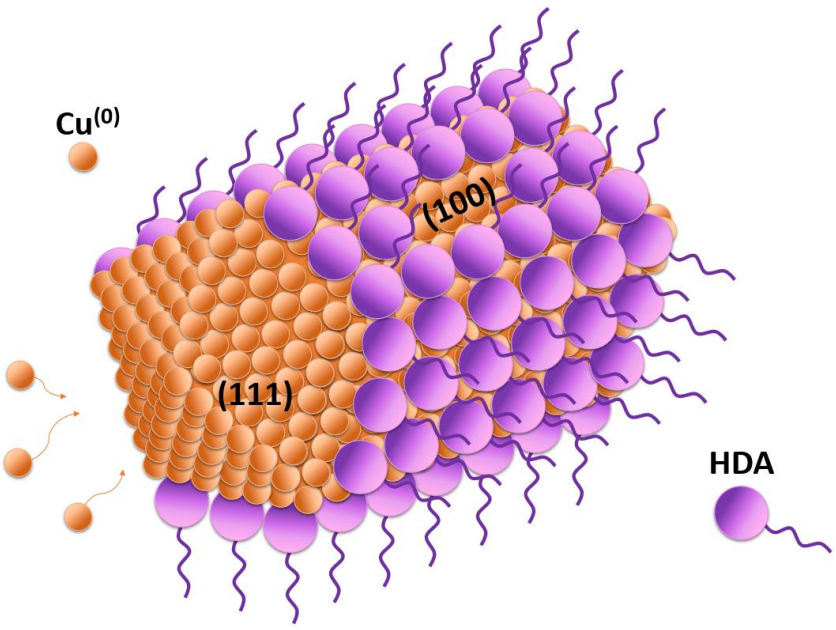


**Figure 2. 9** Schematic representation of the selective adsorption of HDA to (100) planes and anisotropic growth through active (111) planes at [110] direction.

Once, multiply twinned decahedral seeds form in the synthesis solution, HDA (the capping agent) is strongly adsorbed by the {100} facets of these seeds as shown in Figure 2.9. This is because, (100) planes have higher surface energy with respect to the most densely packed plane (111) of face centered cubic (FCC) copper and thermodynamically crystal planes with higher surface energy should primarily lower their energy to minimize the total surface energy. This preferred adsorption provides reduced copper atoms to bind preferentially to the poorly passivated or in other words active {111} facets of decahedral copper seeds that homogenously nucleates in solution. At the end, NW formation takes place through this 1D growth without lateral growth.

Furthermore, it is worth noting that HDA does not only manipulate the shape of Cu nanocrystals; but also prevents their oxidation in the aqueous solution [34]. Therefore, the final copper species obtained are free from oxides, which is very

important to utilize them in TCE applications in where high electrical conductivity is crucial.

Directly after synthesis, purification of Cu NWs was conducted through centrifugation for multiple times using various solvents. First of all, red-brown solution was centrifuged two times at 7000 rpm for 10 minutes with deionized (DI) water (18.3 MΩ) to remove excess HDA. Then slightly modified version of multiphase separation, which was developed by Qian *et al.* was applied to separate all the unwanted by-products from the Cu NWs [37].

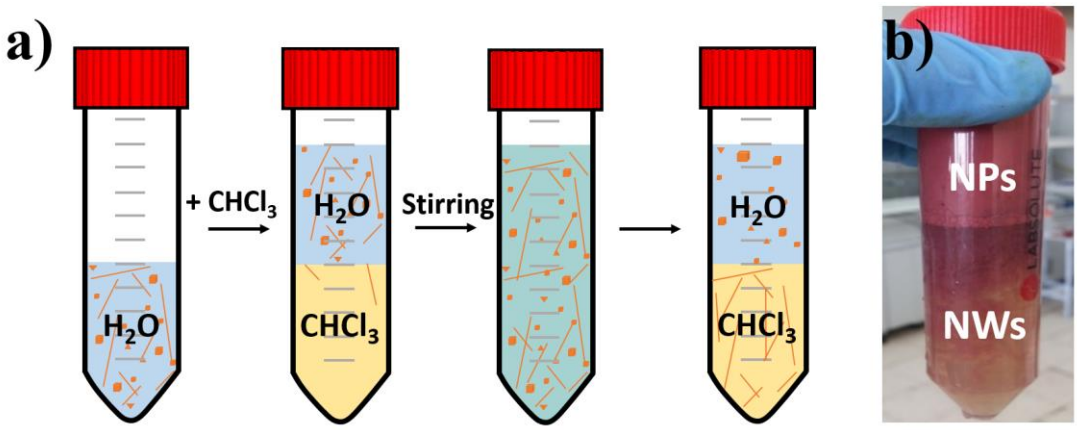


**Figure 2. 10** (a) Schematic representation of the steps followed for multiphase separation. (b) Photograph of separated nanoparticles in DI water and Cu NWs in chloroform ($CHCl_3$).

Figure 2.10 vividly illustrates the procedure followed in multiphase separation method. In this method, the solid composed of both nanoparticles (NPs) and NWs were firstly dispersed in DI water. Then $CHCl_3$, a hydrophobic organic solvent, was added and the solution was stirred vigorously using a magnetic stirrer for 5 minutes. After stirring, two liquid phases separated rapidly from each other. Then, water phase containing by-products was collected using a Pasteur pipette. Figure 2.11, schematically represents how NWs enter chloroform liquid phase. Since (111) facet of NWs are poorly passivated, these ends act as hydrophobic. Therefore, when hydrophobic ends come across the DI water/chloroform interface, NWs prefer to

enter hydrophobic organic solvent. On the other hand, by-products (cubes & bipyramids) prefer to stay in DI water since all their (100) facets are intensively covered by HDA. Furthermore, it should be emphasized that chloroform has dual purpose in this method. In addition to by-product separation, it dissolves all the HDA coating around nanowires (see Figure 2.11) As a result, NWs start to agglomerate to lower their surface energy. Moreover, it should be noted that increase in stirring time cause to dissolution of HDA around by-products. This leads to decrease in efficiency due to by-products transferred to organic solvent. Fabricating TCEs having good optoelectronic performance (high optical transparency along with high electrical conductivity), is not possible with agglomerated NWs. Therefore, subsequent to by-product separation and centrifugation in chloroform at 7000 rpm for 10 minutes, NWs were centrifuged twice at 7000 rpm for 10 minutes with 2 wt% polyvinylpyrrolidone (PVP)-ethanol solution twice to assure good dispersion.

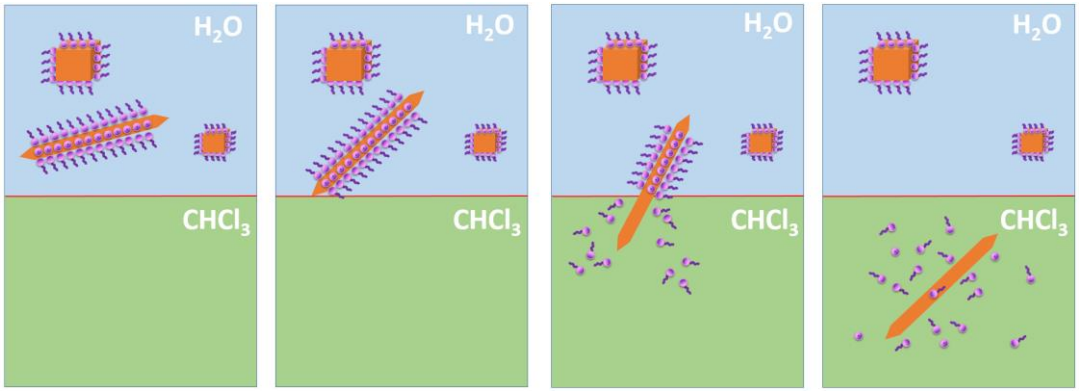


**Figure 2. 11** Schematic representation of separation mechanism proposed (Adapted from [35]).

Following PVP coating of the NWs, two more centrifugation steps at 7000 rpm for 10 minutes with ethanol were applied to remove excess dispersant. At the end, the final product was dispersed in ethanol for further characterization and fabrication of TCEs.

## 2.3 Nanowire Characterization Methods

### 2.3.1 Scanning Electron Microscopy (SEM)

Synthesized Cu NWs were characterized by field emission scanning electron microscopy (FE-SEM) (Nova NanoSEM 430) operated at an operating voltage of 20 kV. SEM samples were prepared by simple drop casting and drying of ethanolic solution of NWs onto silicon wafers. Then, they were fixed onto SEM specimen stubs via conductive carbon tapes. No additional coating was used for SEM analysis.

### 2.3.2 Transmission Electron Microscopy (TEM)

For morphological analysis in atomic scale, transmission electron microscope (TEM), JEOL 2010 high-resolution transmission electron microscopy (HRTEM) operated at 200 kV was used. TEM samples were prepared by simple drop casting of ethanolic solution of NWs onto holey carbon coated 400 mesh copper support grids and dried.

### 2.3.3 XRD Analysis

Phase identification and crystal structure analysis of synthesized Cu NWs were conducted by X-ray diffraction (XRD) analysis. Rigaku D/Max-2000 pc diffractometer with Cu Kα radiation operating at 40 kV range of 20-80° at a scanning rate of 2°/min was used.

## 2.4 Results

SEM was used to analyze the morphological characteristics of synthesized Cu NWs. Figure 2.12 provides both low and high-resolution SEM images of purified Cu NWs. High-resolution SEM image shows NWs with their measured diameters. Moreover, size distribution of the synthesized product in terms of diameter and length is provided in Figure 2.13. Mean diameter and mean length were calculated from 100

NWs randomly chosen from SEM images of several number of different samples. Cu NWs exhibited an average diameter of 45.4 ± 17.4 nm and length of 49.3 ± 19.9 µm.

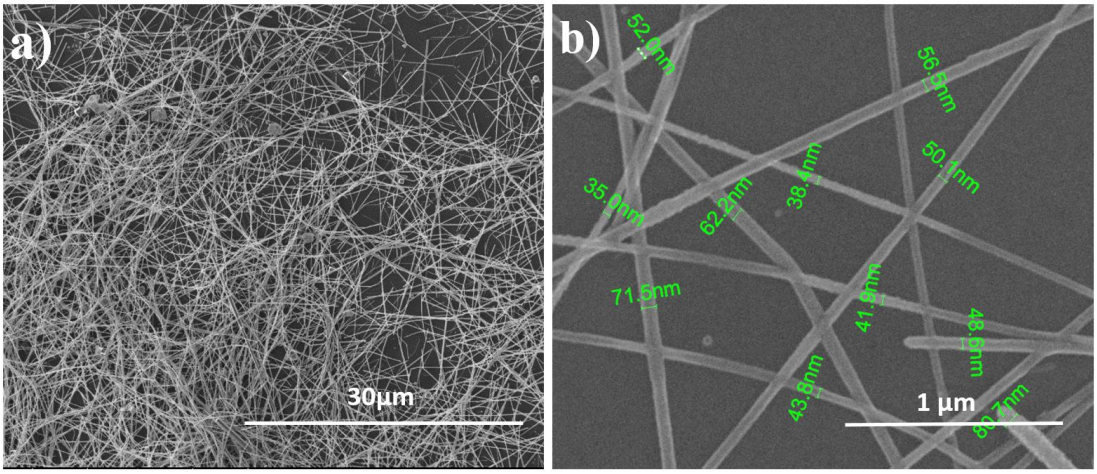


**Figure 2. 12** (a) Low and (b) high resolution SEM images of synthesized Cu NWs via hydrothermal method in this work.

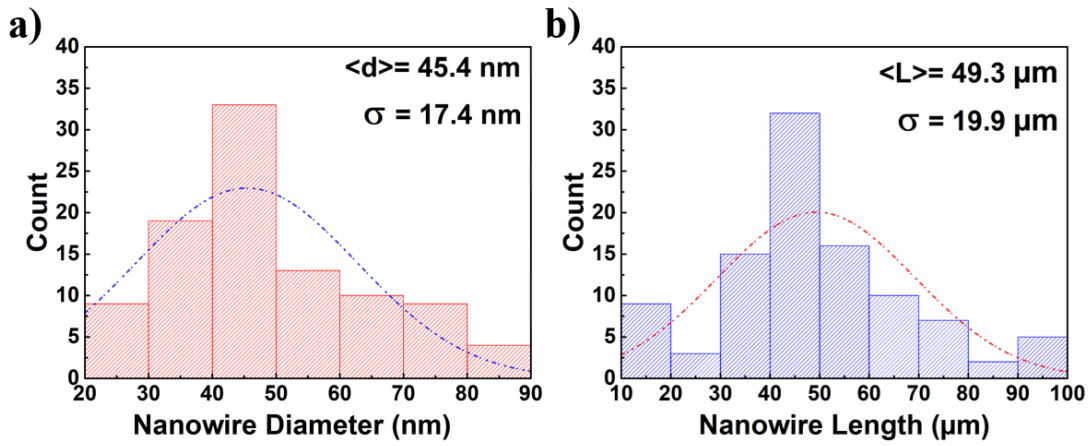


**Figure 2. 13** (a) Diameter and (b) length distribution histograms of synthesized Cu NWs via hydrothermal method in this work.

Figure 2.14 shows TEM and HRTEM images of as-synthesized Cu NWs via hydrothermal method. As it is clearly seen in images, Cu NWs have smooth surfaces and perfect crystallinity. The amorphous layer around the lateral surfaces of NWs, seen in Figure 2.14 (a) and (b), can be explained as the residual PVP shell, similar to TEM images of Ag NWs reported in literature [38]. In addition, focused ion beam (FIB) method was used to prepare cross-sectional TEM samples to examine the cross section of NWs under TEM (courtesy of Meltem Sezen from Sabancı University). HRTEM analysis assured that NWs have pentagonal cross-section with five twins as shown in Figure 2.14 (c) and (d).

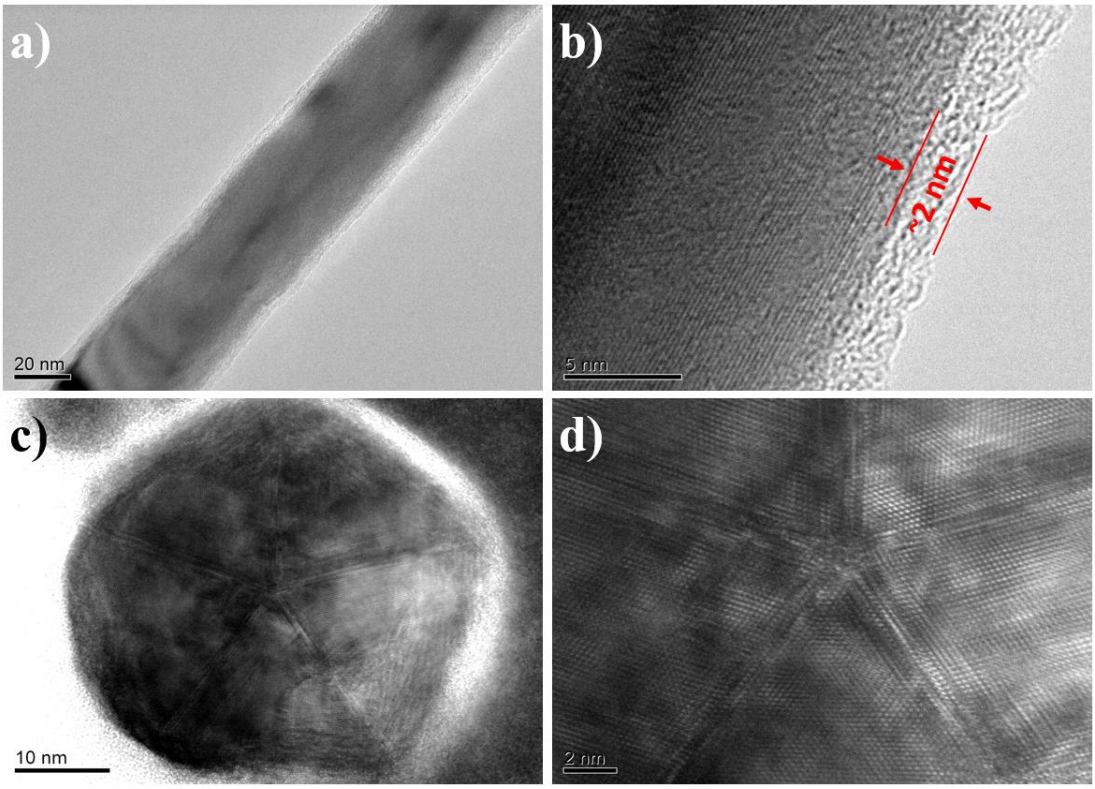


**Figure 2. 14** (a) TEM and (b) HRTEM images of as synthesized Cu NWs via hydrothermal method. (c) TEM and (b) HRTEM images of a FIB prepared cross section of Cu NW.

XRD analysis was used to monitor the purity of Cu NWs. Figure 2.15 shows the XRD pattern of Cu NWs. The XRD patterns of all samples with all diffraction peaks positioned at 2θ values of 43.30°, 50.45° and 74.20° were obtained and these diffraction angles were attributed to (111), (200) and (220) planes of face centered cubic (FCC) structure, respectively. These diffraction peaks perfectly matched with the characteristic peaks of FCC copper (JCPDS 04-0836). Furthermore, no diffraction peak that belong to oxides of copper (CuO, $Cu_2O$) or no any kind of impurities were detected within the detection limit of XRD apparatus, which indicates that as-synthesized NWs are pure and oxide free.

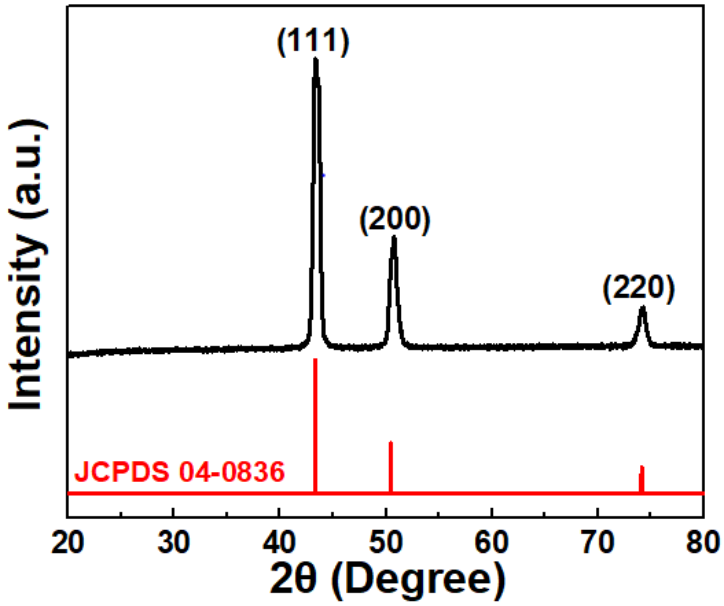


**Figure 2. 15** XRD pattern of Cu NWs synthesized via hydrothermal method.

As explained in experimental details part, multiphase separation was used for the separation of by-products. SEM images provided below in Figure 2.16 confirms the efficiency of this separation method and SEM images of as-syhthesized Cu NWs, Cu NWs and nanoparticles after multiphase separation are provided. It should be noted that the efficient separation depends on the stirring time. Further increase in stirring time causes transfer of particles into organic solvent as well as NWs.

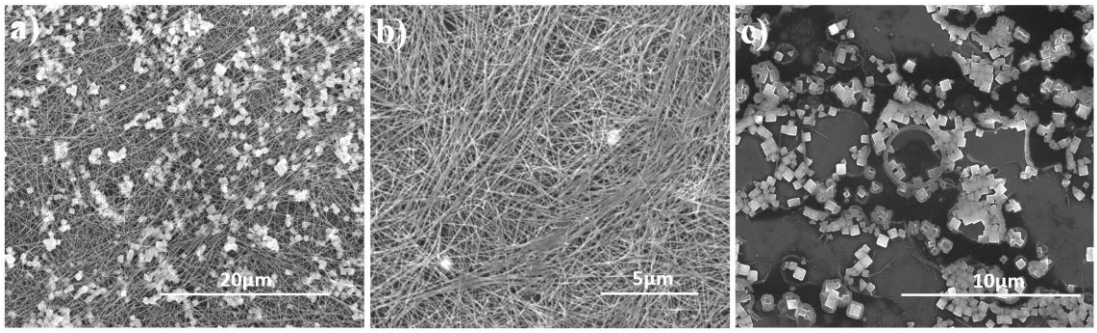


**Figure 2. 16** SEM images of as synthesized Cu NWs (a) before multiphase separation, (b) NWs and (c) NPs after multiphase separation

Additionally, as evidenced from Figure 2.16 (b), Cu NWs start to agglomerate to lower their surface energy. The reason for this agglomeration is the dissolution of the HDA shell around the lateral surfaces of NWs by chloroform. Therefore, PVP coating is a vital step to obtain good dispersion and consequently to fabricate high performance TCEs.

# CHAPTER 3

# TRANSPARENT AND CONDUCTING COPPER NANOWIRE NETWORKS

## 3.1. Introduction

TCEs are thin films of materials that are electrically conductive and at the same time transparent to visible light. Due to their high electrical conductivity in combination with high optical transparency, TCEs are an essential part of optoelectronic devices like organic solar cells, displays, touch screens, smart windows, light emitting diodes (LEDs) and organic light emitting diodes (OLEDs) as well as transparent heaters. The associated market related with TCEs have been growing over the last decade especially with increasing demands of smartphones, large flat panel displays, tablets and smart watches. All these gadgets require at least one transparent electrode in their device structure. Therefore, significant efforts have been continuously spent to fabricate high performance TCEs for the production of innovative, efficient and low cost optoelectronic devices.

### 3.1.1. Common Transparent Electrode Materials

Currently, the most commonly investigated and commercially available TCE material is transparent conducting oxides (TCOs), such as tin doped indium oxide (ITO), aluminum doped zinc oxide (AZO) and fluorine doped tin oxide (FTO). TCOs are visibly transparent since their band gaps are large enough for the transmission of photons in the visible range. Their transparency along with electrical conductivity can be controlled easily by adjusting the film thickness via their deposition method, which is most commonly sputtering [2]. In the market, majority of commercial products are based on thin films of these oxides on glass and polyethylene terephthalate (PET) substrates. In particular, ITO is the most widely investigated and

commercially prevalent one due to its high performance and wide applicability range in a variety of devices. In spite of high performance, ease of controlling film thickness, wide applicability and robustness, ITO has several drawbacks. First, indium (In) -raw material of ITO- is one of the rarest elements in the Earth's crust [39]. Therefore, sustainability of In supply is delicate and In prices have been continuously rising due to its limited availability. Moreover, increasing demand for optoelectronic devices relying on ITO is also increasing the price of this element. When demand grew faster than the production capacity of In, ITO will no longer be a competitive and profitable material for these devices. In addition to the cost of the material itself, manufacturing cost of ITO is also high. ITO is vacuum processed, mostly sputtered, and its deposition requires high temperatures and low vacuum [40]. In addition to economic concerns, ITO is unable to meet the requirement of emerging high-tech electronics that require flexibility. ITO is a fragile ceramic material and cannot maintain its electrical conductivity under mechanical bending due to cracks created throughout the film. Not only ITO; but also, FTO and other TCOs have similar drawbacks. Figure 3.1 shows the degradation in electrical performance of ITO, FTO and silver nanowire (Ag NWs) based transparent electrodes under mechanical bending [38]. Although FTO is better than ITO in terms of flexibility, its electrical conductivity considerably decreases when subjected to bending forces. Moreover, after integration of metal oxide thin films into optoelectronic devices, generally specific metal ions start to diffuse into other layers (like In element in ITO and Zn metal in AZO) [41]. This diffusion process degrades the adjacent layers and consequently shortens the lifetime of the whole device [42].

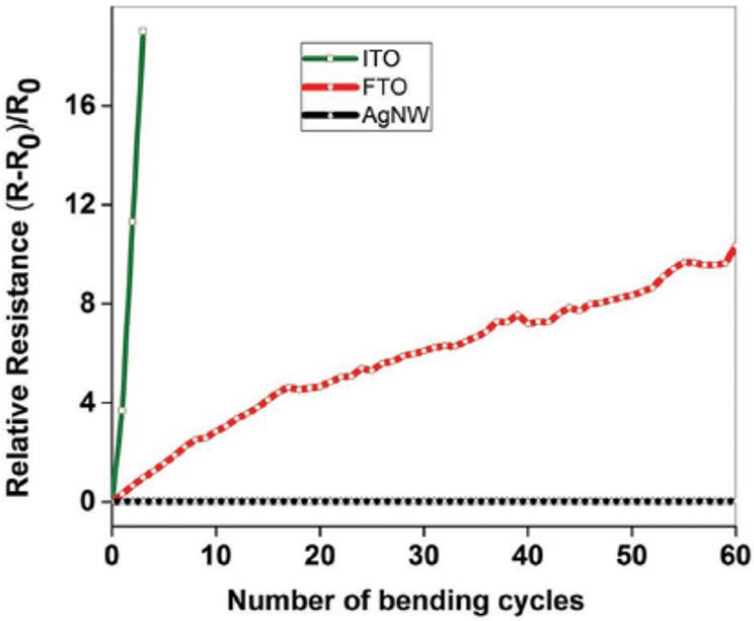


**Figure 3. 1** Change in electrical resistance of various types of TCEs under mechanical bending test. The radius of curvature was set as 5 mm [38].

For these reasons, mechanically flexible, large-scale processable, low cost and light-weight materials have been investigated to use in next generation electronic devices as an alternative to ITO.

### 3.1.2. Alternative Transparent Electrode Materials

Significant number of studies have been devoted to find an alternative transparent electrode material and various potential organic and inorganic candidates have been suggested for the replacement of ITO. However, each alternative material has both strengths and weaknesses. Therefore, there is no unique alternative material that is superior to all others. Among all candidates, the most promising ones can be listed as carbon nanotubes (CNTs), conductive polymers, graphene as organic materials; fine metal meshes and random networks of metal nanowires as inorganic materials.

### 3.1.2.1 Carbon Nanotubes

TCEs made of carbon nanomaterials have attracted significant attention over the past decade especially due to their outstanding mechanical properties and non-toxicity. Promising results have been obtained by the integration of carbon nanotubes (CNTs), particularly single-walled carbon nanotube (SWCNT) random networks, as transparent electrodes into various optoelectronic devices [43][44][45]. Especially with the development in large-scale production of high quality and low cost CNTs, dispersion and deposition processes have made this material more competitive in recent years as an alternative to ITO. However, there still exist challenges that should be overcome. Although electrical conductivity of a single CNT is very high and close to metals, random networks of CNTs suffer from low electrical conductivity due to high contact resistance of nanotubes at their junctions. Many researchers have reported that the conductivity of CNT based TCEs can be improved through chemical doping/modification treatments. For example, Hecht *et al.* demonstrated SWCNT based electrodes with 60 Ω/sq sheet resistance and 90.9 % transmittance, through exfoliation/doping by a superacid [46]. However, doping have made these electrodes temperature, air and humidity sensitive [47]. As a result, CNT based TCEs are still not a strong competitor to replace ITO in terms of cost and performance.

### 3.1.2.2 Conductive Polymers

Suitability of conductive polymers for various number of optoelectronic devices have been demonstrated by many research groups. Among these materials, the most intensively investigated one is poly (3,4-ethylenedioxythiophene):poly(styrene-sulfonate) also known as PEDOT:PSS. PEDOT: PSS is mechanically flexible, light weight, low cost, solution processable and environmentally friendly conductive polymeric material having high transparency in thin film form over a wide spectral range. However, electrical conductivity of this material is significantly lower than commercial ITO ($\sigma_{ITO} = 10^4$ S.cm$^{-1}$) [42][48]. Highest electrical conductivity achieved for PEDOT : PSS with some post treatments is not more than $1.5x10^3$ S.cm$^{-1}$ [49].

Moreover, the current carrying capacity of this polymer by itself is not sufficient to use it in optoelectronic devices like OLEDs, OPVs [42]. Its obvious blue color and temperature instability and absorption of moisture/oxygen are additional drawbacks [50]. Therefore, PEDOT: PSS thin films cannot serve as an efficient transparent electrode in optoelectronic devices. Instead of using it solely as a transparent electrode material, they are more suitable to use as planarization layer and/or hole transfer/injection layers in OPVs and OLEDs [5] [51].

#### 3.1.2.3 Graphene

Graphene is a two dimensional, only one atom thick, single layer of graphite composed of carbon atoms arranged in a hexagonal (honeycomb) lattice. Due to $sp^2$ hybridization and formation of delocalized electrons, planar charge transport in any direction takes place. Theoretically, defect free and single grain graphene has very low sheet resistance due to this movement of electrons in plane. However, no experimental results have been obtained that are compatible with the theoretical results up to date. This is due to the defects and grain boundaries of experimentally produced graphene, which negatively affects the electrical conductivity by introducing energy barriers for the transportation of electrical charges.

Andre Geim and Konstantin Novoselov won Nobel Prize in Physics in 2010 for separating 1 atom thick planar carbon sheets from graphite using a simple scotch tape [52]. This method is called as mechanical exfoliation. Since the breakthrough discovery of graphene in 2004, it has been widely investigated. Due to limited size of graphene flakes produced with mechanical exfoliation, other approaches to synthesize graphene were developed by many researchers. Now the synthesis of graphene is possible with both solution processing and CVD based methods [53][54]. According to literature, general sheet resistance and transmittance values for solution processed graphene based TCEs are higher than 1000 Ω/square at a transmittance of 85% [55]. In case of CVD synthesized monolayer graphene sheets, more promising

results have been reported. However, CVD based synthesis methods are not preferable since large scale production through this method is not practical.

#### 3.1.2.4 Fine Metal Grids

Metals, particularly Ag, Cu and Au are good conductors of electricity. Being conductive especially with respect to the mentioned low conductivity CNT thin films, graphene and conductive polymers makes metals an appealing alternative as a TCE material; but, they do not have transparency. Therefore, metals are generally used in display devices, OLEDs and LEDs as reflective anodes. However, advancement in lithography allowed to process these conductive metals to form fine metal meshes and so to use them as a TCE material. Fine metal grids can be patterned as periodically ordered wires with diameters of about 100 nm. Charge transport occurs through each column and row of periodically arranged wires and light passes through the spaces between wires. Tunable thickness and the pattern size of the grids allow optimization of the conductivity and transparency of the electrodes. Upon optimization of these parameters, metal grids having sheet resistances of 5-24 Ω/sq and transmittance of 70-80% can be obtained [56][57][58]. And this is a significant enhancement in both conductivity and transparency over CNT thin films, conductive polymers, graphene as well as ITO. Fine metal grids can be fabricated through a number of lithographic approaches such as, electron beam lithography, photolithography and scanning-probe lithography. These lithographic techniques; however, are rather costly in terms of equipment used and the quality of resolution achieved by the equipment. Moreover, metals to be processed lithographically should first be thermally evaporated onto a substrate. This thermal evaporation increases the cost of the process. Another disadvantage of fine metal grid electrodes is their extremely high surface roughness.

### 3.1.2.5 Metallic Nanowires

Random networks of metallic NWs have been successfully utilized in a variety of optoelectronic devices in laboratories. NW based transparent electrodes have exhibited performance equivalent to or even better than that of ITO in terms of electrical conductivity and optical transparency. Moreover, they combined their excellent optoelectronic properties with high mechanical flexibility. NWs can be synthesized in solution and can be solution processed as well. Both solution phase synthesis and solution based processing methods are very advantageous since they are simple, economical and scalable methods. Most widely studied metallic NWs are gold (Au), silver (Ag) and copper (Cu) NWs. Figure 3.2 shows SEM images of Ag NW based random networks with different NW densities. NW density is an important factor due to its strong influence on optoelectronic properties. Sheet resistance and optical transmittance of these films can be adjusted through the NW density.

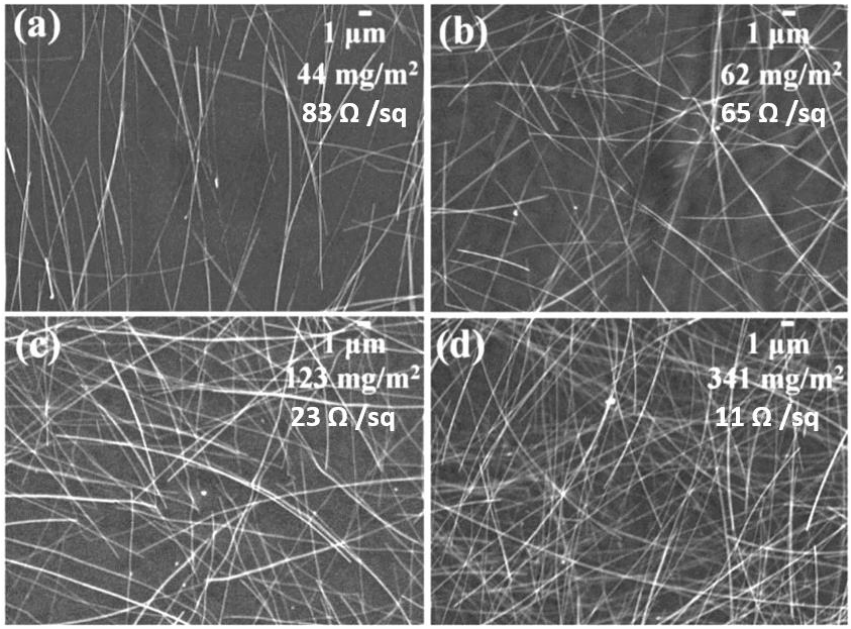


**Figure 3. 2** SEM images of Ag NW films with different densities. The different densities of Ag NW films lead to different sheet resistances of (a) 83, (b) 65 and (c) 23 and (d) 11 Ω /sq. Average diameter of Ag NWs is 30 nm [59].

So far, Ag NW random networks have exhibited outstanding performance as an alternative to ITO. The performance obtained with Cu NW random networks are not so high yet; but, is highly promising.

### 3.2 Copper Nanowire Networks

After successful utilization of Ag NW [60][61] and Au NW[62][63] based transparent electrodes, random network of Cu NWs have been introduced as a promising alternative material for TCEs due to its comparable intrinsic electrical conductivity, low cost and high abundance of Cu. Random networks of Cu NWs can be fabricated with various methods such as vacuum filtration, Meyer rod coating, spin coating and spray coating.

Vacuum filtration is one of the common methods to fabricate uniform NW films. This method relies on suction of a NW suspension through a suitable filter membrane. After suction of the suspension, film is created through interpenetrated and overlapped NWs on the surface of filter membrane. Following filtration, produced film can be transferred to a variety of substrates such as glass, PET, PDMS and Si wafer. Several studies have demonstrated routes to obtain mechanically robust and highly conductive Cu NW networks through vacuum filtration [64][65][66]. Although successful results have been obtained through fabrication of Cu NW networks via vacuum filtration, the size of films created by this method is very limited. Moreover, this process is expensive because it requires expensive filter membranes. Meyer rod coating was also used to create Cu NW random networks using a nitrocellulose based ink [67]. Although this coating method is simple and cost effective, it is necessary to create inks of NWs first with good rheological properties. In spin coating method, excessive amount of NW suspension is placed onto a substrate and the NWs were dispersed onto surface through centrifugal force via rotating this substrate at high speeds. This process is also not scalable. On the other hand using spray coating, Cu NW networks can be created on any type of substrate with curved or irregular surfaces through spraying a dilute NW suspension

using a simple air brush. This method is low cost and is also suitable for roll-to-roll production.

Cu NW networks have exhibited excellent performance in terms of optoelectronic properties, and thus they have been utilized in a variety of applications. Figure 3.3 gives the timeline of development in Cu NW based technologies. In 2008, Cu NWs were first used in nano-electronic circuits [68] and field emission displays [17]. Then, in 2010s, significant amount of studies on random networks of Cu NWs as TCEs were reported by several research groups [67] [69]. More recently, Cu NWs were utilized in solar fuels as water oxidation catalyst [70]. Another exciting and recent application involving Cu NWs is Cu NW aerogel monoliths which were demonstrated in 2014 [71].

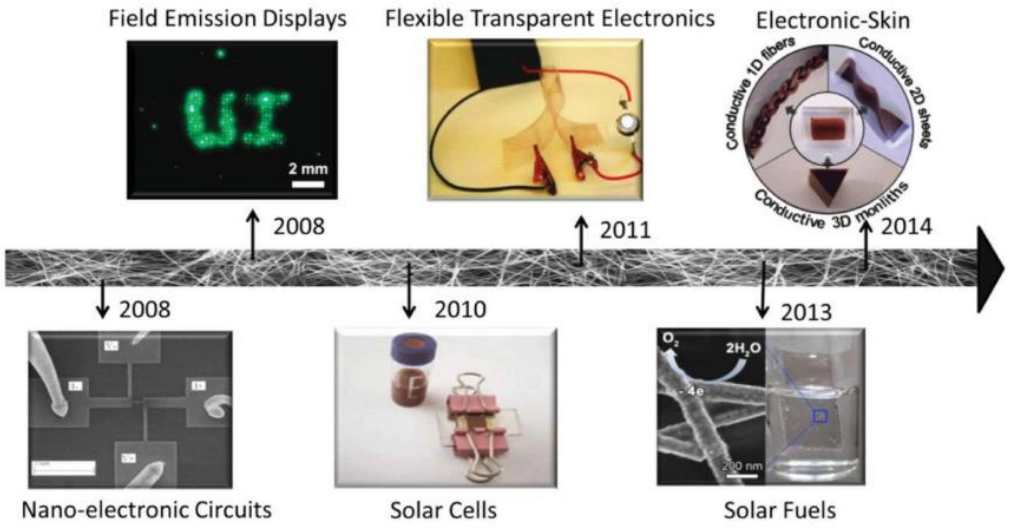


**Figure 3. 3** Timeline of Cu NW based technologies in research laboratories [2].

In addition successful utilization of Cu NW random networks as transparent electrodes for touch screens [72][73] , OLEDs [5] [74], sensors and solar cells [3][4][75] have been demonstrated by many research groups.

In their study, Chen *et al*. demonstrated successful utilization of Cu NW based transparent electrodes as an anode in bulk heterojunction organic photovoltaics [4]. In this study, Cu NWs were embedded into PEDOT: PSS layer to create flexible

transparent electrodes. Cu NWs were spray coated onto spin coated PEDOT: PSS film in a semi-solidified state and this non solidified condition of PEDOT: PSS helped embedding of NWs. Schematic of the preparation procedure can be seen in Figure 3.4 (c). One of the main disadvantage for the utilization of Cu NWs in PVs and OLEDs is their high surface roughness. Embedding NWs into PEDOT: PSS helped to reduce the high surface roughness of the networks. Moreover, embedding also increased the adhesion of networks to the substrate (See Figure 3.4 (e)). Fabricated OPV gave a power conversion efficiency of 1.4%. Although this obtained efficiency was a lot lower than the efficiency of ITO based OPVs, better performance was predicted to be obtained using high aspect ratio Cu NWs. Because in this study, fabricated electrodes' optical transmittance was very low (~ 70% T) due to low aspect ratio of Cu NWs used. SEM images of Cu NWs on PET and Cu NWs- PEDOT: PSS layers on PET are given in Figure 3.4 (a) and (b), respectively.

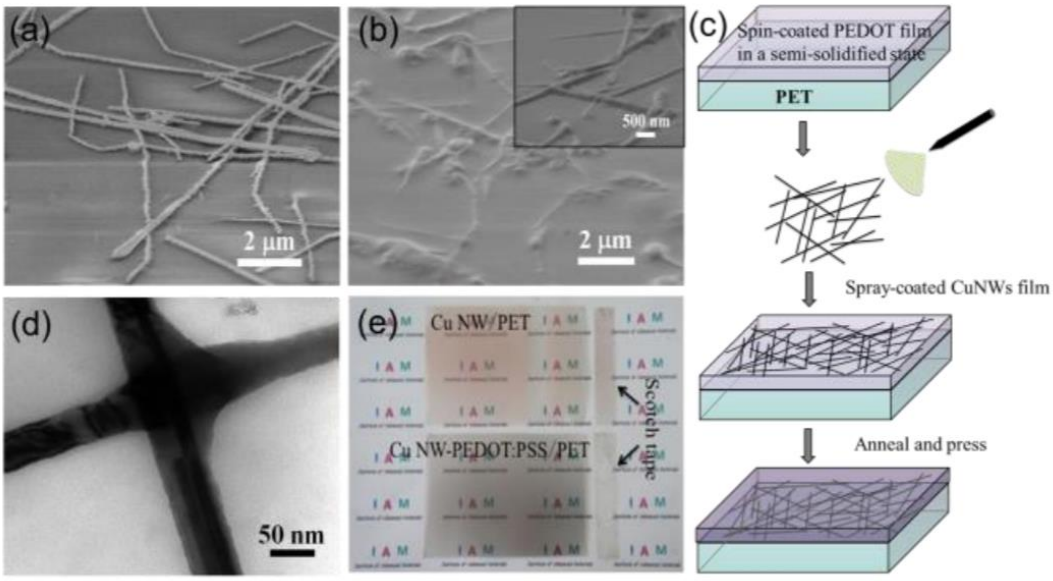


**Figure 3. 4** SEM images of (a) Cu NW/PET and (b) Cu NW-PEDOT:PSS/PET films. (c) Preparation procedure for Cu NW-PEDOT:PSS/PET films. (d) TEM image of PEDOT:PSS-coated Cu NWs. (e) Photographs of adhesion test for Cu NW/PET (top, R = 300 Ω/sq, T = 81%) and Cu NW-PEDOT:PSS/PET films (bottom, R = 15 Ω/sq , T = 76%) [4].

Im *et al.* reported highly flexible composite structure based on Cu NWs and glass fiber reinforced hybrimer (GFRHybrimer) and successfully incorporated these films into OLEDs [5]. In this study, fabricated composite films exhibited 25 Ω/sq sheet resistance and 82% transmittance and used as a bottom electrode in device structure. Device structure is provided in Figure 3.5 (a). Additionally, operation of the fabricated OLED device with Cu NW-GFRHybrimer both in flat and flexed states were demonstrated to verify the independence of performance of electrodes from mechanical bending (See Figure 3.5 (b) and (c)). Moreover, fabricated OLED devices exhibited comparable performances, which confirms suitability of Cu NW networks as a TCE material. Electroluminescence characteristics of the fabricated device can be seen in Figure 3.5.

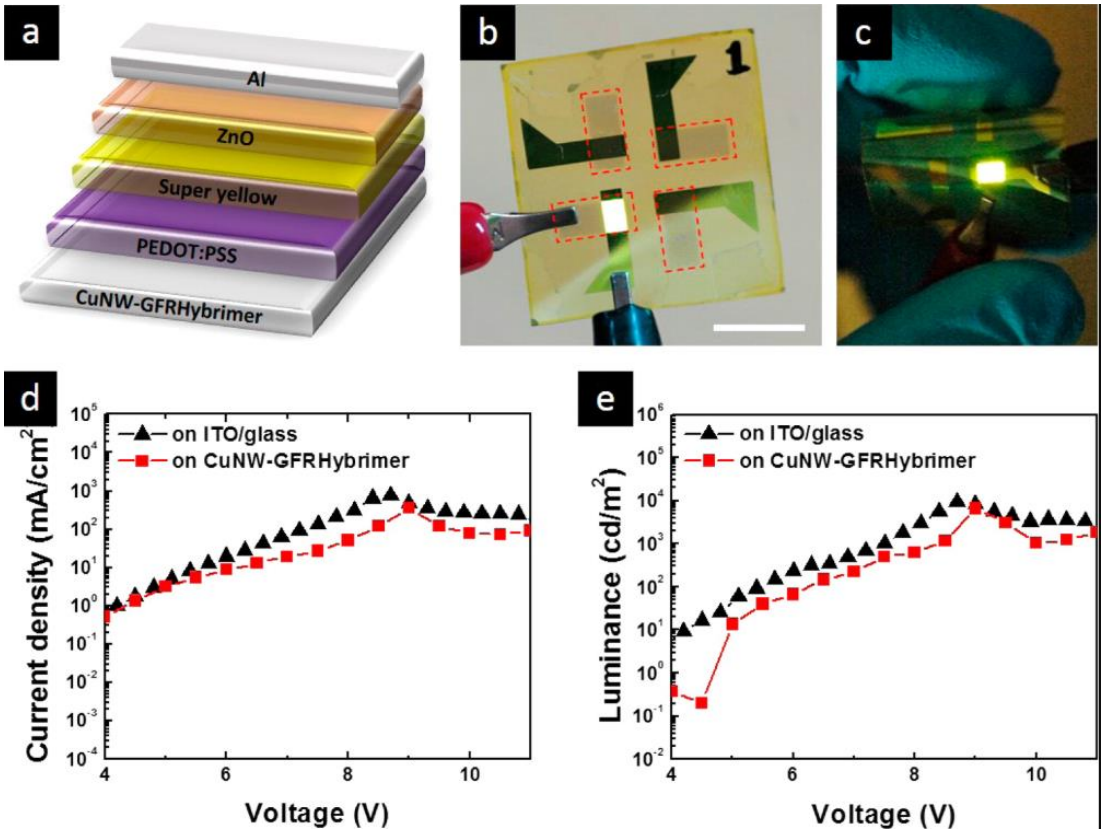


**Figure 3. 5** Demonstration of a flexible OLED on CuNW–GFRHybrimer film. (a) Device structure for the OLED. A photograph of the OLED device operating at (b) flat state (the dashed boxes show the patterned CuNW electrode directly produced by the transfer process) and (c) flexed state. The scale bar is 1 cm. (d) A plot of current density vs voltage (J–V). (e) A plot of luminance vs voltage (L–V). A reference OLED device on ITO/glass is tested for comparison [5].

As a result, all these studies demonstrated the high potential of Cu NW random networks as a promising alternative TCE material.

### 3.3 Experimental Details

All glassware were cleaned using Alconox detergent and rinsed with DI water. Then ultrasonic cleaning were performed in acetone (99.8%), isopropyl alcohol (99.8%)

and finally deionized water (18.3 MΩ) respectively through 15 minutes for each. After sonication steps, all substrates were dried with nitrogen gas. All chemicals were purchased from Sigma-Aldrich and used as received without further purification. Annealing was performed with Aixtron – Nano-instruments Black Magic II plasma enhanced chemical vapor deposition (PECVD) system operated at a base pressure of $2x10^{-5}$ atm.

### 3.3.1 Fabrication of Copper Nanowire Networks

Following purification, Cu NWs were dispersed in ethanol for the fabrication of electrodes via spray deposition. Afterwards, cleaned and dried glass substrates (2.54 x 2.54 cm, 1 mm thick) were secured onto a hot plate via heat resistant kapton tape. Additionally, to characterize the fabricated electrodes easily via SEM, a small piece of silicon wafer was also secured onto the same hot plate. Then, hot plate was heated to 90 °C and the substrates were allowed to reach the target temperature. Heating was necessary for the immediate evaporation of ethanol and leaving only NWs on the surface of the substrates. For spray deposition, a commercial airbrush fed by pure nitrogen gas at a pressure of 1.5 atm was used. NW dispersion was sprayed onto heated substrates repeatedly until a percolative and an electrically conductive network was obtained. Throughout spraying process, the distance between substrates and the nozzle of airbrush was kept constant at 15 cm. The number of spraying cycles was controlled to obtain TCEs with different NW densities. Following deposition, all fabricated electrodes were annealed at 200 °C for 20 minutes to get rid of residual PVP layer around NWs and so, to enhance the connection between NWs at their contact points. Figure 3.6 shows photographs of ethanolic dispersion of NWs and spray deposition system used in this work.

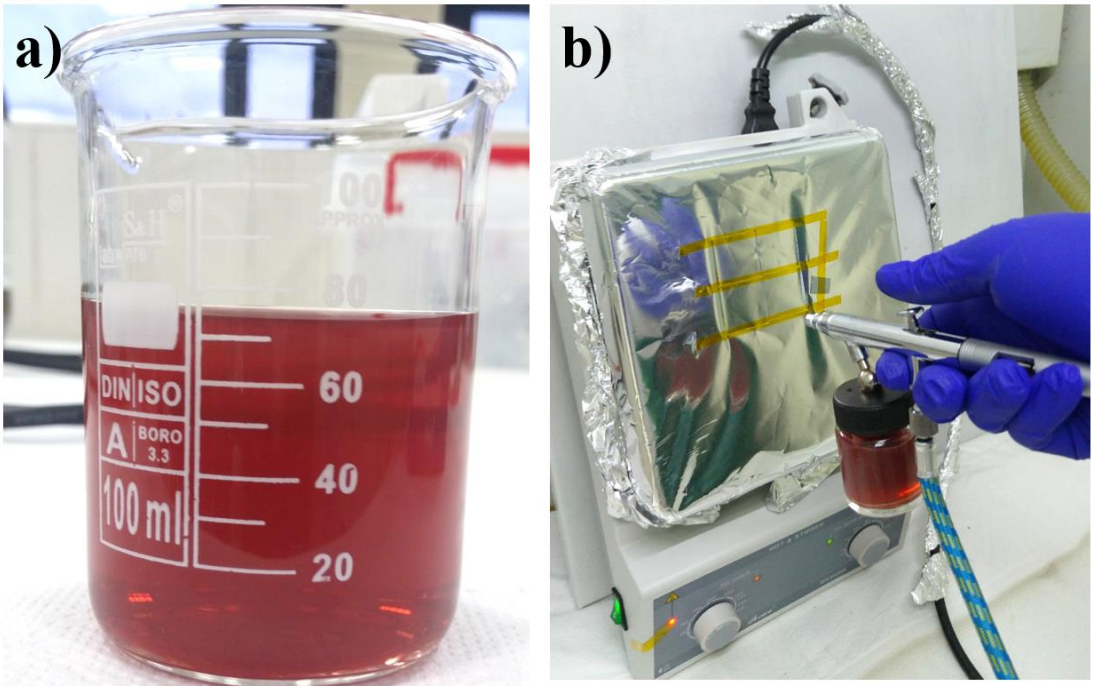


**Figure 3. 6** Photographs of (a) ethanolic solution of Cu NWs and (b) spray deposition of Cu NWs onto glass substrates and Si wafer using a commercial airbrush.

### 3.4 Device Characterization Methods

#### 3.4.1 Scanning Electron Microscopy (SEM) Analysis

Fabricated Cu NW random networks on glass and Si wafer substrates were characterized by FE-SEM (Nova NanoSEM 430) operated at an operating voltage of 20 kV. Electrodes were fixed onto SEM specimen stubs via conductive carbon tapes. No additional coating was used for SEM analysis.

#### 3.4.2 Sheet Resistance Measurements

One of the two elementary characteristics of a TCE is its sheet resistance, which is a critical parameter that should be precisely determined following the electrode fabrication process. For thin films of materials, sheet resistance term is defined and

used rather than resistance. This is because, electrical charges do not pass through the bulk material; but, they rather travel along the surface of the thin films. The exact definition of sheet resistance can be given as the resistance between opposite sides of a square in unit of ohms per square (Ω/sq). Sheet resistance measurement provides an easy comparison between different conducting thin films since the measured value is independent of the size of the square. Direct way to measure sheet resistance is using a four point probe. However, it is also possible to measure sheet resistance via two probe method provided that contact resistance can be ignored.

Resistance ($R$) and resistivity ($\rho$) are related with each other through,

$$R = \rho . \frac{L}{W.t} \quad (1)$$

, where $L$, $W$ and $t$ are length, width and thickness of the conducting bulk material, respectively. On the other hand, sheet resistance is independent from the area of the sample and it is related with resistivity through,

$$R_{sh} = \frac{\rho}{t} \quad (2)$$

However, most of the time, measuring film thickness is not trivial. Additionally, random NW networks do not form a continuous film with a certain and continuous thickness value. However, resistance and sheet resistance are related with each other through,

$$R = R_{sh} . \frac{L}{W} \quad (3)$$

Therefore, if the area between the probes is known, it is easy to determine the sheet resistance of the thin films via two probe method.

Here in this study, sheet resistance values of fabricated Cu NW networks were measured via a Keithley 2400 sourcemeter. In order to measure the sheet resistance of electrodes, two probe measurement set up previously developed by Coskun *et al.* was used [76]. Figure 3.7 shows a schematic of this measurement set up. Keithley sourcemeter were operated with a +/-1V I-V scan at 100 mV/s between two gallium indium eutectic contacts of diameter D = 1.5 mm and separated by a distance L = 3 mm. Measured resistance value was multiplied by D/L (0.5) to obtain the sheet resistance value, which was independent of the surface area.

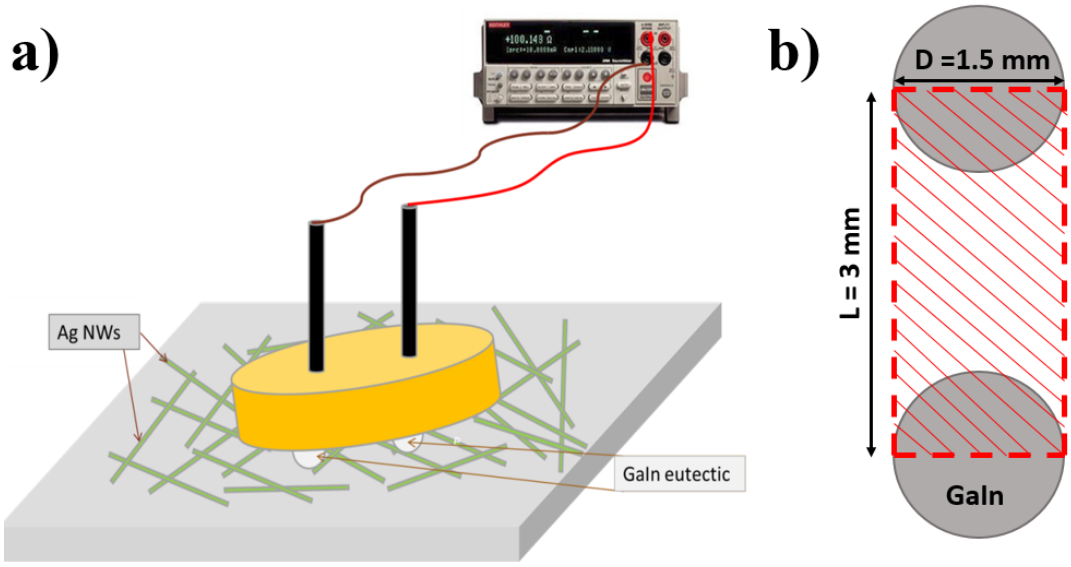


**Figure 3. 7** Schematic of (a) the two probe measurement set-up used for obtaining the sheet resistance values of Ag NW networks [76]. (b) Area covered by the measurement setup.

### 3.4.3 Transparency Measurements

The optical analyses of the Cu NW networks were performed by Agilent 8453 UV-VIS Spectrophotometer within the wavelength range of 400 - 700 nm in normal incidence mode. Here in this study, all transmittance values were stated at a specified wavelength of 550 nm. All transmittance values were reported in reference to the transmittance of cleaned glass substrates.

### 3.4.4 Areal Mass Density calculations

Optoelectronic properties of TCEs completely depend on the density of NWs forming the network. It will also be discussed in Chapter 3 that the rate of electrode degradation also strongly depend on the NW density. Although significant amount of research on random network of NWs exist in literature, most of them do not state the density of fabricated networks. For this reason, it is very difficult to compare optoelectronic performance of the nanowire networks to those in literature unless the SEM image provided in literature is analyzed to determine the NW density. Here in this study, density of networks as areal mass density (amd) in unit of $mg/m^2$ were calculated for each electrode. To determine amd of each network, several SEM images were taken from each sample. Then these images were analyzed under MATLAB software. For image analysis, developed code can be found in the Appendix. With the help of this code, firstly, SEM images were converted into grey scale images. Then contrast of the images was adjusted so that the wires in the image became white in color and the background became dark in color as shown in Figure 3.8. Then the fraction of white pixels to total number of pixels were calculated. This fraction approximately gives the percentage of the area covered by the NWs. This fraction parameter was called as $x$, which was used for further calculations, where $0 < x < 1$.

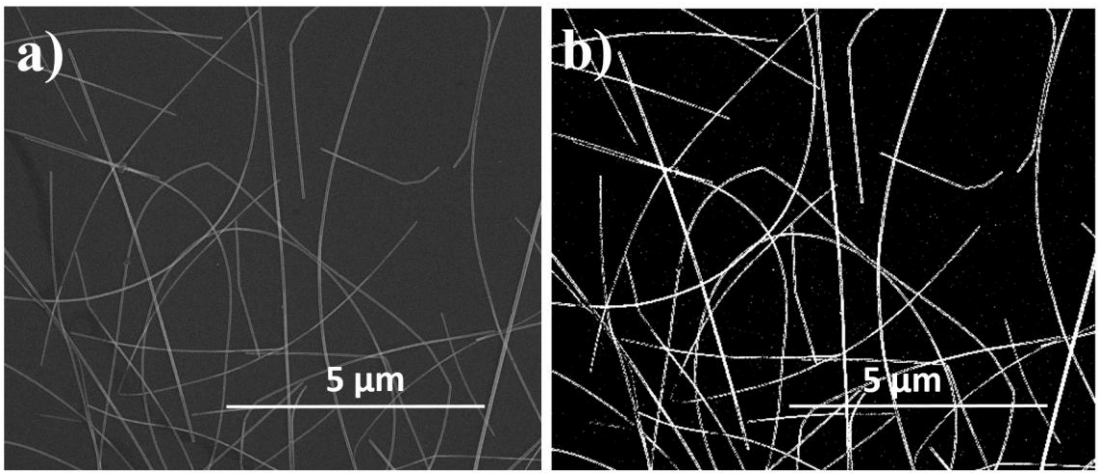


**Figure 3. 8** An SEM image of Cu NW network that is (a) unprocessed and (b) with adjusted contrast via MATLAB.

Then, by considering the scale bar given in SEM images, area of the whole image (*A*) was calculated in $m^2$ unit. The area covered by NWs was given as *A.x* (multiplication of the whole area and the fraction covered by NWs). Then, it was assumed that all NWs have cylindrical shape and have the same diameter (the average diameter calculated from randomly selected 100 NWs in Section 2.7 of Chapter 1. By this assumption we have,

$$A.x = D.l = 2.r.l \qquad (4)$$

, where *l* is the sum of lengths of all NWs that appear in the image and *r* is the average radius.

On the other hand, mass of NWs (*M*) can be calculated through;

Mass of NW = Volume of NW x Density of Copper

$$M = \pi.r^2.l.\rho_{cu} \qquad (5)$$

By substituting *r.l = A.x/2* into equation (5), one can obtain that;

$$M = \pi.r.\left(\frac{A.x}{2}\right).\rho_{cu} \tag{6}$$

Then amd than can be simply calculated as;

$$\text{amd} = \frac{M}{A} = \frac{\left(\pi.r.\left(\frac{A.x}{2}\right).\rho_{cu}\right)}{A} = \frac{(\pi.r.x.\rho_{cu})}{2}$$

### 3.5 Results

Figure 3.9 (a) shows an SEM image of Cu NW networks deposited onto Si wafer. Moreover, a photograph of a glass substrate with Cu NW network is shown in Figure 3.9 (b). This photograph reveals the transparency of the networks with clearly apparent METU logo behind the sample.

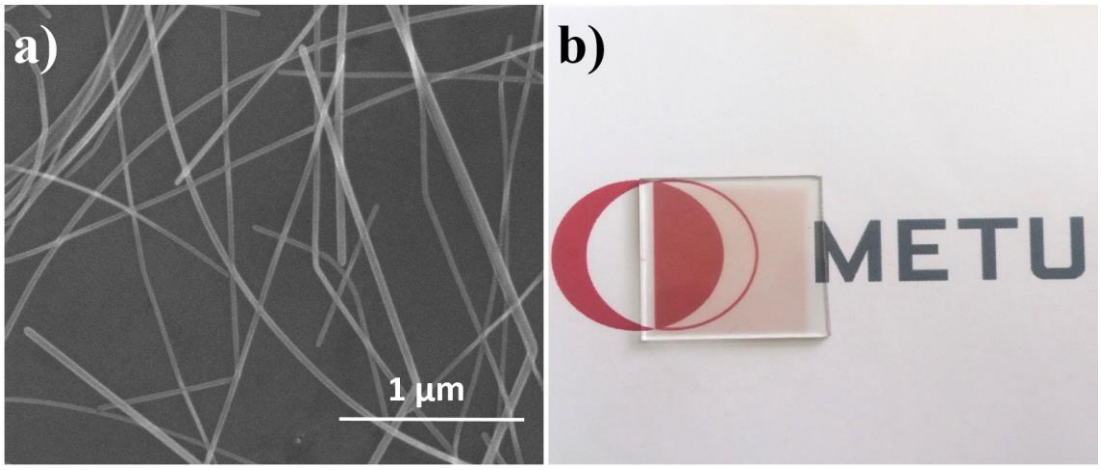


**Figure 3. 9** (a) SEM image of Cu NW networks on a Si wafer. (b) Photograph of a glass substrate with Cu NW network.

### 3.5.1 Effect of Annealing Temperature

Following spray deposition of the networks, all samples were annealed under vacuum at different temperatures for 20 minutes. Then, all the samples were analysed using SEM. Corresponding SEM images for the samples annealed at 100, 200, 300, 400 and 500°C are provided in Figure 3.10 (b)-(f), respectively. For comparison, as-deposited sample's SEM image is also provided in Figure 3.10 (a). As it clearly seen in the figure, there exist thick residual PVP layer around the nanowires since purification steps applied after PVP coating are insufficient for the complete removal of this dispersant. This PVP layer deteriorates the electrical performance of the networks by preventing connection between NWs at their contact points and thus, an annealing treatment was necessary.

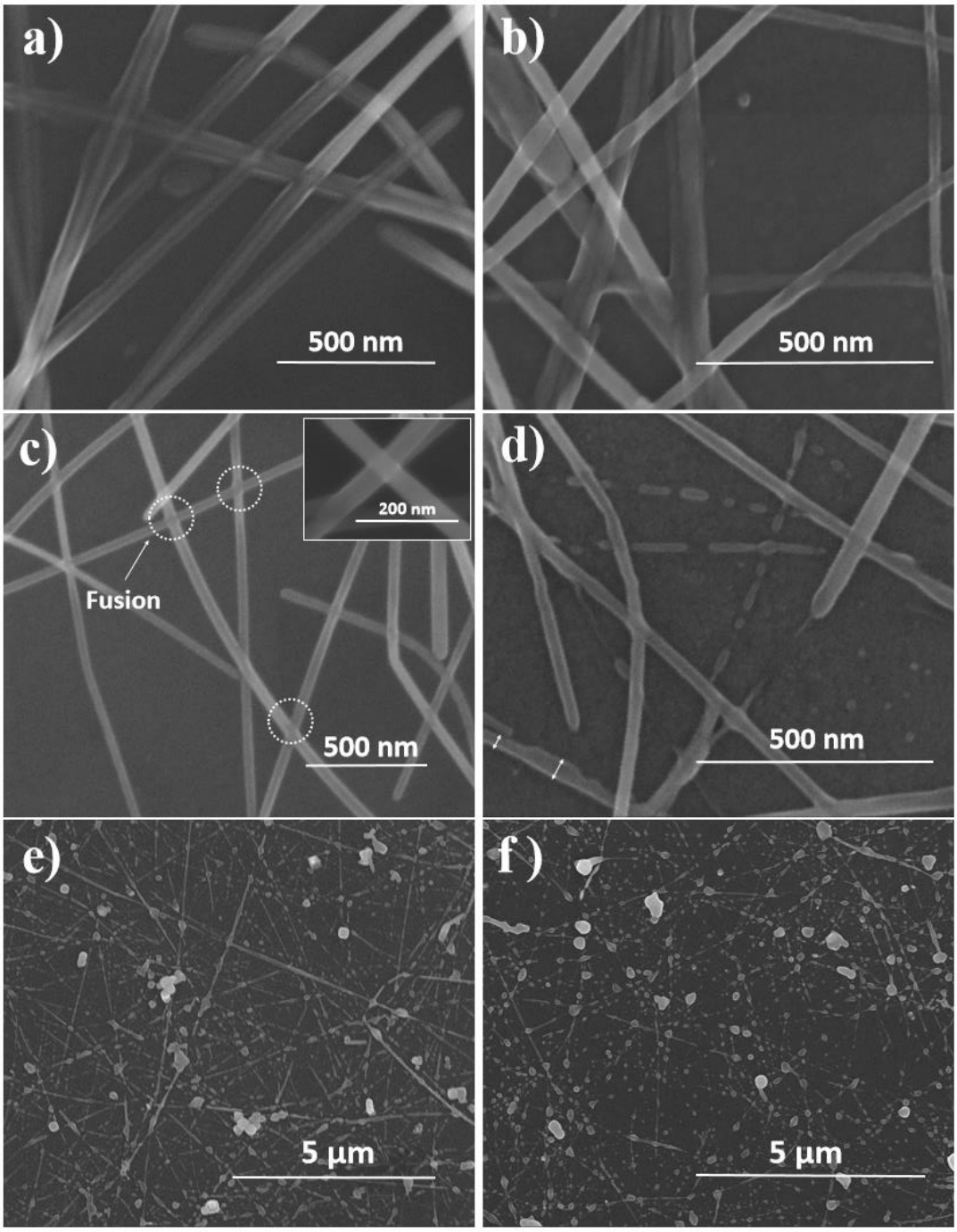


**Figure 3. 10** SEM images of Cu NW networks that are (a) as-deposited and annealed at (b) 100, (c) 200, (d) 300, (e) 400 and (f) 500°C for 20 minutes.

Firstly, annealing temperature was set to 100°C. It was found that annealing at this temperature was insufficient to completely remove PVP by considering residual thin PVP layer around the NWs in SEM image (Figure 3.10 (b)). Then annealing temperature was increased to 200°C. This temperature was determined as the optimum annealing temperature due to two reasons. First, annealing at 200°C provided the complete removal of the residual PVP layer as shown in Figure 3.10 (c). Second, it was observed that adjacent NWs started to fuse together at their contact points, which can be clearly seen from the dashed white circles on Figure 3.10 (c). This local sintering of NWs provided better electrical conductivity for the networks by decreasing the contact resistance due to enhanced connection between the Cu NWs. After annealing at 300°C, NWs started to fragment into number of ordered, discrete nano droplets. In addition, diameters of the NWs start to change. This signifies local melting within the NWs at 300°C, even though the melting temperature of bulk copper is around 1084°C [77]. Decrease in melting temperature can be explained by Lindemann's law of melting, while size variation in diameter and fragmentation of nanowires into spheriodized nano droplets can be explained by Plateau-Rayleigh instability of solids [78]. Simply, melting of materials occur when the vibration of surface atoms are much higher than the atoms in the bulk according to Lindemann [79]. Therefore, melting strongly depends on the fraction of surface atoms to total atoms, or in other words the surface to volume ratio, for all types of materials. Nanomaterials' surface to volume ratio is very high. In particular, Cu NWs investigated in this study had a very high aspect ratio of 1100. As a result, it can be stated that melting temperature of nanomaterials differs from the melting temperature of their bulk counterparts. Moreover, most of published studies in literature also show that the melting temperature decreases as the size of material decreases, especially in micrometer and nanometer scale [80][81][82][83]. On the other hand, Plateau-Rayleigh instability states that cylindrical shapes with high surface energy are unstable so that, as the temperature increases, first perturbation in radius forms then cylinder decay into fragmented spheriodized droplets to decrease the total energy. Variation in diameter and formation of spheriodized nano droplets after

annealing at 300°C therefore can be explained by Rayleigh instability. Further increase in annealing temperatures (400 and 500°C) resulted in total destruction of NW networks and formation of more fragmented spherical nano droplets, which can be seen in Figures 3.10 (e) and (f). Moreover, it was clear that at this high annealing temperatures, growth of some droplets at the expense of others took place.

### 3.5.2 Effect of Annealing Time at 200°C

After determining the optimum annealing temperature as 200°C, the effect of annealing time at this temperature was investigated. Figure 3.11 shows the variation in the sheet resistance of electrodes that were annealed at 200°C for different periods. To obtain statistical results, 3 different samples with same NW density were annealed at each temperature. First data point belongs to an un-annealed sample and the resistance of this sample was in the order of mega ohms. This high resistance of the as deposited sample was due to PVP layer covering the lateral surfaces of NWs. It was also mentioned in the previous part that this insulating polymer creates high contact resistance along the network. 10 minutes of annealing was insufficient as it can be observed from the graph provided in Figure 3.11. 20 minutes of annealing at 200°C was found to be sufficient for the complete removal of PVP layer according to the obtained sheet resistance values of the sample. No further decrease or increase in sheet resistance was observed for higher annealing times since annealing was performed under ultra-high vacuum ($2x10^{-5}$ atm).

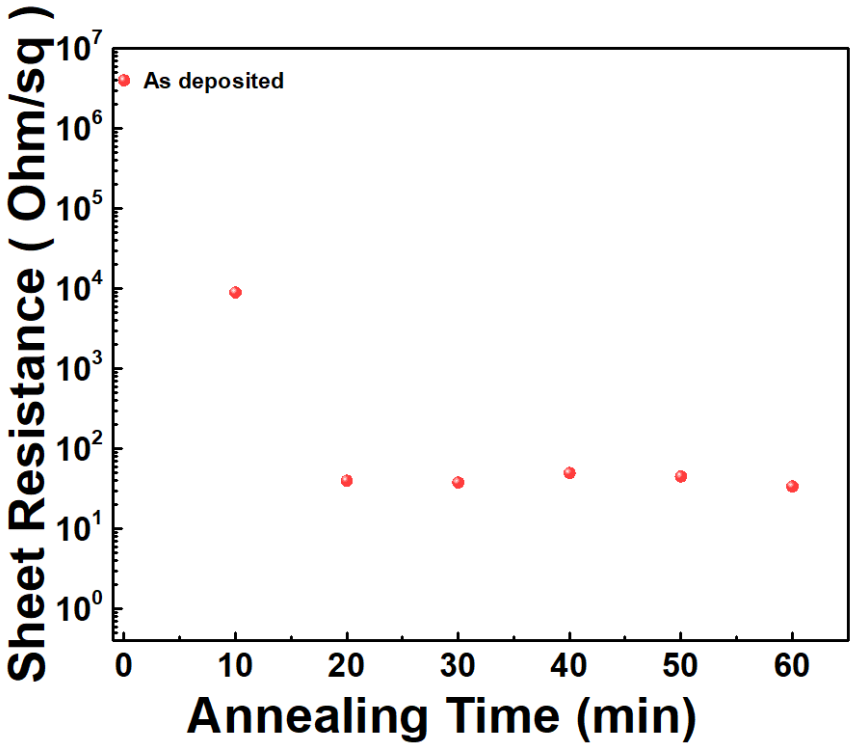


**Figure 3. 11** Change in sheet resistance of Cu NW networks annealed at 200°C for different annealing times.

### 3.5.3 Effect of Nanowire Density on Optical and Electrical Properties of Networks

To investigate the effect of NW density on the optoelectronic performance of electrodes, electrodes with different NW densities were fabricated through changing the number of spray cycles. SEM images of Cu NW networks with 10 different NW areal mass densities (amd) are provided in Figure 3.12. Subsequent to density determination, transmittance measurements of networks with different amd values were conducted and respective spectra are provided in Figure 3.13 (a). As it is clear from the figure, an increase in amd of networks resulted in a decrease in optical transparency. This was due to an increase in the area covered by the NWs and thus a decrease in the area of the holes that allows light to pass through. So, it was found that this parameter, amd, has strong influence on the optical transmittance of the

electrodes. Moreover, change in transmittance with respect to amd of the networks were plotted in order to determine whether their dependence is linear or not and provided in Figure 3.13 (b). Additionally, sheet resistance versus amd graph was also plotted and provided in Figure 3.14 (a). It was found that an increase in the amd of the networks resulted in a linear decrease in transmittance while a power law decrease was observed in electrical resistance. These obtained results are in agreement with a previously published study on Ag NW networks by Lagrange *et al.* [84]. The explanation for power law relation between electrical resistance and amd can be explained by non-linear increase in possible charge transport paths in the NW network on each spray cycle during deposition.

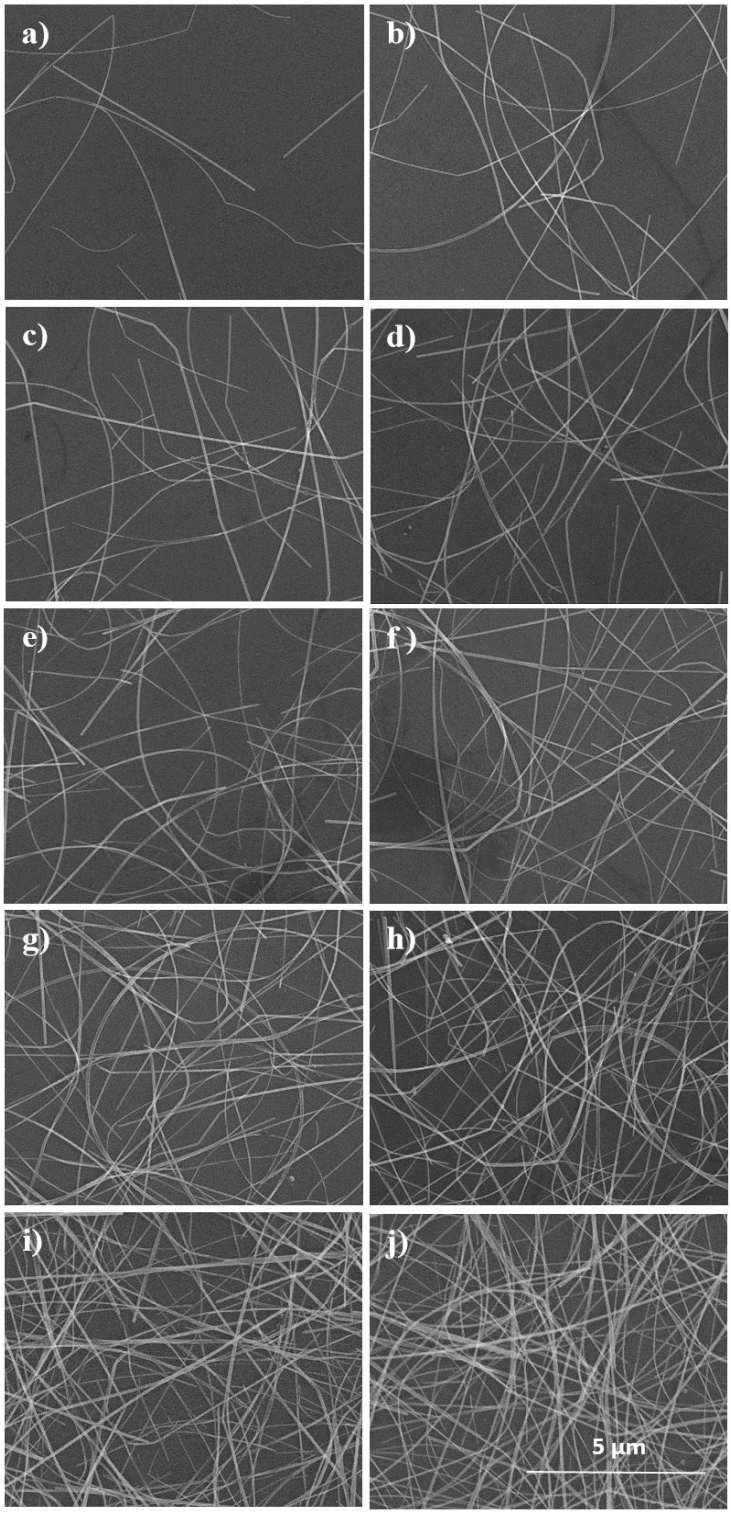


**Figure 3. 12** SEM images of Cu NW networks with different amds of (a) 8, (b) 22, (c) 28, (d) 32, (e) 40, (f) 50, (g) 70, (h) 88, (i) 112 and (j) 132 mg/m$^2$.

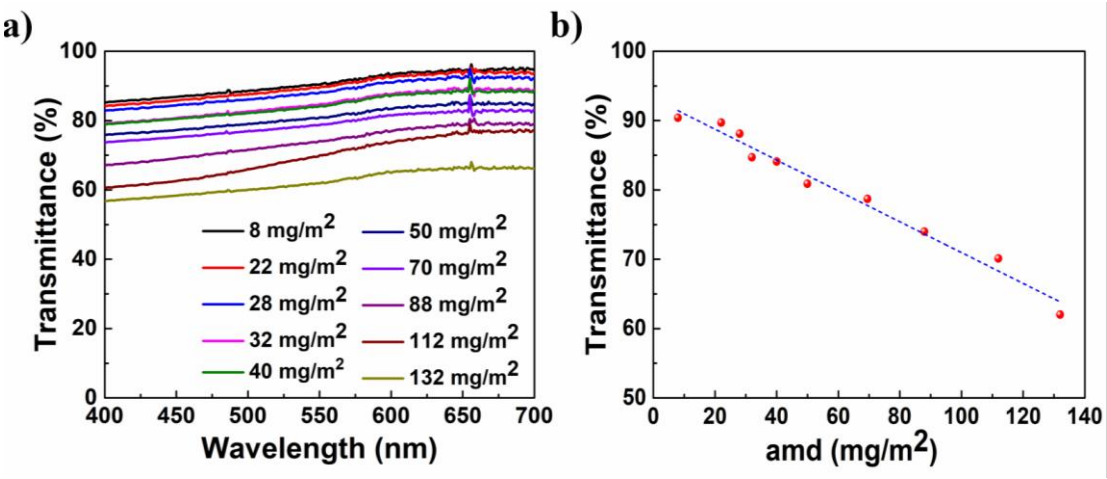


**Figure 3. 13** (a) Transmission spectra of Cu NW networks with different amd values. (b) Change in transmittance with respect to change in amd of Cu NW networks. Dashed blue line is for visual aid.

Moreover, as a figure of merit, dependence of transmittance on the sheet resistance of the network is provided in Figure 3.14 (b). Over 50 samples were used to collect this statistical data. It is clear that the deviation in sheet resistance was higher at highly transparent networks whereas almost no deviation in sheet resistance was observed for networks with poor transparency. Additionally, there was an obvious trade-off between sheet resistance and optical transmittance. An optimum value for both conductivity and transmittance should be achieved to obtain electrodes with high optoelectronic performance. As explained in the experimental section, this optimum value can be obtained by changing the number of spraying cycles, which controls the NW density within the networks. In addition, post treatment to decrease contact resistance between the NWs should be practiced carefully.

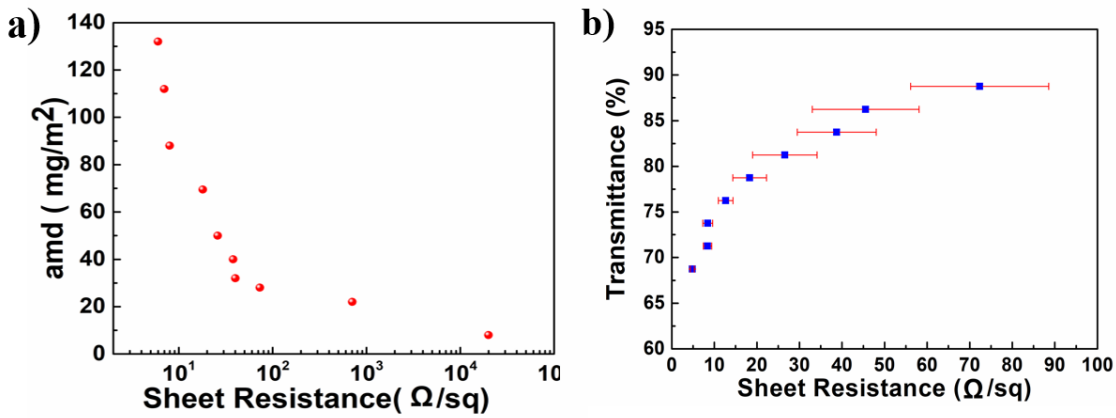


**Figure 3. 14** Dependence of the experimental values of sheet resistance of Cu NW networks on (a) optical transmittance at 550 nm and (b) amd of Cu NW networks ($mg/m^2$).

# CHAPTER 4

# STABILITY OF COPPER NANOWIRES

## 4.1. Introduction

The most critical issue with the large scale utilization of Cu NWs in commercial electronics is their oxidation under atmospheric conditions. In addition to intrinsically poor oxidation resistance, high aspect ratio makes Cu NWs even more sensitive to oxygen. Thus they easily oxidize, and become non-conducting. Therefore, the most crucial challenge for researchers to utilize Cu NWs in commercial products is the efficient protection of Cu NW networks from atmospheric corrosion without deteriorating their optoelectronic performance. Since not only NWs but also bulk copper is susceptible to oxidation, corrosion and passivation strategies of both bulk Cu and Cu NW will be discussed in this chapter.

### 4.1.1 Bulk Copper Corrosion and Its Corrosion Inhibitors

Copper is the third most commonly used metal in the world after iron/steel and aluminum and is very useful in both pure and alloyed forms [85]. Brass, copper-nickel, bronze are the examples of the most known and widely used copper alloys. Copper and its alloys are being used in a variety of fields in industry since they offer good combination of high electrical and thermal conductivity, mechanical workability, wear resistance and malleability. In particular, important part of today's electronic industry relies on copper due to its high electrical conductivity ($5.95 \times 10^7$ S/m [85]) and its high abundancy in earth's crust.

Normally, copper is considered as a noble metal with certain corrosion resistance in atmosphere due to the formation of a thin protective natural oxide layer providing passivation [86]. However, the formation of this few nanometers thick cupric oxide

($Cu_2O$) layer at the surface of copper takes place in low pollutant environments. In contrast, in highly pollutant environments with gases (i.e. $SO_2$, $O_3$, $Cl_2$, $NO_2$) or ionic constituents (e.g. $Cl^-$, $SO_4^{-2}$) this native oxide layer cannot form [87].

Since corroded surface have different properties than those of copper, this creates detrimental effects on a system constructed from copper, thus copper metal needs a protection in aggressive environments. Power plants, desalination plants, heat exchangers and in particular electronics are the prominent copper based industries suffering from corrosion. Moreover, the corroded layer is generally non-conductive and this adversely affect the performance of copper based components in electronics such as electrical boards and circuits. For this reason, corrosion of copper and corrosion protection of copper has been studied for many years. In this respect, researchers proposed considerable number of corrosion protection methods to enhance the stability of copper under different environments.

Protection against oxidation can be provided via three main ways, which are *(i)* controlling the exposure environment such as purifying atmosphere, decreasing relative humidity and temperature, cleaning surface from dust, *(ii)* the use of protective coatings such as painting, metal coating, polymer coating, sacrificial coating, vitreous enamel coating and temporary wrapping, *(iii)* the use of corrosion inhibitors such as inorganic inhibitors (chromates, molybdates and tetraborates), organic inhibitors (azoles, amines, amino acids, self-assembled monolayers) [87]. Since most of the time environmental control is not possible, one needs to use other two protection methods. The use of coatings provides good corrosion resistance for copper; however, they may fail to be suitable regarding the application area of copper. For example, thick polymeric and vitreous enamel coatings are not suitable to increase corrosion resistance of copper used in electronics, since they are insulating. Additionally, metal coatings generally involve electrodeposition process, which requires the use of a current source and complex steps. Corrosion inhibitors, on the other hand, are easy to apply since they are adsorbed by the copper surface when dipped in a solution containing inhibitors.

Therefore, corrosion inhibitors can be accepted as a strong alternative to the coatings for the protection of copper. There exist numerous organic and inorganic corrosion inhibitors providing protection for copper and its alloys. Examples of inorganic corrosion inhibitors include molybdates ($MoO_4^{-2}$), chromates ($CrO_4^{-2}$) and tetraborates ($B_4O_7^{-2}$) [88]. However, inorganic corrosion inhibitors provide weak corrosion inhibition efficiency when compared to organic ones [87]. Therefore, organic corrosion inhibitors and their derivatives are more commonly used for the corrosion protection of copper. Amongst organic inhibitors, azoles are the most prominent ones thanks to their high corrosion inhibition efficiency. Azoles are the organic compounds containing nitrogen atoms in their molecular structure. Free electron pairs in nitrogen atom acts as a potential site for bonding with copper and provide inhibition. Commonly used azoles for the corrosion protection of copper are imidazole, thiadaziazole, thiazole, pyrazole and benzotriazole e[87][89][90].

#### 4.1.1.1 Benzotriazole (BTA) and Its Corrosion Inhibition Mechanism

Benzotriazole is a heterocyclic organic compound composed of fused benzene and triazole rings with a chemical formula $C_6H_5N_3$, which can exist in two tautomeric forms as provided in Figure 4.1 [87].

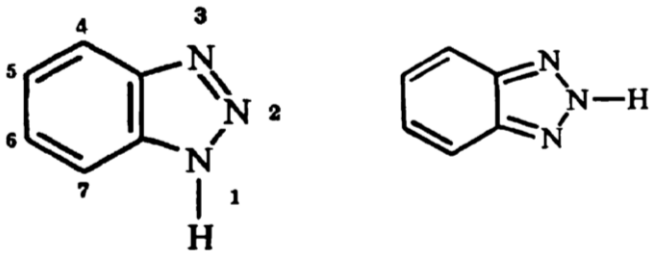


**Figure 4. 1** Tautomeric structure of BTA [87].

Benzotriazole (BTA) has been in use for many years for the prevention of corrosion of copper and its alloys in packaging and particularly in the protection under immersed conditions [91]. It was shown to be the most effective organic corrosion inhibitor in various aggressive environments [87].

To understand the mechanism of inhibition, many research groups have studied the properties of organic corrosion inhibitors. These include molecular dimensions, charge transfer, the number of adsorption sites, and the type of interaction between BTA and oxide-free and oxidized copper surfaces and the properties of the resulting protective film such as thickness, composition and detailed structure [87]. It was shown that the interaction between inhibitor and metal's surface is dominantly controlled by the molecular structure of the inhibitor [92]. Zucchi *et al.* demonstrated that heteroatoms such as nitrogen, oxygen, sulphur in inhibitor molecular structure acts as an adsorption site and promotes electron exchange between inhibitor and copper having vacant d orbital [89]. Therefore, adsorption of inhibitor molecules on the surface of copper results in the formation of a strong protective layer, which prevent its corrosion.

In addition to presence of heteroatoms in the molecular structure of inhibitor, bonding strength between inhibitor and metal, Van der Waals and $\pi$- $\pi$ interactions, film growth by polymerization are the key factors that determines the corrosion inhibition efficiency of an inhibitor [93]. Moreover, pH, temperature and aggressiveness of the environment are the other external factors that affect the corrosion inhibition efficiency.

Adsorption of inhibitor may be physical or chemical. Physical adsorption involves the electrostatic attraction between metal surface and inhibitor with opposite charges. Chemical adsorption involves coordination through the lone electron pairs of mentioned heteroatoms in the molecular structure of an inhibitor. In the case of BTA, chemical adsorption results in the formation of bonds between copper and BTA through lone pair electrons of nitrogen atom present in the molecular structure of BTA [88]. Through chemical adsorption, monolayer or multilayer protective films form at the surface of copper. This protective layer has been identified as a compact film of polymeric complex between Cu and BTA via spectroscopic analysis [94]. The polymeric complex layer may be Cu(I)BTA, Cu(II)BTA or Cu(0)BTA depending on the adsorbed copper surface [95]. If the surface of copper is cuprous

oxide ($Cu_2O$), adsorption results in Cu(I)BTA complex. If adsorption onto cupric oxide (CuO) takes place then Cu(II)BTA complex forms. If the oxide free copper surface is involved in adsorption, then Cu(0)BTA complex forms [95]. But, since in general, very thin layer of cuprous oxide almost always occur at the surface of copper, Cu(I)BTA polymeric complex is the most widely observed protective layer. The reactions taking place through chemisorption of BTA on cuprous oxide are:

$$Cu(s) + BTA\ (aq) = Cu{:}BTA\ (ads) + H^{+}(aq)$$

$$Cu{:}BTA\ (ads) = Cu(I)BTA(s) + H^{+}(aq) + e^{-}$$

It was proposed that the formed polymeric chain has alternating BTA molecules and Cu atoms with the structure provided in Figure 4.2 [92].

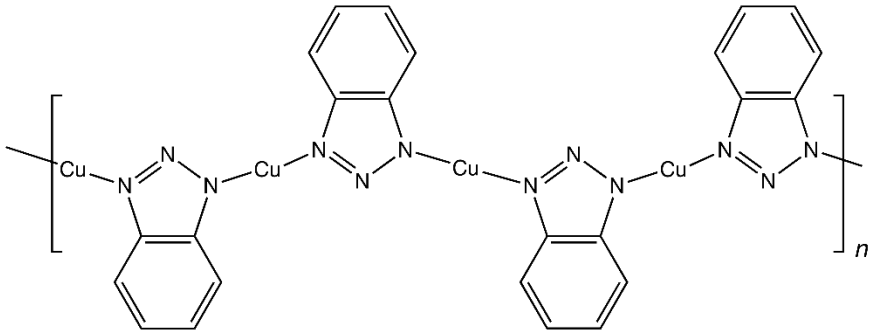


**Figure 4. 2** Structure of the Cu(I)BTA polymeric complex formed at the surface of Cu upon treatment with BTA solution [92].

It was reported that formed polymeric barrier film is insoluble in water and various organic solvents [91][94][95]. Cotton demonstrated that this film is completely resistant to rinsing and washing with water or alcohol [94]. Xue *et al.* prepared passivated copper plates by simply immersing the chemically cleaned plates in BTA-ethanol solution and showed that formed film is also stable in dry air and provides protection against oxidation under both atmospheric and immersed conditions [95]. Brusic *et al.* tested both unprotected (control) and BTA passivated Cu films under humid environment with 80% RH at 80°C for two weeks [88]. Their results showed that the rate of oxidation of BTA passivated Cu films was significantly slower than

the bare Cu films. This is because the thickness of oxide layer on bare Cu films was 2 times that of BTA passivated Cu films. Faltermeier reported corrosion inhibitor effectiveness of BTA for Cu plates that are immersed in 3 wt% BTA-ethanol solution as 99% upon storage under atmospheric conditions [90]. In addition, it was shown that BTA is also an effective corrosion inhibitor for copper and its alloys under environments such as neutral solutions, alkaline and acidic solutions as well as chloride containing solutions [92]. For instance, it was demonstrated that BTA completely inhibits the corrosion of Cu-Ni alloys in salt water [96] and in acidic media [97].

Additionally, Brusic *et al.* reported that Cu-BTA polymeric complex is thermally stable up to 200°C even though the evaporation of BTA occurs at temperatures about 100°C [88]. Christensen and co-workers also studied the thermal stability of BTA on copper foils under atmospheric conditions within the temperature range of 30 to 200°C [98]. First, they heated BTA passivated Cu foils to 100°C in air and monitored the amount of BTA on the surface of Cu foil by analyzing the ratio of the N1s and Cu2p XPS signals. It was observed that BTA get rapidly lost from the surface within a few hours and more gradually get lost at longer time (see Figure 4.3 (a)). Moreover, the loss of BTA occurred in shorter times at higher temperatures. Figure 4.3 (b) shows the remaining BTA on the surface after heating samples for 5 and 10 minutes in air at different temperatures. It is clear in the graph that the loss of BTA at temperatures higher than 150°C was so quick. Thus, this temperature was determined as the maximum temperature at which BTA is thermally stable. These results were different than the results of study reported by Brusic and co-workers, because the film preparation steps and film thickness have strong influence on the thermal stability of BTA on copper surfaces [98].

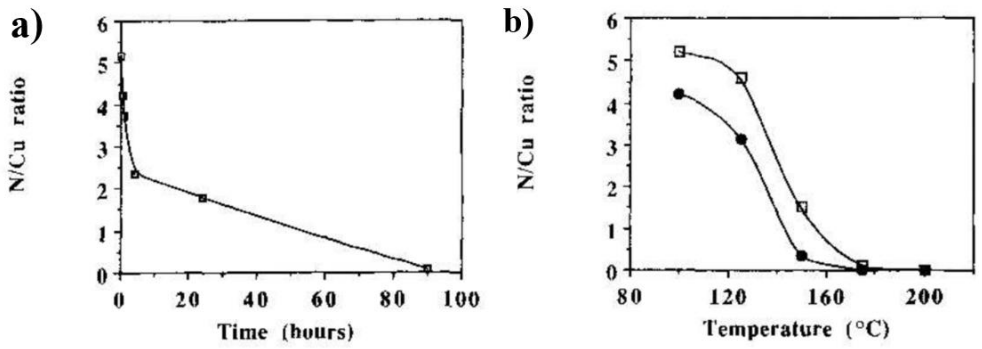


**Figure 4. 3** (a) Graph showing the loss of BTA from the Cu surface at 100°C in air (b) The stability of BTA on Cu surface in air at various temperatures for 5 (□) and 10 (●) min exposures [98].

Moreover, the type of corrosion inhibitor is determined by the act of inhibitor to reduce anodic or cathodic reaction rates. The corrosion inhibitor is called as anodic inhibitor if it reduces the rate of anodic dissolution of copper in corrosive environment. And it is called as cathodic inhibitor if it reduces the rate of cathodic reactions such as oxygen or hydrogen reduction. According to the literature, BTA is a mixed type inhibitor like all nitrogen containing heterocyclic compounds that simultaneously controls the rate of both anodic and cathodic reactions [87][99]. Therefore, this is also one of the reasons which makes BTA an efficient corrosion inhibitor.

### 4.1.2 Copper Nanowire Corrosion and Passivation Strategies

#### 4.1.2.1 Corrosion at Nanoscale

Surface area to volume ratio is an important factor determining the physical and chemical properties of materials such as, color, melting point and reactivity. The key point that correlates high surface to volume ratio with reactivity is the surface energy. Atoms at the surface of a particle are different from those at the interior. Since the number of bonds made by a surface atom is less than the expected coordination number, surface atoms have unsatisfied bonds also known as dangling

bonds. These are the ones that do not participate in bonding [100]. The number of dangling bonds is the fundamental quantity to determine the surface energy and higher number of dangling bonds means higher surface energy. Thermodynamically, high surface energy is unfavorable, thus surface atoms react with the surrounding environment to decrease the number of dangling bonds causing high surface energy [101]. As a result, metallic nanostructures are highly reactive and so inherently less stable than their bulk counterparts due to their extremely high surface area to volume ratio. This is why nanomaterials have a high tendency to agglomerate as well as to corrode.

#### 4.1.2.2 Copper Nanowire Corrosion

The oxidation rate of bulk Cu is significantly high even at room temperature. However, generally compact natural oxide "$Cu_2O$" layer forms at the surface of bulk Cu immediately after exposure to air. And this $Cu_2O$ layer, even though cannot completely stop further oxidation, can significantly reduce the rate of oxidation and so, provide good passivation for bulk Cu. However, this is not true for Cu nanostructures since the compactness of this native oxide layer has critical importance for passivation. Oxidation behavior of Cu nanostructures significantly differs from that of bulk. It was demonstrated by Bando *et al.* that Cu nanorods upon exposure to air react with oxygen immediately and completely oxidize before the formation of a compact protective oxide layer [102]. In their study, Cu nanorods were synthesized through vacuum vapor deposition (VVD) method, which is explained in Section 2.2. Synthesis was performed in a TEM and Cu nanorods with diameters in the range of 50-200 nm and lengths in the range of 2-4 μm were obtained. Then the room temperature oxidation behavior of nanorods was studied using TEM. TEM images of both as-synthesized and oxidized nanorods are provided in Figure 4.4 (a) and (b), respectively. It is clear in the TEM images that nanorods with smooth surface initially became very rough during oxidation. Moreover, TEM

image of oxidized nanorods showed that oxide layer formed around the nanorods was unstable and significant amount of oxide were spilled over the TEM grid.

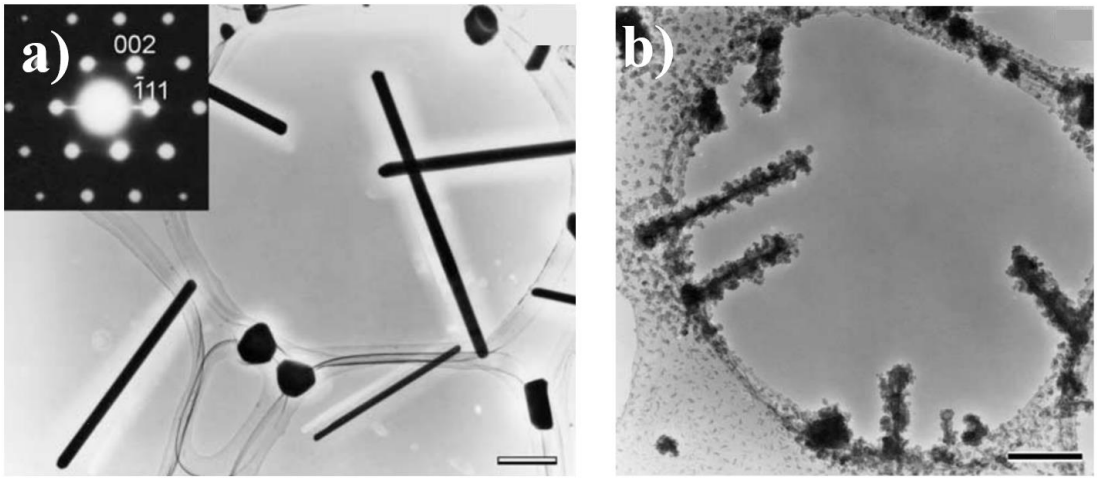


**Figure 4. 4** (a) TEM image of the as-synthesized Cu nanorods prior to oxidation. Scale bar corresponds to 500 nm. The inset is a nanobeam electron diffraction pattern of one of the Cu nanorods in [110] zone axis. (b) TEM image of collapsed nanorods due to oxidation. Scale bar corresponds to 200 nm [102].

Therefore, it can be concluded that the oxide layer formation in Cu nanostructures cannot grow dense enough to provide protection for the underlying copper atoms.

However, it should also be noted that the stability of NWs is substantially influenced by their synthesis route, morphology (i.e. average diameter and length), their surface-capping chemistry, purification and subsequent steps. For example, Liu *et al.* reported that Cu NWs with different diameters have different resistance against oxidation. Moreover, the diameters have also influence on the final morphology after oxidation [103]. In their study, the electrochemically synthesized Cu NWs had diameters in the range of 80-200 nm. Figure 4.5 (a) shows a TEM image of as synthesized NWs with very smooth surfaces in this work. In order to observe the morphological changes, NWs were exposed to atmospheric air for 24 h. After exposure to air, NWs were analyzed with TEM and it was concluded that NWs with small diameters (d < 100 nm) was totally consumed by the oxygen and the

morphology was quite similar to the morphology of oxidized NWs reported by Bando and co-workers [102]. One of these oxidized NWs with a small diameter is marked as 1 in the TEM image provided in Figure 4.5 (b). On the other hand, no porous oxide was observed on the surface of NWs with large diameters (~ 200 nm). Within the same TEM image, one of the NWs with a large diameter is marked as 3. Moreover, same porous oxide layer was observed on the surface of NWs with a moderate diameter which, is marked as 2 in the TEM image.

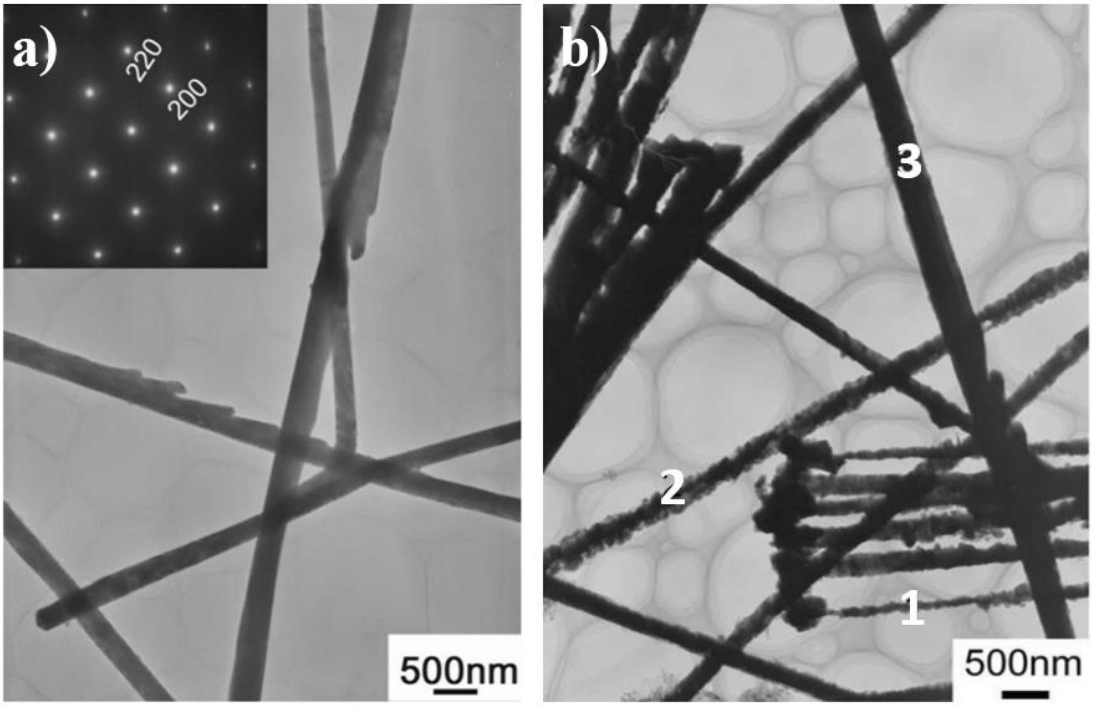


**Figure 4. 5** TEM image of (a) as synthesized Cu NWs with a diameter of about 150 nm and corresponding SAED pattern, (b) Cu NWs after 24 h atmospheric air exposure [103].

Therefore, the diameter of NWs does not only affect their stability; but also the final morphology after oxidation. In the same study, after electrodeposition of NWs into porous alumina membranes (PAM), NWs were released under two different conditions to see the effect of sample treatment on stability. In the first case, NWs were liberated from the PAM template under ambient atmosphere. On the other

hand, second procedure was performed in a glovebox under argon atmosphere. Then NWs were kept under ambient atmosphere for 30 days. After 30 days, EDS analysis showed that oxygen content of Cu NWs passivated under argon atmosphere was about half of that passivated under the ambient atmosphere [103].

In addition to room temperature atmospheric corrosion of NWs, limited number of studies on the stability of NWs at elevated temperatures were also reported. Luo and co-workers studied the oxidation kinetics of Cu NWs synthesized by AC electrodeposition [104]. Diameter of the Cu NWs' obtained in this work was about 25 nm. After heating Cu NWs with different heating rates, XRD analysis were performed. According to the XRD results, oxidation of Cu to $Cu_2O$ occurs for temperatures up to 175°C. For temperatures higher than 175°C, both Cu and $Cu_2O$ were transformed into CuO. In addition to XRD, morphology of NWs were investigated via TEM analysis. Figure 4.6 provides the TEM images of a single as-synthesized Cu NW, oxidized Cu NW heated up to 175°C and oxidized Cu NW heated up to 350°C.

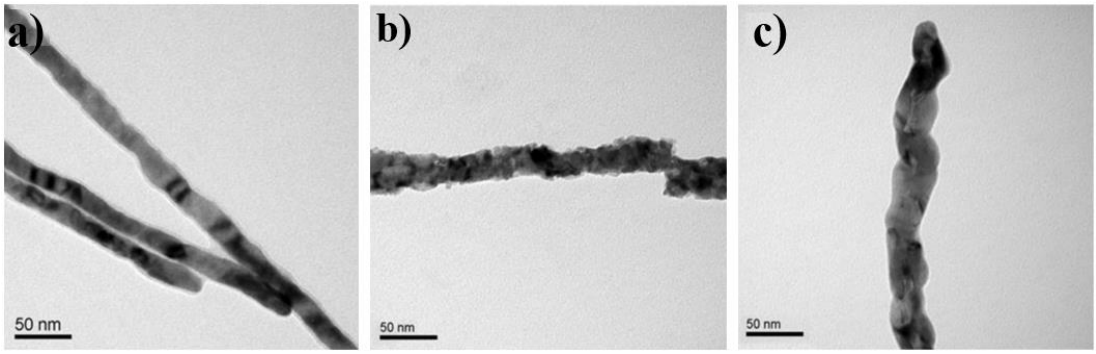


**Figure 4. 6** TEM images of Cu NWs (a) as-synthesized, (b) oxidized after heating up to 175°C and (c) oxidized after heating up to 350°C [104].

TEM analysis showed that the surface of NWs was rougher when Cu was oxidized to $Cu_2O$ with a diameter of 25±6 nm. On the other hand, CuO NWs was thicker than the Cu NWs with a diameter of 32±6 nm.

Recently, Xu *et al.* studied the stability of Cu NWs in the liquid and gas phases by monitoring the changes in their morphology and phase [105]. In their work, Cu NWs were synthesized by the EDA mediated synthesis route, which is explained in Section 2.4.1. It was demonstrated that the oxidation of Cu NWs in the liquid phase strongly correlates with the oxygen solubility of solvents. In the gas phase, oxidation of Cu NWs was investigated through thermogravimetric analysis (TGA). Cu NWs were found to oxidize to $Cu_2O$ upon heating to 200°C and they were oxidized to CuO at temperatures higher than 200°C. Following oxidation, TEM analysis were performed for both $Cu_2O$ and CuO NWs and a hollow morphology with a very thin oxide shell was observed (see Figure 4.7).

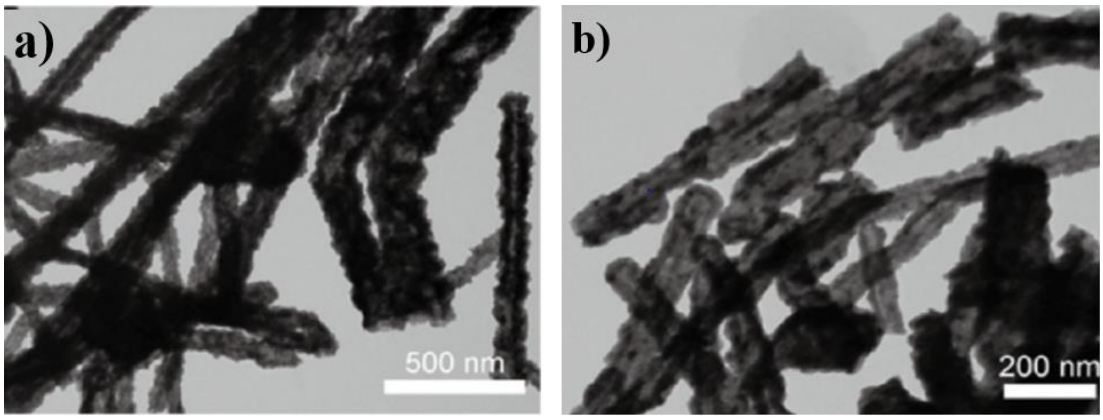


Fi**gure 4. 7** TEM image of oxidized Cu NW after heating (a) up to 200°C and (b) above 200°C [104].

Although this study is quite similar to the one reported by Luo and co-workers, the resulting morphology following the oxidation of NWs were different. This difference can be attributed to the different synthesis routes. Because many researchers stated that the oxidation mechanism and rate as well as the final morphology is influenced by the synthesis method, initial morphology of NWs, purification and other types of treatments applied [102][103][105][106].

#### 4.1.2.3 Passivation Strategies for Copper Nanowires

In literature, nearly all proposed methods to obtain stable Cu NWs and/or random networks of Cu NWs are mainly based on minimizing the oxygen exposure of Cu NWs by coating them with a protective layer. Numerous methods to coat various materials as a passivation layer have been investigated. The most important passivation strategies can be categorized into four as *(i)* metal coating, *(ii)* metal oxide coating, *(iii)* coating with carbon-based materials and *(iv)* polymer coating.

##### 4.1.2.3.1 Metal Coating

Base metal/noble metal core/shell nanowires provide resistance to oxidation with minimum amount of expensive noble metal use. Therefore, it is very common to coat instable nanostructures with noble metals like gold (Au), silver (Ag), platinum (Pt) and palladium (Pd) to achieve oxidation and corrosion stability. So far, to improve the oxidation stability of Cu NWs, relatively inert metallic coatings such as Ag, Au, Pt and nickel (Ni) were investigated using different deposition methods [75][107] [108][109][110].

###### 4.1.2.3.1.1 Ag Coating

Amongst all aforementioned noble metals (Au, Ag and Pt), Ag is a relatively cheap metal. Moreover, both electrical conductivity and stability of Ag are better than those of Cu. Therefore, Ag is a prominent candidate as a metallic protective shell. Wei *et al.* developed Cu/Ag core/shell NWs by facile galvanic replacement reaction resulting from the different electrochemical potentials of $Ag^{+}$/Ag and $Cu^{2+}$/Cu redox pairs (Figure 4.8 (a)) [108]. It was demonstrated that Cu NWs coated with a thin Ag layer are more resistant to oxidation when compared to bare Cu NWs, which was simply traced by monitoring the changes in sheet resistance with time (see Figure 4.8 (b)). At the end of 24 h air exposure, resistance of bare Cu NW networks increased by 1500%, while the initial resistance was maintained for Cu/Ag NWs. XPS results provided in Figure 4.8 (c) further verified the oxidation of Cu NWs to CuO without

protection of the Ag shell, after 24 h exposure to air. Although this facile method provide quite efficient protection for NWs; base Cu metal corrodes and oxidizes since deposition of Ag onto Cu proceeds through galvanic replacement [111]. It is also clear in the TEM image of Cu/Ag NW provided in Figure 4.8 (a) that the diameter of the wire is not uniform. This is because, oxidation and dissolution of Cu template take place throughout galvanic replacement in addition to the reduction of noble Ag. And this is the major drawback of Ag coating of Cu NWs through galvanic replacement.

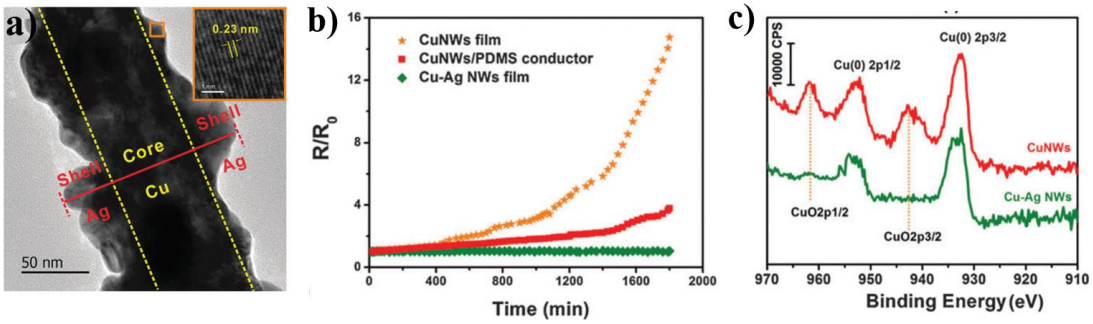


**Figure 4. 8** (a) TEM image of an as-prepared Cu/Ag NW. (b) Normalized resistance of NW based electrodes as a function of exposure time. (c) XPS spectra of Cu NWs and Cu/Ag NWs after exposure to air for 24 h [108].

Wiley's group further improved the route for the synthesis of Cu/Ag core/shell NWs and reported an extensive study on room temperature solution phase synthesis of Cu/Ag, Cu/Pt and Cu/Ni core/shell NWs. In this work, ascorbic acid was used to reduce noble metal ions onto the surface of Cu NWs while preventing galvanic replacement [107].

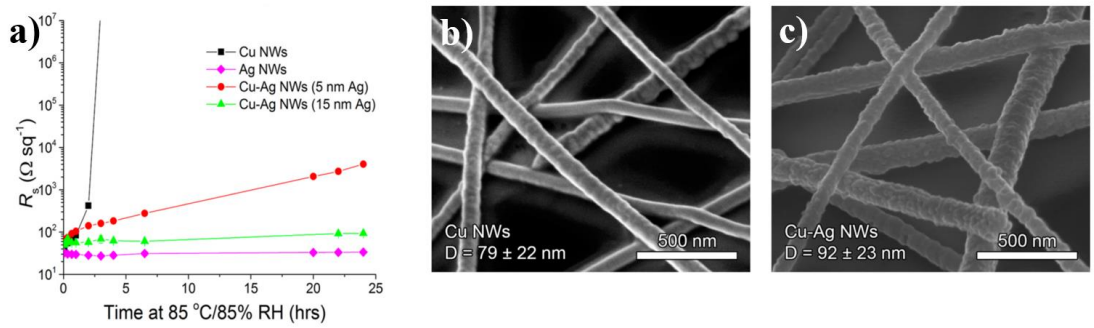


**Figure 4. 9** SEM image of (a) Cu NW (b) Cu/Ag core/shell NWs. (b) Plots of sheet resistance versus time for Cu NWs, Ag NWs and Cu/Ag NWs at a humid environment (85% RH) at 85°C.

The effect of shell thickness on oxidation resistance was also investigated in this work and it was found that the increased shell thickness increases the resistance to oxidation. It can be observed from Figure 4.9 (a) that the rate of oxidation of 5 nm Ag coated Cu NWs was much slower than that of bare Cu NWs; but, the result was not sufficient to consider it as a significant improvement in oxidation resistance. Better results were obtained with 15 nm thick shells in terms of oxidation protection since the initial sheet resistance of 15 nm Ag coated Cu NWs remained the same up to six days under humid environment (85% RH) at 85°C. However, the optoelectronic performance was adversely affected with an increase in the shell thickness. This is because the aspect ratio of the NWs decreased down to 260 with an increase in shell thickness to 13 nm. Aspect ratio was 360 for uncoated Cu NWs in this study. A significant increase in the diameter of NWs is also clear when the SEM images provided in Figure 4.9 (b) and (c) are compared.

#### 4.1.2.3.1.2 Ni Coating

When exposed to air, nickel oxide (NiO) forms at the surface of Ni. Once this native oxide layer reaches a certain thickness of 3-4 nm, it provides passivation for the underlying Ni metal [112]. Although electrodeposition of Ni onto Cu NW random networks were demonstrated by several research groups [113][114][115], it should

be noted that electrodeposition method is way too complicated since it requires access to a current source. More importantly, electrodeposition of Ni uniformly over a large area of NW random networks is very difficult due to resistance of the networks. Wiley's group demonstrated that Cu NWs can simply be coated with Ni by dipping random networks of Cu NWs in an electroless nickel plating solution [75]. Ni coating was very conformal; but, diameters of NWs increased from 67±15nm to 90±31nm (see Figure 4.10 (a)). Increase in diameter resulted in a dramatic drop in transmittance of the films by about 7%, particularly for the ones with low sheet resistance (see Figure 4.10 (b)). Afterwards, the stability of Ni coated Cu NW random networks were tested under humid environment (85% RH) at 85°C by monitoring the changes in sheet resistance with respect to time. While bare Cu NWs became completely insulating in 1 h, the initial resistance of Ni coated Cu NWs were preserved up to 5 h under the same humid environment. These results were valid for 20% Ni coated Cu NW random networks. To further improve the resistance to oxidation, Cu NWs were coated with a thicker Ni shell of 28% Ni. These thicker Ni shells were found to show better performance under the same testing conditions. Although it was not mentioned in the paper, the detrimental effect of thicker NWs on transmittance should be more dramatic with 28% Ni coated Cu NW random networks.

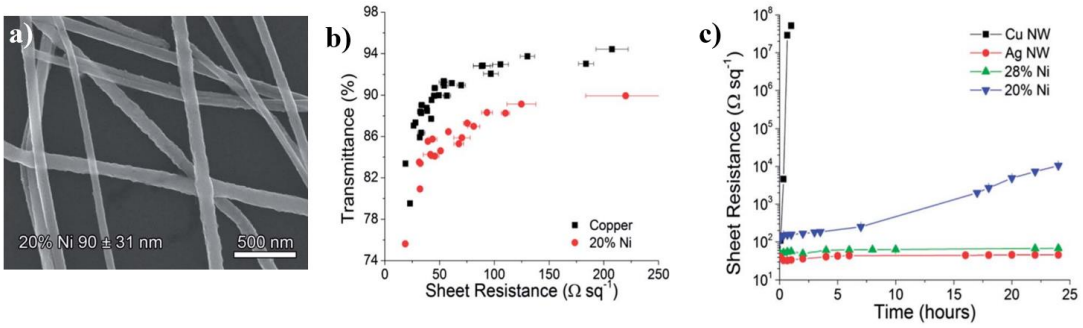


**Figure 4. 10** (a) SEM image of 20% Ni coated Cu NWs. (b) Transmittance versus sheet resistance for Cu NW random networks before and after Ni plating (c) Sheet resistance change over 24 hours for Cu NWs, 20% and 28% Ni coated Cu NWs and Ag NWs (for comparison) under humid conditions (85% RH at 85°C) [75].

#### 4.1.2.3.1.3 Au and Pt Coating

Au and Pt are other noble metals employed as a protective shell for Cu NWs. Recently, Yang and coworkers synthesized ultrathin Cu/Au core/shell NWs by epitaxial deposition of a conformal gold shell with only 2 nm thickness onto the surface of Cu NWs [110]. To prevent galvanic replacement, trictyohosphine as a strong binding ligand was used in this study. The average diameter of the Cu/Au NWs were only 21±4 nm. Therefore, random networks of Cu/Au NWs exhibited better figure of merit transmittance and electrical conductivity values compared to aforementioned core/shell NWs. Moreover, Cu/Au core/shell NWs' oxidation resistance was quite high compared to that of bare Cu NWs when tested under humid environment (80% RH 80°C). It took almost 48 hours for only 6 fold increase in the sheet resistance of Cu/Au NWs while 3 hours was enough for complete oxidation of bare Cu NWs. This synthetic epitaxial growth is a challenge since galvanic replacement is generally unavoidable. And most of the time hollow structures are obtained instead of a conformal shell layer around the NWs when galvanic replacement dominates the growth [116]. Moreover, it should be noted that a minute variation of synthesis parameters could dramatically affect the quality of core/shell

NWs synthesized via epitaxial growth. Pt was also investigated and deposited onto surface of Cu NWs to improve the oxidation stability via galvanic replacement [109] and electrodeposition [107].

#### 4.1.2.3.2 Metal Oxide Coating

Electrically conductive metal oxides such as zinc oxide (ZnO) and its doped versions are alternative passivation materials used for the protection of random networks of NWs against oxidation without deteriorating their optoelectronic performance. This is because these conducting metal oxides are not only electrically conductive but also transparent to visible region of the spectrum by virtue of their wide band gaps. For example, the band gap of aluminum doped ZnO (AZO) thin films is around 3.5 eV while the band gap of pure ZnO thin films is around 3.26 eV [117]. As a result, metal oxide coatings can prevent the corrosion and oxidation of NW networks by maintaining their optical and electrical performance in aggressive environments. Up to now, AZO, aluminum oxide ($Al_2O_3$), zinc, tin and indium oxide shells were reported as an effective passivation layer for Cu NW random networks [3][118][119].

Hsu *et al*. demonstrated a powerful passivation layer composed of outer $Al_2O_3$ layer and inner AZO layers onto electrospun Cu nanofibers via atomic layer deposition (ALD) (see Figure 4.11) [118]. In this study, highly transparent and conductive AZO layer was deposited to protect the NWs against oxidation. However, additional very thin layer of $Al_2O_3$ (1 nm thick) was also deposited onto AZO layer to improve the resistance to chemical corrosion since AZO has very poor chemical stability against especially acidic corrosion [118]. As a result, not only oxidation stability but also chemical corrosion stability of random networks of Cu NWs were enhanced. A 10% increase in resistance of passivated fibers upon exposure to 160°C in dry air and 80°C in humid air with 80% RH (Figure 4.11 (b) and (c)) was reported. Moreover, initial sheet resistance of bare electrodes increase 30 folds times which was more

than that of passivated electrodes under PEDOT: PSS layer. This clearly verifies the enhancement in the corrosion resistance of Cu NWs.

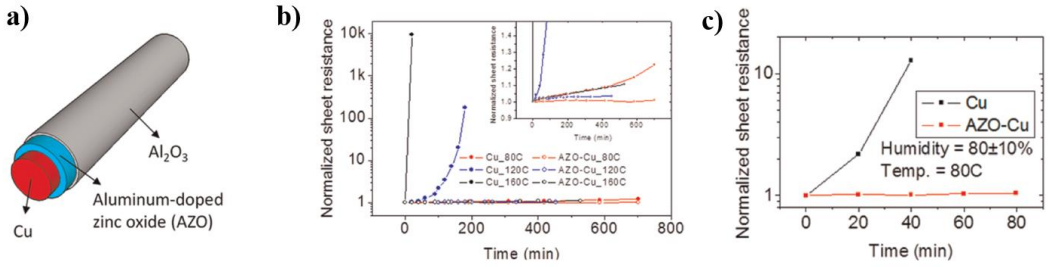


**Figure 4. 11** (a) Schematic core-shell structure of Cu/AZO/$Al_2O_3$ nanofibers. (b) Normalized sheet resistance versus baking time at 80, 120 and 160°C. (c) Change in normalized sheet resistance with respect to time under humid air with 80% RH at 80°C [118].

A similar passivation method were also investigated by Moon and co-workers [3]. A significant enhancement in both thermal and oxidation stability of Cu NW random networks sandwiched between two thin layers of AZO (55 nm thick) was reported. The AZO/Cu NW/AZO electrodes exhibited high optoelectronic performance with a transmittance and sheet resistance of 83.9 % and 35.9 Ω/sq, respectively. To fabricate electrodes, radio frequency (RF) magnetron sputtering of initial AZO layer onto a glass substrate were first performed. Then, random networks of Cu NWs were deposited onto this top of AZO coated glass substrate via spray deposition. Following network deposition, 55 nm thick top AZO layer were deposited again through RF magnetron sputtering. The HRTEM image of cross-sectioned sandwich structure is provided in Figure 4.12 (a). No change in sheet resistance was reported upon the composite electrodes were exposed to ambient atmosphere for 5 months. Moreover, AZO/Cu NW/AZO electrodes were heated to 80°C in order to investigate their thermal stability. The change in sheet resistance as a function of exposure time is provided in Figure 4.12 (b) in comparison to bare Cu and Ag NW random networks. Evidenced by the provided graph in Figure 4.12 (b), composite electrodes maintained their initial sheet resistance for up to 166 hours.

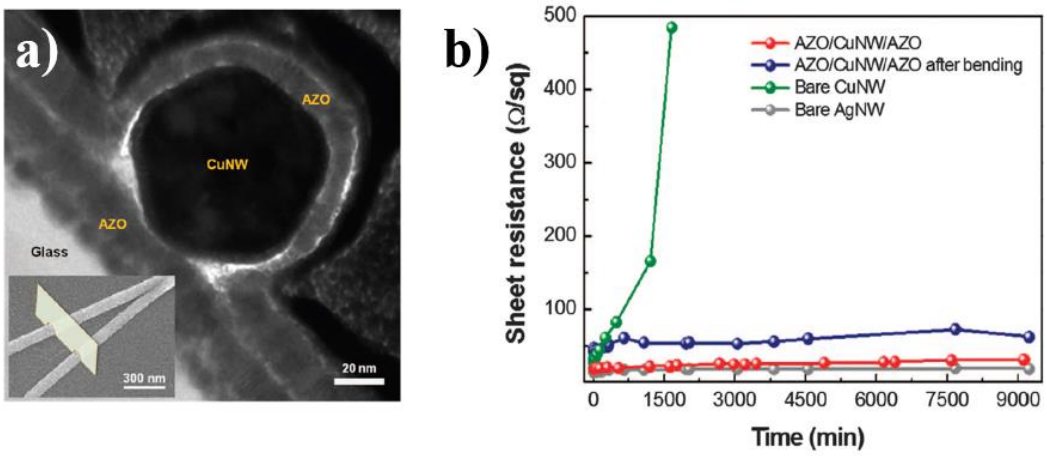


**Figure 4. 12** (a) HR-TEM image of a cross-sectioned AZO/Cu NW/AZO composite. (b) Variations in the sheet resistance for AZO/Cu NW/AZO composite electrode at 80°C in comparison to bare Cu NW and Ag NW random networks and composite electrode fabricated on PET after bending test [3].

Although, this core/shell structure created by AZO/$Al_2O_3$ and only AZO coatings significantly enhanced the durability of NW random networks, both ALD and sputtering are quite expensive techniques that are suitable for small area devices not compatible yet with large area and low cost roll-to-roll production.

Recently, Wiley's group reported a solution phase method to fabricate metal oxide coated random Cu NW networks [119]. This was established first by electrodeposition of some metals (Sn, Zn and In) onto the Cu NW random networks and followed by oxidation of these metal coatings through dipping these electrodes into a 2 wt% hydrogen peroxide ($H_2O_2$) solution to form transparent Zn, Sn and In oxide shells. The main reason to form oxide shells was to recover the decreased transmittance by electroplating. Passivated electrodes were tested under humid air (85 % RH at 85°C) and under dry air at 160°C. Plots showing the change in sheet resistance of ZnO coated Cu NW network along with bare Cu NWs as a function of time in both aforementioned testing conditions are provided in Figure 4.13. Humid conditions severely affected bare Cu NW electrodes and they became non-conducting in less than 30 minutes. On the other hand, the sheet resistance of

passivated electrodes only increased from 25 to 300 Ω /sq within 24 hours under severe humid conditions (see Figure 4.13 (b)).

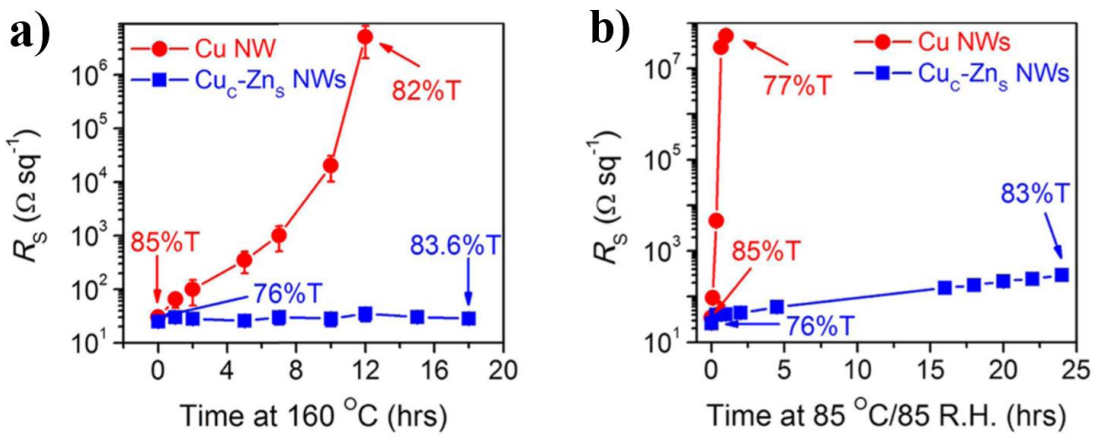


**Figure 4. 13** Plots of sheet resistance of ZnO coated Cu NWs ($Cu_{core}$-$Zn_{shell}$) and bare Cu NWs with respect to time (a) in a dry oven at 160°C and (b) at 85°C and 85%RH [119].

Although this solution phase method to improve the oxidation stability of Cu NW random networks is cost effective and simple with respect to ALD and sputtering, it is time consuming. This is because treatment a $H_2O_2$ treatment is necessary subsequent to the electrodeposition. Moreover, as also mentioned before, electrodeposition of metals onto large area random networks of NWs is impractical in terms of obtainment of a uniform coating.

#### 4.1.2.3.3 Carbon-Based Material Coating

Three types of carbon-based materials were used for the passivation of Cu NWs, these are graphene/reduced graphene oxide, carbon nanotubes (CNT) and carbon itself. Although some groups have demonstrated novel methods to synthesize Cu-CNT and Cu-C core shell NWs, stability of these composite NWs have not been studied yet. However, it can be expected that both coating types could improve the oxidation resistance of Cu NWs since numerous studies in literature showed that CNTs were employed to improve the stability and performance of Ag NWs

[120][121]. Yan *et al.* demonstrated a novel technique to synthesize Cu-CNT core shell nanowires by self-scrolling CNTs onto Cu NWs using forced field based molecular dynamic (MD) simulations. In this method, CNTs collapsed and rolled onto Cu NWs with strong van der Waals bonds [122]. Deng *et al.* synthesized carbon coated Cu nanocables via hydrothermal reduction and consequent carbonization [123].

#### 4.1.2.3.3.1 Graphene/Reduced Graphene Oxide

In addition to outstanding mechanical and electrical performance, high impermeability of graphene is what makes it attractive as a passivation material for the protection of NW random networks against oxidation. It has already been demonstrated by several research groups that graphene layers on top of random networks of NWs creates impermeable barrier that do not allow inter-diffusion and thus prevent oxidation of Cu NWs [124][125][126][127]. Theoretically, coating or wrapping Cu NWs with graphene enhance not only oxidation stability but also the electrical and thermal conductivity of the random networks. However, direct synthesis of graphene onto random networks of Cu NWs is not possible since CVD growth of graphene takes place at temperatures around 1000°C [54]. Even below these temperatures NWs melt and break due to Rayleigh instability as mentioned in Section 3.4.1. Alternatively, Shi and coworkers demonstrated that CVD grown graphene can be transferred onto Cu NW random networks via a wet transfer method [124]. In wet transfer method, firstly a PMMA layer was spun onto graphene coated Cu foils. Then Cu foil was etched with a specific copper etchant. Remaining PMMA/graphene was then transferred onto Cu NWs and PMMA was removed simply by rising in acetone. Obtained Cu NW/ graphene hybrid electrodes were tested under accelerated ageing under different conditions to confirm oxidation protection.

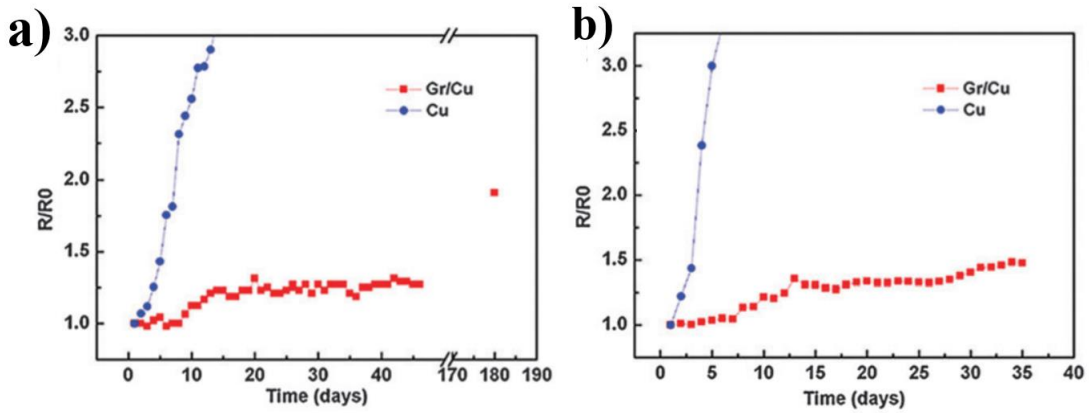


**Figure 4. 14** Change in the resistance ratio ($R/R_0$) of Cu NW-graphene hybrid electrodes compared to bare Cu NW electrodes tested at (a) room temperature and (b) 60°C [124].

The sheet resistance of graphene passivated electrodes was significantly enhanced with respect to that of bare electrodes when stored at room temperature. Sheet resistance of Cu NW/graphene hybrid electrodes increased only 91% after 6 months while bare electrodes' sheet resistance doubled within only 8 days (Figure 4.14 (a)). The rate of oxidation increased when electrodes were stored at 60°C. At this temperature, bare Cu NW electrodes sheet resistance doubled within 4 days. On the contrary, Cu NW/graphene electrodes initial sheet resistance increased by 14 times after 6 months of storage at 60°C (Figure 4.14 (b)).

In another study, Yang's research group demonstrated Cu NW/graphene oxide (GO) as well as Cu NW/ reduced graphene oxide (rGO) core/shell NWs [128]. In this study, Cu NWs were wrapped with 1.5 nm thick and uniform GO nanosheets. However, obtained electrodes showed lower performance in terms of conductivity since GO is electrically insulating. Then GO was reduced to rGO by annealing the networks at 260°C. Fabricated Cu NW/rGO core/shell random networks exhibited outstanding stability with no significant change in sheet resistance after 48 h under 80 °C and 80 ± 5% RH conditions. These results together with a TEM image of a single Cu-rGO core shell NW are provided in Figure 4.15. Moreover, Cu NW/rGO

electrodes stored under ambient atmosphere maintained their initial sheet resistance up to 200 days due to the limited diffusion of oxygen molecules through this protective shell (Figure 4.15 (c)).

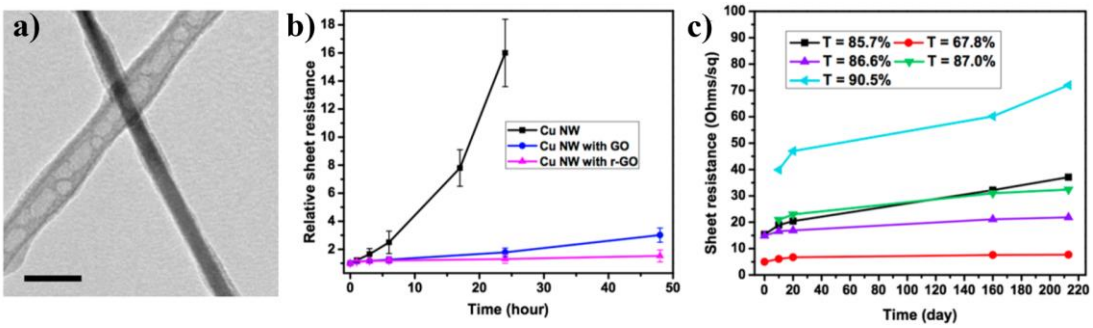


**Figure 4. 15** (a) TEM image of Cu NW/rGO core-shell NW. Scale bar corresponds to 50 nm. Stability of (a) different types of TCEs tracked at 80 °C in air and (b) five individual Cu-rGO films with different transmittance values tracked under ambient storage for over 200 days [128].

However, conflicting results have been reported recently by Zhou *et al*. [129]. They showed that graphene promotes the long term oxidation of Cu in ambient atmosphere although graphene is an effective corrosion inhibitor against short term oxidation. Ineffective long term protection of graphene was ascribed to its conductive nature, which enhances the electrochemical corrosion process.

#### 4.1.2.3.4 Polymer Coating

Both electrically conducting and insulating polymers have been employed as a passivation layer to prevent oxidation of Cu NWs and/or Cu NW random networks. Particularly, PEDOT: PSS were studied due to its high conductivity and strong adhesion to various substrates [130]. Chen *et al*. demonstrated that PEDOT: PSS coated Cu NW random networks are very stable while the resistance of bare Cu NW random networks only increased by a factor of 4 on exposure to air for 30 days (see Figure 4.16 (a) ) [4].

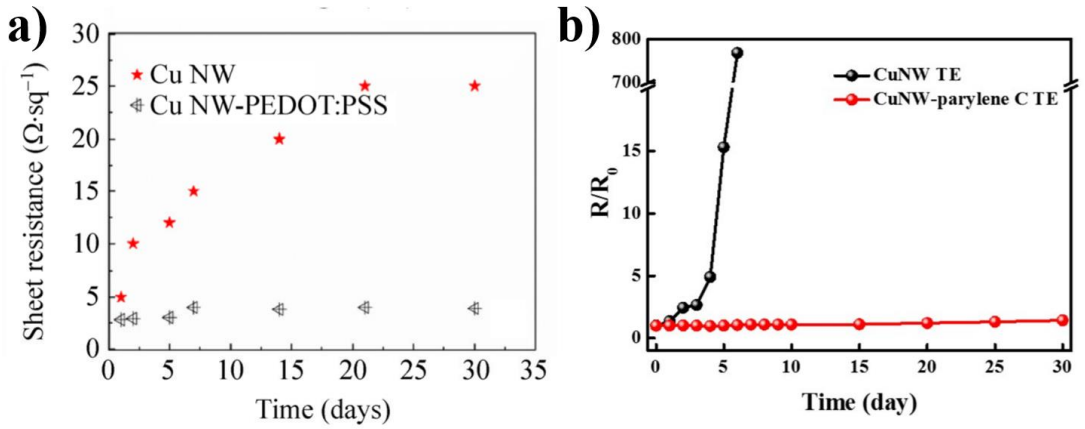


**Figure 4. 16** (a) Change in sheet resistance with time for Cu NW/PET (T = 55%) and Cu NW–PEDOT:PSS/PET (T = 55%) films [4]. (b) Sheet resistance change of Cu NW and Cu NW-parylene C transparent conducting electrodes (TCEs) during the long-term stability test under ambient condition for 30 days [131].

Ahn *et al.* fabricated high performance Cu NW-parylene C TCEs using pyrolytic deposition of parylene C passivation layer onto Cu NW random networks at room temperature [131]. Graph showing the changes in sheet resistance with time for both bare Cu NW TCE and passivated Cu NW-parylene C TCE is provided in Figure 4.16 (b). Cu NW-parylene C TCEs (94.7% transmittance and 41.6 Ω /sq sheet resistance) exhibited significantly enhanced oxidation stability compared to that of bare TCEs.

## 4.2 Characterization Methods

### 4.2.1 Scanning Electron Microscopy (SEM)

Transparent Cu NW random networks on glass substrates were characterized by FE-SEM (Nova NanoSEM 430) operated at 20 kV. Electrodes were fixed onto SEM stubs via conductive carbon tapes. Only oxidized Cu NW networks on glass substrates were coated with gold using SC7640 Quorum Technologies high resolution sputter coater operated at an operating voltage of 1.5 kV with 10 mA current for 1 minute. This roughly deposits 5 nm of gold onto samples.

### 4.2.2 Transmission Electron Microscopy (TEM)

Furthermore, detailed morphological and elemental analysis were performed via transmission electron microscopy (TEM). A JEOL 2010 high-resolution transmission electron microscopy (HRTEM) operated at 200 kV was used for this purpose. TEM samples were prepared through the removal of Cu NWs from glass substrates using ultrasonication. Then, Cu NWs were diluted in an ethanolic solution and transferred onto holey carbon-coated 400 mesh Cu support grids by drop casting.

### 4.2.3 X-ray Photoelectron Spectroscopy (XPS)

PHI 5000 Versa Probe spectrometer was used to collect XPS spectra. C (1s) line was set as 284.8 as a reference and charge correction of the binding energies (BE). Depth profiles were obtained by sputtering with an argon plasma at a voltage of 0.5 kV. XPS peak deconvolution was performed in OriginPro software to resolve each peak by fitting Gaussian-Lorentzian Function subsequent to baseline correction.

### 4.2.4 Attenuated Total Reflectance Infrared Spectroscopy (ATR-IR)

ATR-IR measurements were performed on a Bruker Alpha spectrometer equipped with a Bruker ATR attachment and a DLaTGS detector. Each ATR-IR spectrum was acquired with a frequency resolution of 4 $cm^{-1}$ by averaging 32 scans. Then, these samples were heated in air for 5 min at temperatures of 50, 75, 100, 125, 150, 175, 200 and 250°C and cooled to room temperature in ambient conditions for subsequent ATR analysis. In order to eliminate atmospheric water and carbon dioxide vibrational signatures, a background spectrum of air was acquired before each sample spectrum.

### 4.2.5 Resistance Measurements

In order to create conductive contacts for resistance measurements, two parallel sides of electrodes were coated with a thin layer of silver colloid. For each electrode, the

distance between contacts were set as 1.5 cm. In ageing processes (high relative humidity and high temperature conditions), all contacts were covered with a commercial temperature and humidity resistant silicone sealant. This was done to prevent corrosion on contacts and thus to obtain reliable measurements. The electrical resistance measurements were done via two-probe method using a digital multimeter. Moreover, the ratio of sheet resistance to initial sheet resistance ($R/R_0$) also called as normalized resistance was used to represent the changes in resistance with respect to time.

### 4.2.6 Humidity Measurements

For humidity measurements, Weather Forecast digital hygrometer with a remote probe was used. (Temperature range: ~0°C to +50°C. Humidity range of 20% RH to 98% RH. Thermometer Accuracy ± 1°. Humidity Accuracy ±5%) Continuous humidity and temperature control were performed with the chamber mounted remote probe.

## 4.3 Experimental Details

### 4.3.1 Passivation of Copper Nanowire Networks

3 wt. % BTA-ethanol solution was prepared and magnetically stirred at 300 rpm for 10 minutes in a tightly sealed glass vial at room temperature. Then, the solution was spin coated onto deposited Cu NWs networks at a spin coating speed of 3000 rpm for 30 seconds. Then, samples were dried at 70°C under 0.8 bar vacuum for 30 minutes. A day later, samples were rinsed by simply dipping in ethanol to get rid of excess BTA. Samples were then left to dry at room temperature.

### 4.3.2 Relative Humidity System

The use of saturated salt solutions is a very practical method to test and calibrate hygrometers at certain constant temperatures above 0°C. The saturated salt solutions

are the slushy mixtures of distilled water and chemically pure salts [132]. When these solutions are enclosed in a tightly sealed glass chamber at a certain temperature and equilibrium is reached, relative humidity reaches a constant value that is specific to both the type of the salt used and the temperature. The relative humidity of some saturated salt solutions is given in Table 4.1.

**Table 4. 1** Relative humidity of saturated salt solutions at different temperatures [133].

| Temperature | Relative humidity of saturated salt solution | | | | | | | |
|---|---|---|---|---|---|---|---|---|
| | $LiCl \cdot H_2O$ | $MgCl_2 \cdot 6H_2O$ | $Na_2Cr_2O_7 \cdot 2H_2O$ | $Mg(NO_3)_2 \cdot 6H_2O$ | NaCl | $(NH_4)_2SO_4$ | $KNO_3$ | $K_2SO_4$ |
| °C | % | % | % | % | % | % | % | % |
| 0 | 14.7 | 35.0 | 60.6 | 60.6 | 74.9 | 83.7 | 97.6 | 99.1 |
| 5 | 14.0 | 34.6 | 59.3 | 59.2 | 75.1 | 82.6 | 96.6 | 98.4 |
| 10 | 13.3 | 34.2 | 57.9 | 57.8 | 75.2 | 81.7 | 95.5 | 97.9 |
| 15 | 12.8 | 33.9 | 56.6 | 56.3 | 75.3 | 81.1 | 94.4 | 97.5 |
| 20 | 12.4 | 33.6 | 55.2 | 54.9 | 75.5 | 80.6 | 93.2 | 97.2 |
| 25 | 12.0 | 33.2 | 53.8 | 53.4 | 75.8 | 80.3 | 92.0 | 96.9 |
| 30 | 11.8 | 32.8 | 52.5 | 52.0 | 75.6 | 80.0 | 90.7 | 96.6 |
| 35 | 11.7 | 32.5 | 51.2 | 50.6 | 75.5 | 79.8 | 89.3 | 96.4 |
| 40 | 11.6 | 32.1 | 49.8 | 49.2 | 75.4 | 79.6 | 87.9 | 96.2 |
| 45 | 11.5 | 31.8 | 48.5 | 47.7 | 75.1 | 79.3 | 86.5 | 96.0 |
| 50 | 11.4 | 31.4 | 47.1 | 46.3 | 74.7 | 79.1 | 85.0 | 95.8 |

In this work, constant relative humidity chambers were designed using saturated salt solutions. A commercial glass jar (400 ml capacity) with a tight silicone cap was employed as a chamber. A hygrometer was used to track the humidity and temperature throughout the experiments. A small hole was opened on the silicone cap to mount and fix the hygrometer probe. Cables with crocodile clips were also mounted through the same procedure. Electrodes were secured with crocodile clips. Then as mentioned before, contact areas outside crocodile tooth were totally covered with a silicone sealant. A schematic presentation and a photo of the utilized humidity chamber in this work are provided in Figures 4.17 (a) and (b), respectively.

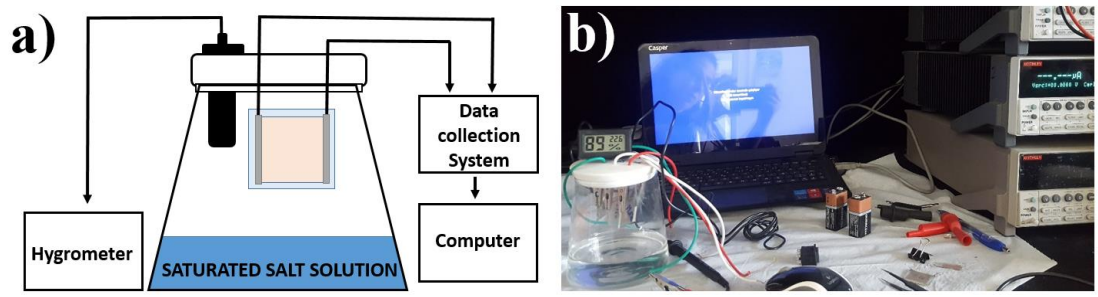


**Figure 4. 17** (a) Schematic and (b) photograph of the humidity measurement setup in this work.

In order to obtain 75% RH and 90% RH at room temperature, sodium chloride (NaCl) and potassium nitrate ($KNO_3$) salts were used. Excess amount of salts were mixed with deionized water inside the chamber and waited for the system to reach equilibrium after chamber was sealed with the cap. Wexler and Hasegawa reported that the time necessary to achieve desired equilibrium humidity with saturated salt solutions depends on *(i)* the ratio of free surface area of the solution to the total chamber volume, *(ii)* the presence of hygroscopic materials, and *(iii)* the amount of air stirring [133]. By considering these factors, a unique jar shape was chosen which expands from top to bottom. In this way, the ratio of free surface area of the solution to chamber volume was increased and thus the time to reach equilibrium was shortened. No hygroscopic materials were involved and no air stirring was applied. In both cases, it took 15 minutes to reach equilibrium humidity level.

### 4.4 Results and Discussions

To see the effect of BTA coating on optoelectronic performance of the electrodes, both sheet resistance and transmittance measurements were performed before and after BTA coating. Figure 4.18 (a) and (b) shows the photographs of bare and BTA passivated Cu NW networks, respectively. The METU logo behind the networks were clearly visible for both electrodes. The sheet resistance of bare electrode was 25 Ω/sq at a transmittance of 85% (at 550 nm). After BTA coating, resistance was measured as 26 Ω/sq at a transmittance of 83% (at 550 nm). Transmittance spectra of

these electrodes are provided in Figure 4.18 (c). It can be stated that no significant change was observed in terms of both sheet resistance and transmittance. Although rinsing was done by dipping networks into ethanol, this method is not effective for the complete removal of residual BTA that is present on the substrates. So, this 2% decrease in transmittance can be attributed to the residual BTA on the substrate surface.

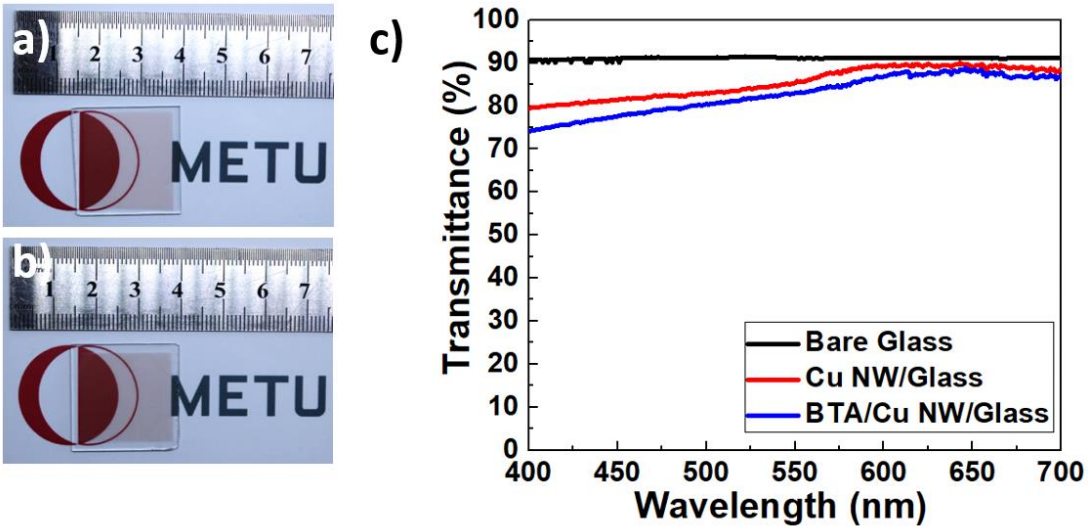


**Figure 4. 18** Photographs of (a) bare and (b) BTA passivated Cu NW networks. (c) Transmittance spectra of bare and BTA passivated Cu NW networks. Spectrum of bare glass is also provided for comparison.

### 4.4.1 Oxidation Stability of Networks under Ambient Conditions

In order to compare the oxidation resistance performance under atmospheric conditions, sheet resistances of bare Cu NW and BTA passivated Cu NW networks were monitored up to a year. Throughout resistance monitoring, all electrodes were kept under atmospherically regulated laboratory conditions (average temperature 22±2 and average humidity 25±5%). Figure 4.19 shows the graph of normalized resistance versus time for bare and BTA passivated Cu NW networks. Bare Cu NWs lost their conductivity within 12 days due to oxidation of NWs while the sheet

resistance of BTA passivated networks increased only by a factor of 1.1. The inset in Figure 4.19 clearly shows the first 12 days of bare Cu NWs and it is obvious that a rapid increase in sheet resistance occurs in the last 4 days of the measurement prior to complete failure. This can be the indication of non-linear decrease in the number of possible charge transport pathways.

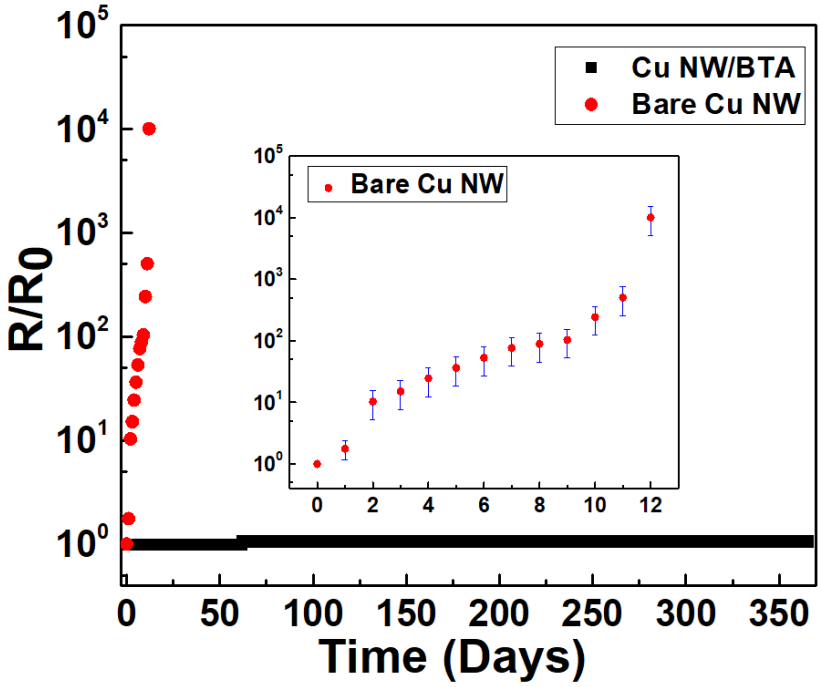


**Figure 4. 19** Change in electrical resistance of bare and BTA passivated Cu NW networks while kept under ambient atmospheric conditions.

Figure 4.20 (a) shows SEM image of bare Cu NW networks before exposure to ambient atmosphere. As it can be seen from the figure, Cu NWs have very smooth side surfaces. BTA passivated Cu NW networks exhibited superior stability against atmospheric corrosion with respect to the reference bare Cu NW network and no morphological change was observed at the end of the test (see Figure 4.20 (b)).

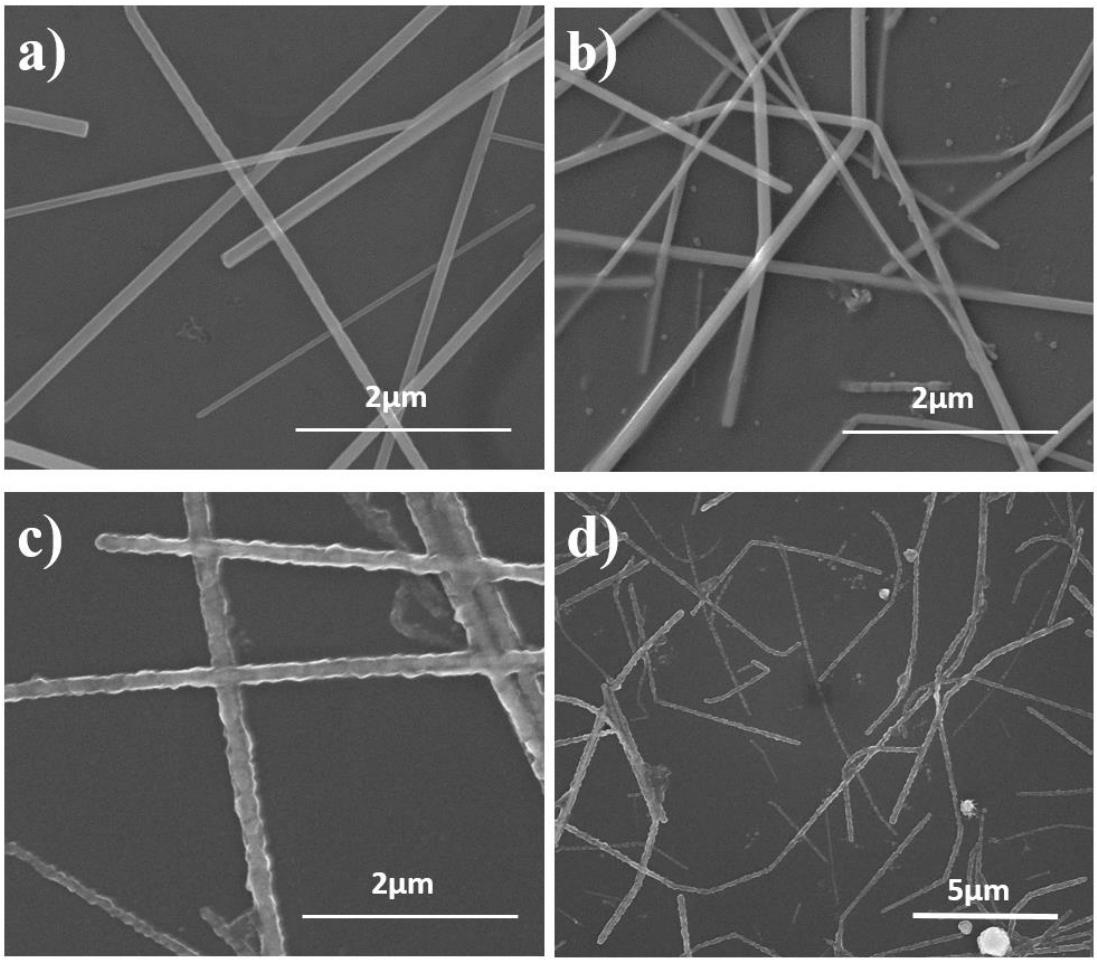


**Figure 4. 20** SEM images of (a) bare Cu NWs before test, (b) BTA passivated Cu NW networks after being kept under ambient conditions for 1 year (c) and (d) bare Cu NW networks after being kept under ambient atmospheric conditions for 1 year.

However, as the bare Cu NWs were kept in ambient conditions, the surface roughness of NWs increased dramatically. Due to severe corrosion, some NWs with small diameters even broke into nanorods and the integrity of conductive network was lost due to the rupture of NWs (see Figure 4.20 (c) and (d)). This result is in agreement with the work reported by Liu (which was mentioned in Section 4.3.2). The degree of corrosion of NWs is related to their diameters. Also in this work, NWs with small diameters were consumed totally due to corrosion while the others (with the large diameters) only showed surface roughness. Moreover, it can be observed

from Figure 4.20 (c) that the non-conducting rough shells of NWs appear lighter compared to the NW cores due to the charging effect in SEM.

To further characterize the compositional change in both BTA passivated and bare networks after exposure to ambient atmosphere and to verify that loss in conductivity and change in morphology is due to the formation of oxides (not other compounds of Cu), the X-ray photoelectron spectroscopy (XPS) analysis was performed. XPS analysis can be used to distinguish between Cu metal, $Cu_2O$ and CuO. The CuO has specific high intensity shake-up satellite peaks, which is approximately 9 eV higher than the main peaks of Cu $2p_{3/2}$ and Cu $2p_{1/2}$ [105]. However, Cu metal and $Cu_2O$ have an overlapping binding energy range, where Cu $2p_{3/2}$ peak appears [134]. So, Cu and $Cu_2O$ cannot be distinguished by only analyzing Cu $2p_{3/2}$ spectra. Cu LMM Auger electron spectra can also be used as a powerful way to distinguish between Cu metal and $Cu_2O$.

Figure 4.21 (a) and (b) provide the XPS results of bare networks after 13 days and 1 year exposure to ambient atmosphere, respectively. Upon their oxidation, the peaks of Cu $2p_{3/2}$ and Cu $2p_{1/2}$ appeared at 932.8 and 952.7 eV with weak satellites. This spectra was attributed to $Cu_2O$ due to the presence of this weak satellite peaks. After completion of 1 year test period, bare samples' XPS spectra showed that 2p peaks at 933.1 and 952.9 eV with strong satellite peaks at 943.6 and 962.0 eV. These spectra agreed with the presence of CuO due to appeared strong satellite peaks. Therefore, it can be concluded that Cu (0) metal first oxidizes to $Cu_2O$ and then oxidation of $Cu_2O$ to CuO takes place through long term NW oxidation in ambient conditions. This result is in agreement with the previous reports [135]. Since the Gibbs free energy of $Cu_2O$ is lower than CuO, thermodynamically, formation of $Cu_2O$ is primary.

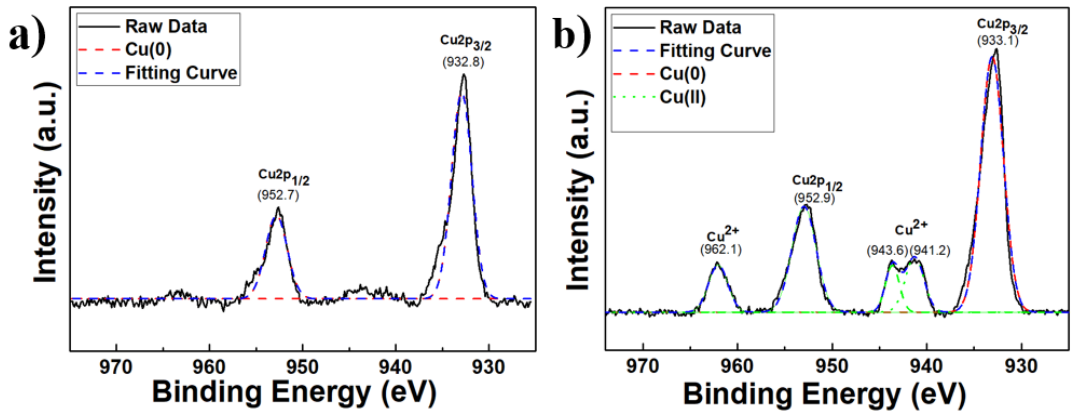


**Figure 4. 21** XPS spectra of bare Cu NW networks after (a) 13 days and (b) a year exposure to ambient atmosphere.

Moreover, XPS analysis of BTA passivated samples also showed weak satellite peaks together with Cu $2p_{3/2}$ and Cu $2p_{1/2}$ peaks at 932.7 and 952.6 eV (Figure 4.22 (a)) at the end of a year exposure to ambient atmosphere. These spectra were attributed to surface oxides of $Cu_2O$ and CuO. These oxides of Cu do not have metallic conductivity and since, there were no significant loss in electrical conductivity for BTA passivated networks after a year. Depth profiling was performed to reveal the subsurface composition. Etching surface layers resulted in the satellite intensity being significantly reduced and completely extinguished with 4 minutes of etching (Figure 4.22 (b)-(c)). After 4 minutes of etching, Cu $2p_{3/2}$ and Cu $2p_{1/2}$ peaks appeared at 932.5 and 952.3 eV (Figure 4.22 (c)).

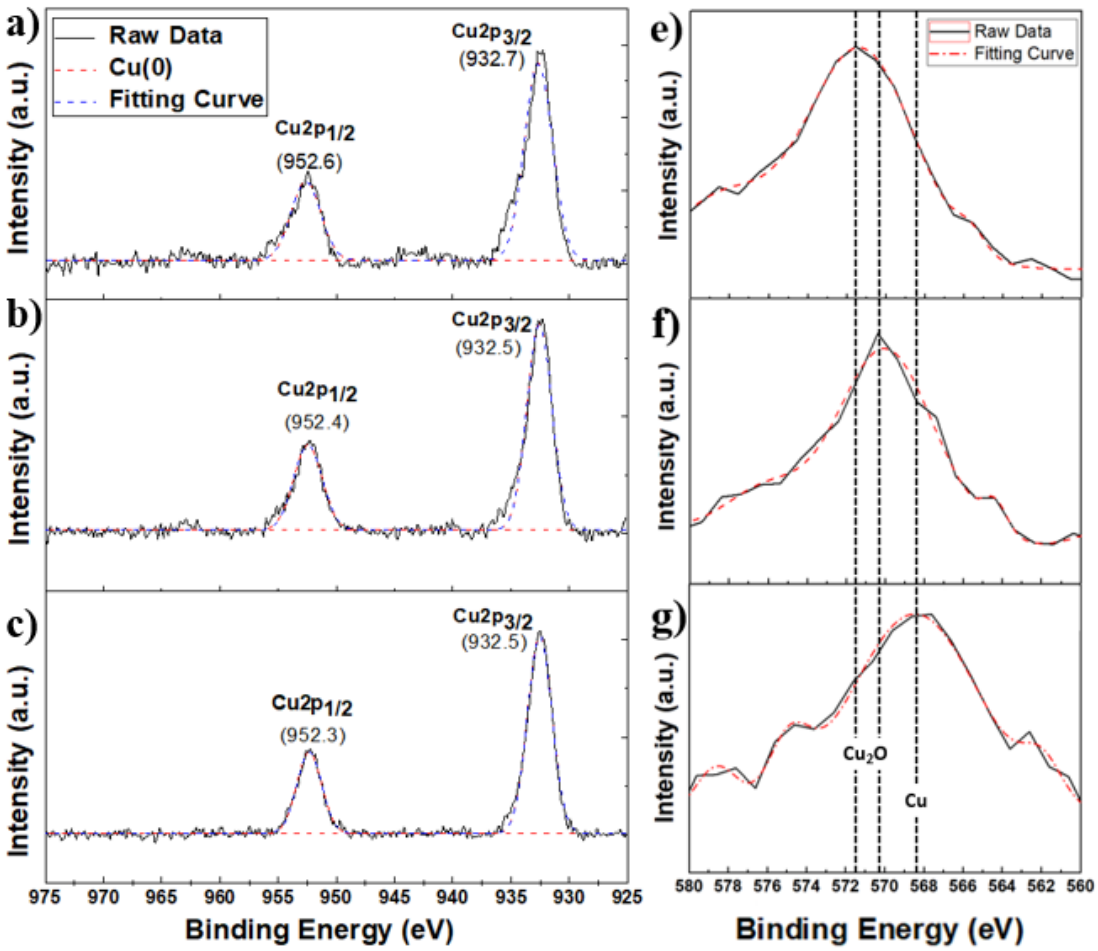


**Figure 4. 22** Changes in Cu 2p spectrum that is (a) un-etched, (b) etched for 1 minute and (c) etched for 4 minutes. Changes in spectrum of Cu LMM Auger that is (e) un-etched, (f) etched for 1 minute and (g) etched for 4 minutes.

To distinguish Cu and $Cu_2O$, Cu LMM Auger spectra were also analyzed. Figure 4.22 (d) to (f) shows the Cu LMM spectra of BTA passivated networks with etching times of 1 and 4 minutes. The peaks for un-etched and 1 minute etched conditions appeared at 571.2 and 570.0 eVs, which are the characteristic LMM of $Cu_2O$. The spectra collected after 4 minutes of etching shifted towards lower binding energies and showed Cu(0) metal peak appearing at 568 eV. Therefore, the presence of thin layers of surface oxides together with the core Cu (0) metal was revealed. This thin

surface oxide layer may be formed during either network fabrication steps or passivation steps.

### 4.4.2 Oxidation Stability of Networks at High Relative Humidity Conditions

One of the main factors leading to corrosion is high RH of the environment. The corrosion rate of metals increase under humid environments [136]. Therefore, to accelerate the corrosion rate and thus to determine the corrosion inhibition efficiency of BTA for Cu NW random networks, degradation of electrodes under different high humidity environments (75% and 90% RH) was investigated for 10 days through sheet resistance measurements, XPS, SEM and TEM analysis. Networks to be aged at two different humidity conditions were prepared with similar NW densities to eliminate the effect of NW density on the degradation of electrodes. Obtained results are tabulated and provided in Table 4.2 as sheet resistance, transmittance and density of networks.

**Table 4. 2** Optoelectronic properties of Cu NW networks before tested under 75% and 90% RH environments.

| | **Sheet Resistance (Ω/sq)** | **%Transmittance (@550nm)** | **amd ($mg/m^2$)** |
|---|---|---|---|
| **Bare Cu NW @ 75%RH** | 9 | 72 | 162 |
| **BTA/Cu NW @75% RH** | 12 | 71 | 150 |
| **Bare Cu NW @90% RH** | 15 | 76 | 148 |
| **BTA/Cu NW @90% RH** | 11 | 72 | 155 |

Figure 4.23 (a) and (b) shows the variation in sheet resistance of the electrodes under 75% and 90 % RH.

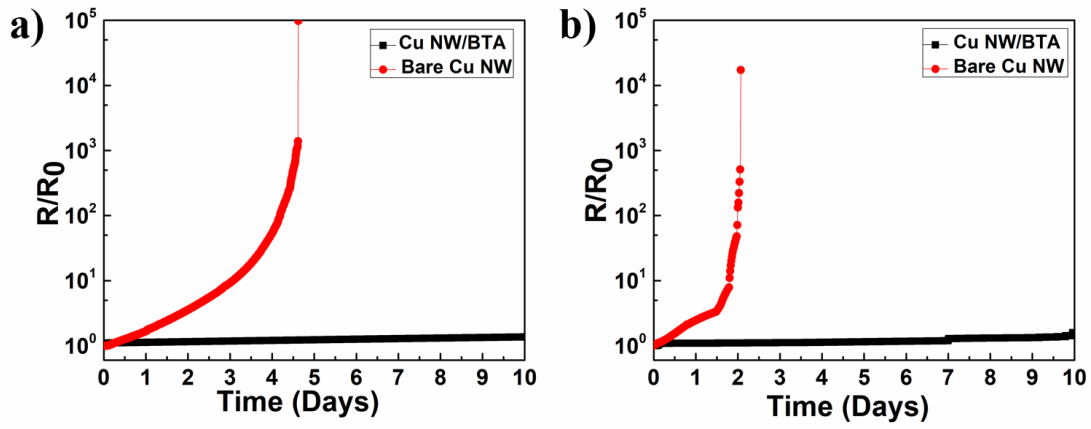


**Figure 4. 23** Change in sheet resistances of bare and BTA passivated Cu NW random networks at (a) 75% and (b) 90% RH for 10 days.

Increase in humidity severely affected the stability of bare Cu NW random networks. In Section 4.6.1, it was demonstrated that bare Cu NW random networks get totally oxidized in 12 days under laboratory conditions within 25±5% RH. However, it took only approximately 5 days for the complete oxidation of bare Cu NW networks at 75% RH. The oxidation rate was much higher at 90% RH for bare Cu NW networks so that they became non-conducting only at the end of 2 days. In sharp comparison, the resistance change for BTA passivated networks were negligible. Only after 7$^{th}$ day, the sheet resistance of BTA passivated networks that are kept under 90% RH were started to increase with a very slow pace. The normalized resistance was increased from 1.2 to 1.7 within the last 3 days of the experiment which ran for 10 days.

Moreover, it was mentioned that the degradation of metallic NW random networks strongly depend on the NW density. To see the effect of NW density, ageing tests at 75% RH was performed for 3 samples with 3 different NW densities. Figure 4.24 shows the change in sheet resistance for these electrodes over time.

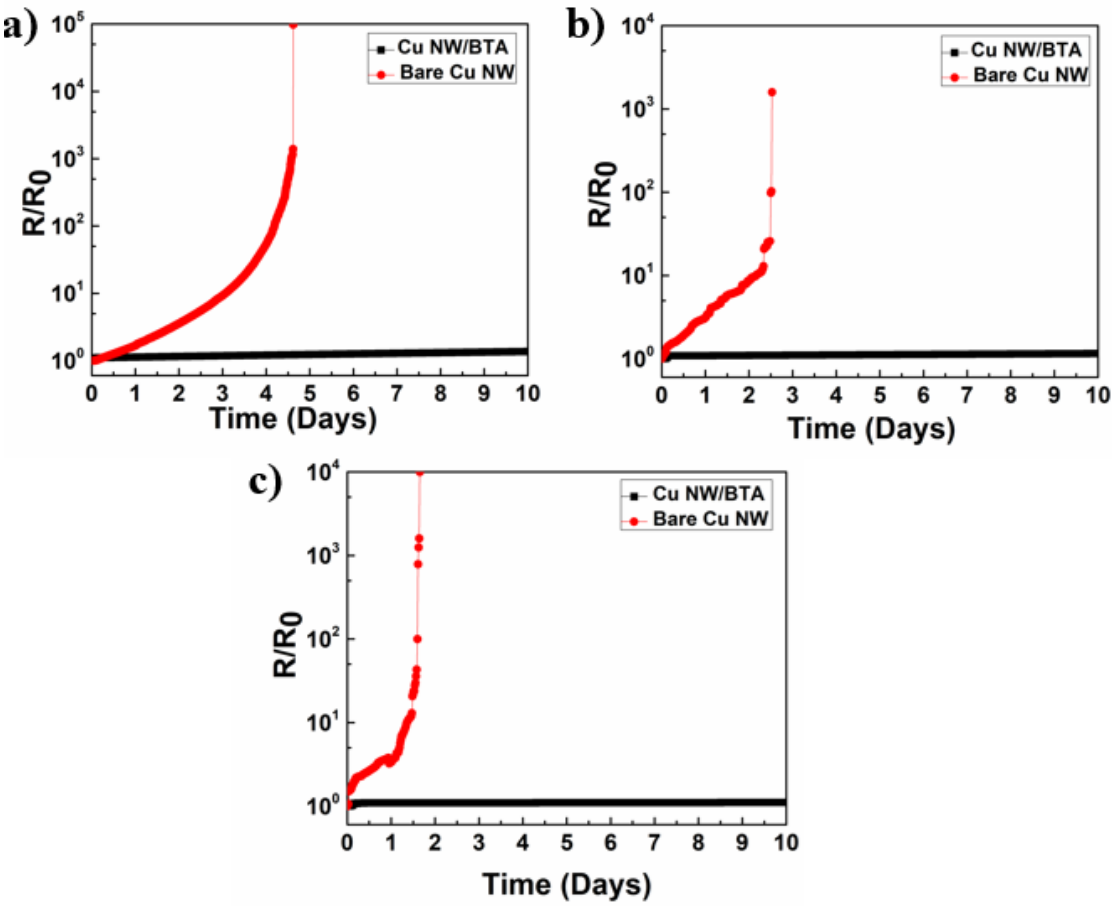


**Figure 4. 24** Change in sheet resistance of bare and BTA treated Cu NW networks with different NW densities of (a) 16, (b) 38 and (c) 156 mg/m$^2$ under 75% RH.

As shown in Figure 4.24, the sheet resistance of dense networks reached to megaohms in 5 days (Figure 4.24 (c)), while less dense and bare networks' resistances reached to the order of mega ohms in less than 3 days (Figure 4.24 (a) and (b)). Bare Cu NW network with a NW density of 38 mg/m$^2$ became non-conducting in approximately 2 days and bare Cu NW network with a NW density of 16 mg/m$^2$ became non-conducting in approximately one and a half day. Slower increase in resistance of dense networks was possibly due to the presence of higher number of alternative pathways for charge transport. This is because one when one path gets destroyed, charge transport is conveyed to the other available pathways. Rapid degradation of less dense electrodes can be explained in same way. Sheet

resistance of BTA passivated Cu NWs, in strong contrast, remained almost unchanged throughout this study for all NW densities investigated.

Table 4.3 summarizes the optoelectronic properties of Cu NW networks with different NW densities before tested under 75% RH environment.

**Table 4. 3** Optoelectronic properties of Cu NW networks with different NW densities before tested under 75% RH environment.

| | **Sheet Resistance (Ω/sq)** | **%Transmittance (@550nm)** | **amd ($mg/m^2$)** |
|---|---|---|---|
| **Bare Cu NW (a)** | 5000 | 85 | 14 |
| **BTA/Cu NW (a)** | 4900 | 83 | 18 |
| **Bare Cu NW (b)** | 103 | 82 | 35 |
| **BTA/Cu NW (b)** | 91 | 80 | 41 |
| **Bare Cu NW (c)** | 9 | 72 | 162 |
| **BTA/Cu NW (c)** | 12 | 71 | 150 |

To see the morphological changes in NWs after ageing under high humidity conditions, SEM and TEM analysis were performed and respective SEM images are provided in Figures 4.25 (a)-(d).

In SEM and TEM images, nanoparticle formation was observed on the surface of Cu NWs exposed to high humidity conditions. Since as the polycrystalline oxide layer forms throughout the surface of NWs, formed grain boundaries and other types of defects acts as a nucleation site for particle formation [135]. Therefore, further oxidation gives rise to the formation of CuO particles at these sites. As particles grow throughout surface, the diameter of NWs starts to increase and deviate from each other.

To characterize the chemical composition of NWs after exposure to high humidity conditions, XPS analysis was performed. Appearing characteristic strong satellite

peaks as well as Cu $2p_{3/2}$ and Cu $2p_{1/2}$ peaks at 933.3 and 953.1 eV revealed that the Cu NWs were oxidized to CuO (see Figure 4.26).

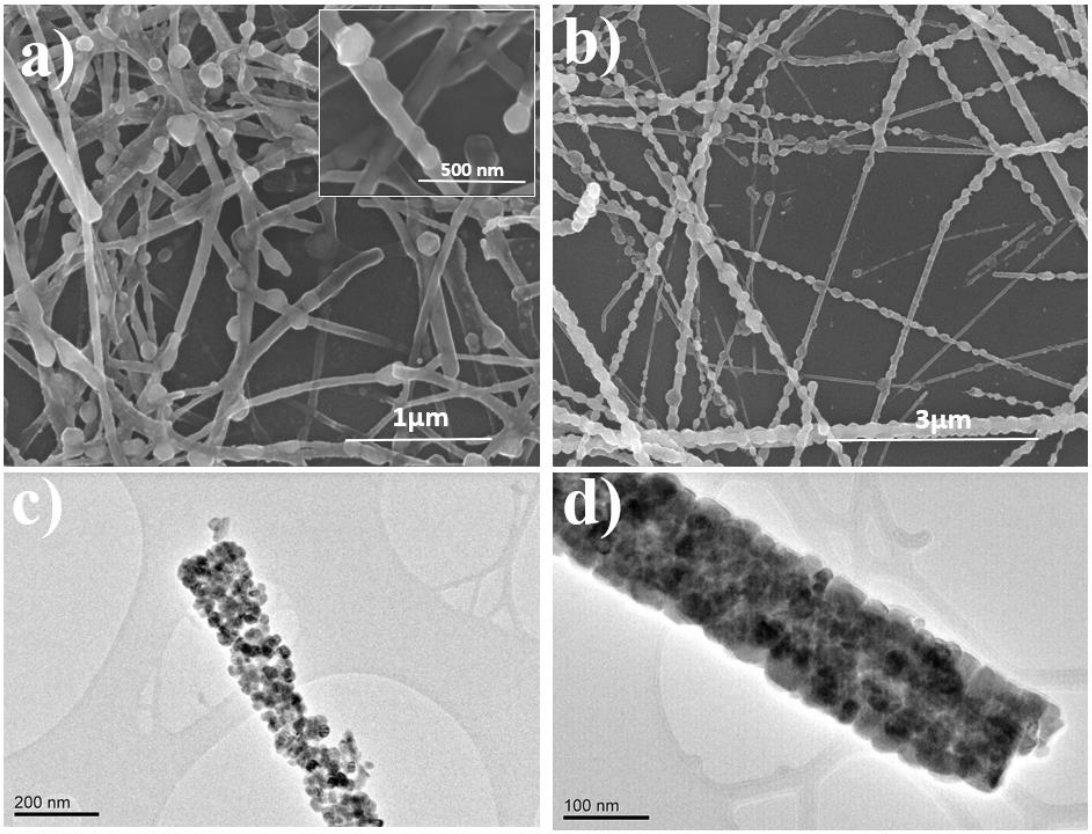


**Figure 4. 25** SEM images of bare Cu NW network aged under (a) 90± 5% and (b) 75± 5% RH. TEM images of bare Cu NWs aged under (a) 75± 5% and (b) 90± 5% RH

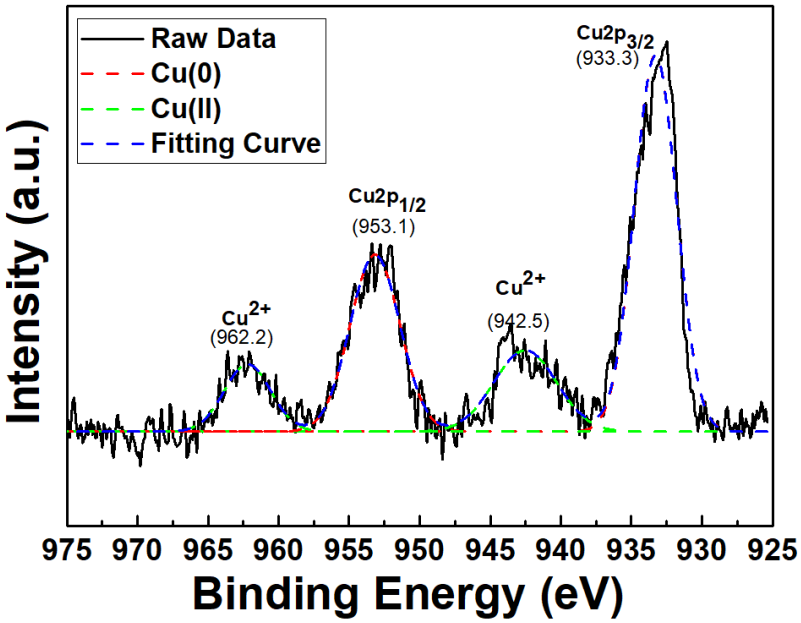


**Figure 4. 26** Cu 2p XPS spectra of bare Cu NW networks upon exposure to high humidity.

### 4.4.3 Oxidation Stability of Networks at Elevated Temperatures

Since typical optoelectronic device fabrication processes involve high temperature annealing steps, Cu NW networks should be thermally stable and robust. For this reason, thermal oxidation stability of Cu NWs are also of great interest. In order to compare the thermal stability of bare and BTA passivated Cu NW random networks, thermal ageing tests at temperatures of 75, 125 and 150°C under ambient conditions were performed. The average initial sheet resistance of networks was 19±3.8 Ω/sq. Areal mass density of networks was in the range of 120 to 150 mg/m$^2$. For all thermal ageing tests, oven was firstly set to the specified temperature then samples were placed inside the oven for the measurements. Figures 4.27 (a)-(c) show the change in resistance for both bare and BTA passivated Cu NW random networks over time at temperatures 75, 125 and 150°C, respectively. At 75°C, BTA passivated networks exhibited superior thermal stability with respect to the bare networks as shown in Figure 4.27 (a).

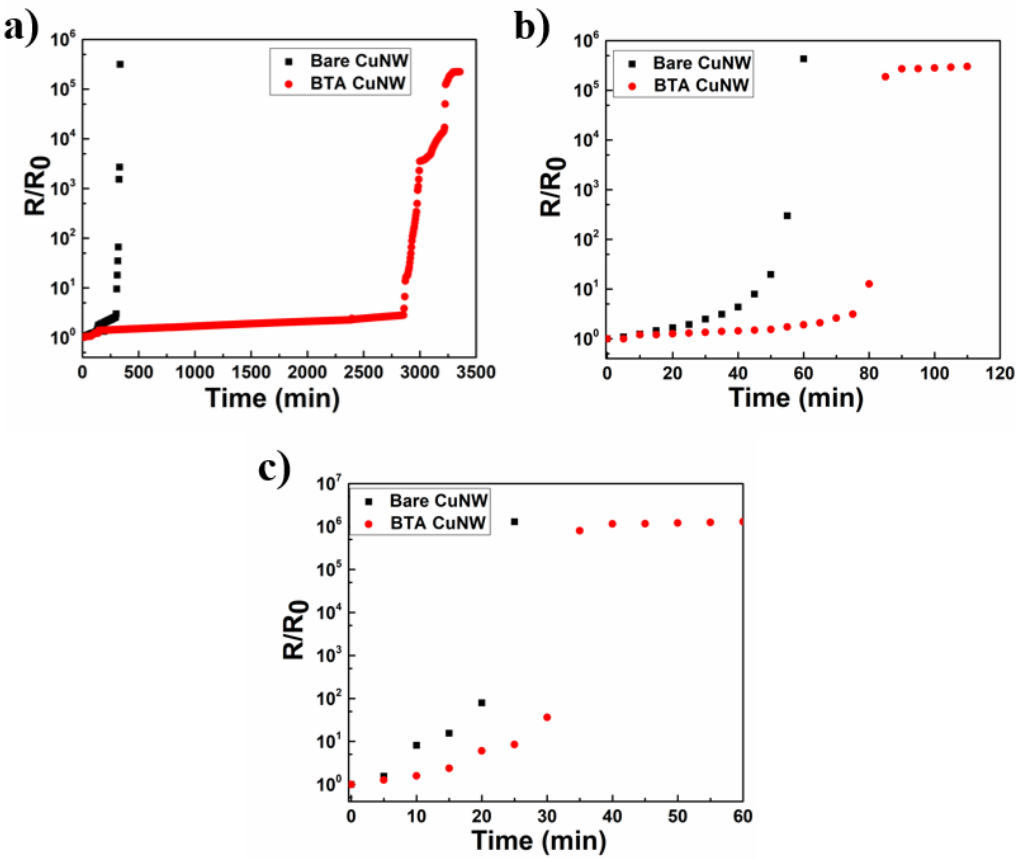


**Figure 4. 27** Change in sheet resistance of Cu NW and BTA passivated Cu NW electrodes over time at different temperatures of (a) 75, (b) 125 and (c) 150°C.

Although it took approximately 250 minutes for bare Cu NW network to be totally non-conducting at 75°C, immediate failure of bare Cu NW networks occurred only within 50 and 20 minutes, when they were exposed to ambient atmosphere at 125°C and 150°C, respectively. On the other hand, BTA passivated Cu NW networks also could not maintain their conductivity at these temperatures (125°C and 150°C). Failure of BTA's corrosion inhibition at 125 and 150°C can be explained through the thermal stability of benzotriazole on bulk Cu during atmospheric corrosion reported by Christensen and Sorensen [98]. It was demonstrated that BTA is thermally stable on the surface of bulk copper up to 150°C and BTA immediately get lost from the surface at higher temperatures due to evaporation of the polymeric complex film. In addition, it was also reported that the loss of BTA from the surface of Cu at elevated

temperatures (100°C) is rapid during the first few hours then gradual at longer times (see Figure 4.3 (a)). And in our results, resistance of BTA passivated Cu NW networks increased quickly for shorter times and the rate of change of resistance decreased as time passes. Especially before the degradation of electrodes, resistance nearly remained constant in the order of mega ohm. Therefore, regarding the results of Christensen and Sorensen, very slow rate of change of sheet resistance was attributed to gradual loss of BTA at longer times. To verify the BTA loss at elevated temperatures, ATR-IR analysis were performed after heating the samples at the specified temperatures for 5 minutes. ATR-IR spectra of the samples are provided in Figure 4.28.

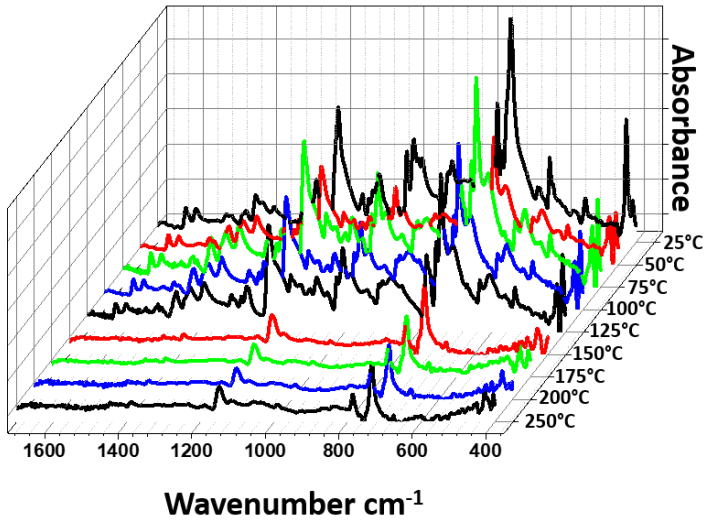


**Figure 4. 28** ATR-IR spectra of BTA passivated Cu NW networks at different temperatures.

It is apparent that most of the vibrational features either totally disappeared or attenuated their intensities significantly when samples were heated at 150°C. BTA remained intact for samples heated at temperatures between 25 to 125°C, which confirms that the BTA is only thermally stable up to 125°C. Moreover, it can also be observed that the degradation time of bare Cu NW electrodes decrease with increasing temperature. Time to total loss in conductivity was approximately 250, 60

and 25 minutes at temperatures of 75, 125 and 150°C, respectively. This is because, at elevated temperatures oxidation kinetics become faster.

Morphological analysis was performed via SEM and TEM to compare the changes that occur at high temperatures compared to those reported in Section 4.3.2.

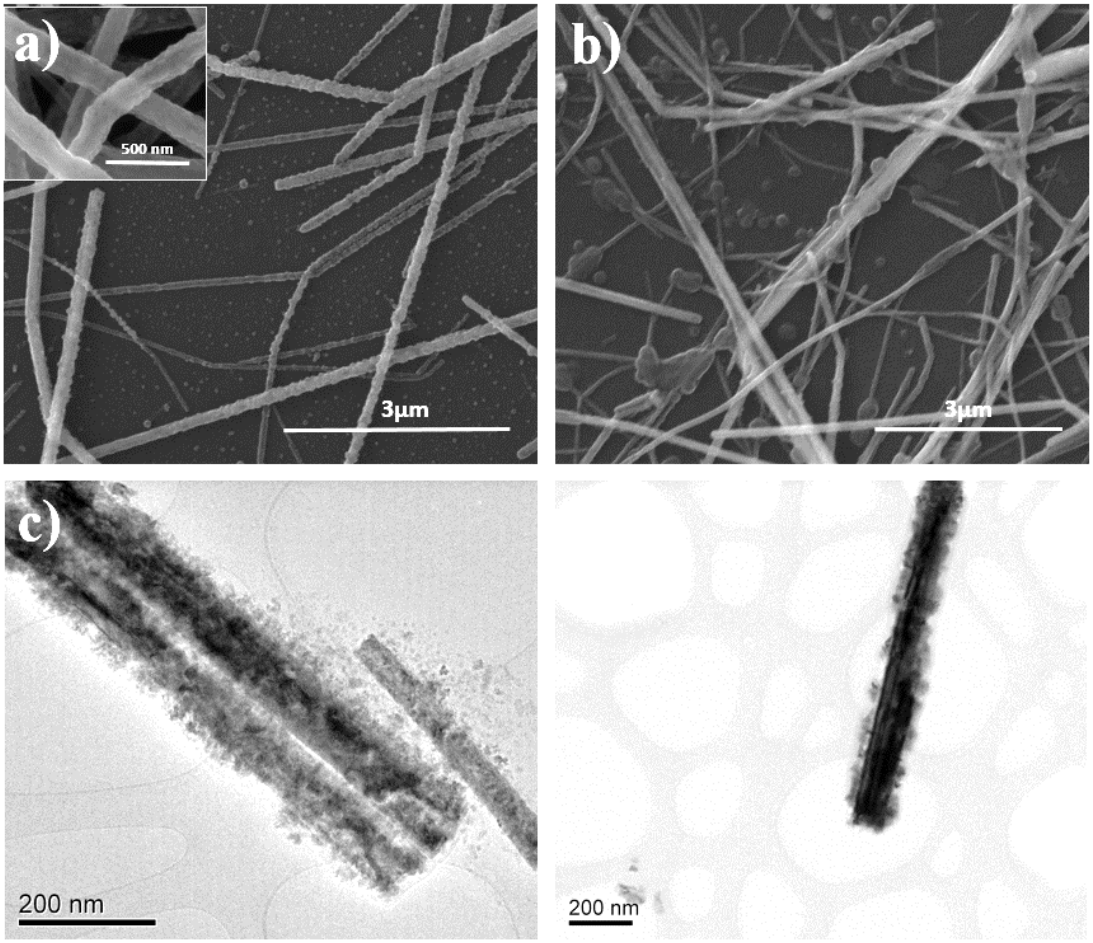


**Figure 4. 29** SEM images of (a) bare and (b) BTA passivated Cu NW networks annealed at 125°C. (c) and (d) TEM images of bare Cu NW networks annealed at 125°C.

After oxidation at 125°C, bare Cu NWs surface was found to be significantly rough (see Figure 4.29 (a)). An SEM image of BTA passivated Cu NW network after complete oxidation at 125°C is provided in Figure 4.29 (b). Although no significant

change in morphology of the BTA treated Cu NWs was observed, some polymeric melts on the substrate surface and on some NWs with large diameters were observed.

TEM images provided in Figure 4.29 (c) and (d) showed that oxide particles formed at the lateral surfaces of NWs were not stable since most of them were found to spill over the TEM grid. This result is in agreement with Bando's work mentioned in section 4.2.1 [102].

### 4.4.4 Oxidation Stability of Networks under Constant 2 Volt Bias

Since Cu NW networks are designed to be used in optoelectronic devices, their long term stability under continuous biasing is an important parameter. Significant amount of research in literature demonstrated that NWs corrode or oxidize over a limited time period when kept under atmospheric conditions. However, limited number of studies investigated the stability of NW random networks during their use as a transparent electrode in devices (when they are carrying current). For example, Goldthrope *et al.* showed that Ag NW networks lose their electrical conductivity within hours or days when they are exposed to a certain voltage pointing out that Joule heating might be the reason for failure [137]. A similar study published by Simonato *et al.* showed that the sheet resistance of networks increases due to Joule heating when they are biased [106]. To simulate the operating conditions of optoelectronic devices, bare and BTA passivated Cu NW networks were subjected to a constant 2 V bias, which is an ideal operating voltage of many optoelectronic devices. Figure 4.30 (a) shows the change in sheet resistance with respect to time for both bare and BTA passivated Cu NW networks.

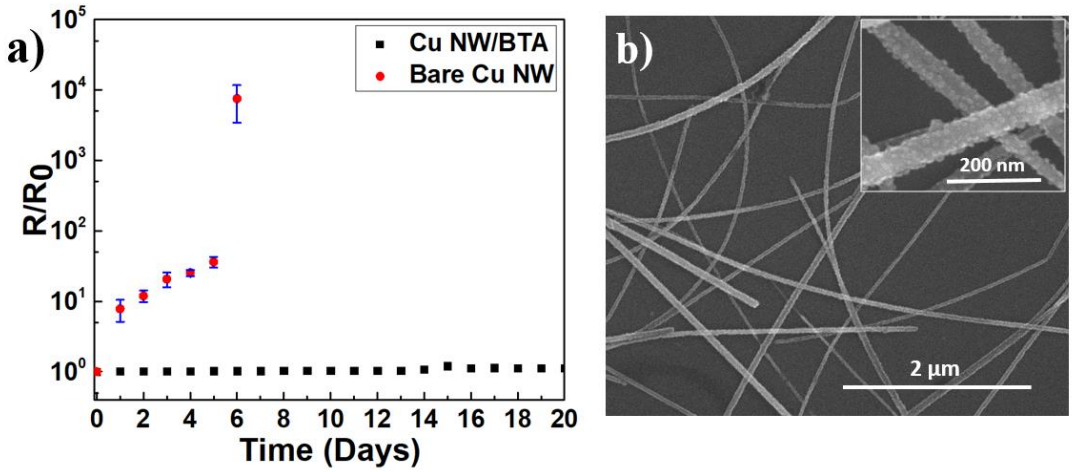


**Figure 4. 30** (a) Change in sheet resistance with respect to time for bare and BTA passivated Cu NW networks. (b) SEM image of a non-conducting Cu NW network at the end of 2 V biasing for 8 days.

The average initial sheet resistance of bare and BTA passivated Cu NW networks were 14±2 Ω/sq and 16 ± 1 Ω/sq, respectively. Three set of samples were used for each type of network. Upon the application of 2 V bias, both samples' temperature was rised to approximately 50°C ($T_{CuNW}$ ~ 52°C, $T_{CuNW/BTA}$ ~ 47°C) as a result of Joule heating. Cu NWs are instable even at room temperature under ambient conditions. Previous studies have also demonstrated that the rate of oxidation increases at elevated temperatures [103][137][118][102]. Therefore, this initial increase in temperature increased the resistance of NWs by approximately 900% due to fast oxidation kinetics. Increase in the resistance resulted in a decrease in temperature; but, resistance continued to increase in a slower pace due to atmospheric corrosion of Cu NWs. And bare Cu NW networks became non-conducting at the end of 7 days (see Figure 4.30 (a)). After the test, morphology of the bare Cu NW networks was analyzed with SEM. SEM image of a bare Cu NW network at the end of biasing test is provided in Figure 4.30 (b). An increase in the surface roughness and the presence of numerous nanoparticles at the lateral surfaces of NWs were observed. This morphological change was due to oxidation of Cu NWs. To verify the oxidation, XPS analysis was performed and $Cu_2O$ oxide was detected.

On the other hand, resistance of BTA passivated Cu NW networks remained constant with a constant temperature of ~50°C also (see Figure 4.30 (a)).

### 4.4.5 Chemical Corrosion Stability of Networks under PEDOT: PSS Layer

Chemical corrosion stability against acidic environment is one of the other crucial requirements for TCEs to be integrated into optoelectronic devices. Because, either as a hole injection or hole transport layer, electrodes are generally in contact with acidic PEDOT: PSS layer in device structure. So far, many studies have demonstrated that the interface layer is susceptible to the corrosion by PEDOT: PSS and thus performance of the devices deteriorate [106][118]. Therefore, long term stability of Cu NW networks coated with PEDOT: PSS layer is an important parameter that predominantly determines the lifetime of the optoelectronic devices that utilize Cu NWs.

In this study, bare and BTA passivated Cu NW networks were spin coated with PEDOT: PSS (pH ~3) layer at 1500 rpm for 30 s. This corresponds to thickness of around 50 nm. After spin coating, all the samples were directly placed into a glovebox filled with argon. Then, the stability of both BTA passivated and bare samples coated with PEDOT: PSS layer were investigated by monitoring the change in their sheet resistance for 4 months. Since PEDOT:PSS is sensitive to ambient atmosphere and its electrical properties degrade in time due to absorption of oxygen/water, all samples were kept under controlled glovebox atmosphere throughout the test period to assure that the change in resistance is not related with PEDOT: PSS degradation. Samples were exposed to air only when measurement was conducted for about 5 minutes each time. Figure 4.31 shows the change in resistance with respect to time for both bare and BTA passivated Cu NW electrodes that were spin coated with PEDOT: PSS.

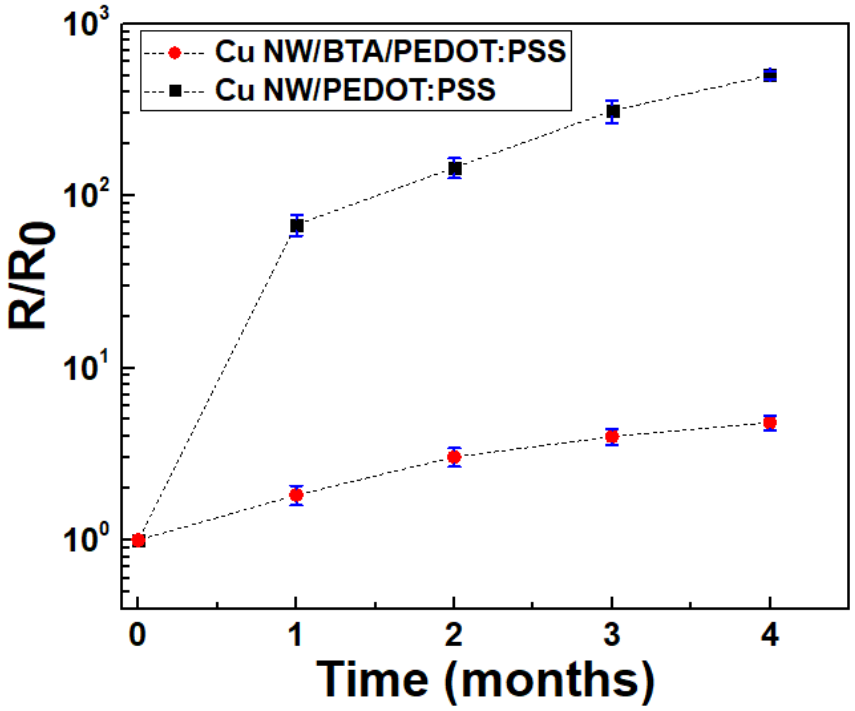


**Figure 4. 31** Change in sheet resistance of PEDOT: PSS coated bare and BTA passivated Cu NW networks with time. Lines are for the visual aid.

To obtain these results, 4 samples of bare Cu NW/PEDOT: PSS and 4 samples of Cu NW/BTA/PEDOT: PSS were used. The initial average resistance for Cu NW/PEDOT: PSS samples were 27 ± 4 Ω/sq, which was measured after the deposition of PEDOT: PSS. The initial average resistance for Cu NW/BTA/PEDOT: PSS samples were 25±2, Ω/sq, which was again measured after PEDOT: PSS deposition. At the end of 4 months, the resistance of Cu NW/PEDOT: PSS samples increased by approximately 500 times, while the resistance of Cu NW/BTA/PEDOT: PSS samples increased by only 5 times. It should also be noted that the maximum resistance of Cu NW/BTA/PEDOT: PSS samples at the end of 4 months was below 300 Ω/sq, which is still sufficient for many applications. Moreover, morphological analysis was conducted by SEM analysis. Figure 4.32 (a) and (b) show the SEM images of bare and BTA passivated Cu NW networks that were spin coated with PEDOT: PSS layer, respectively.

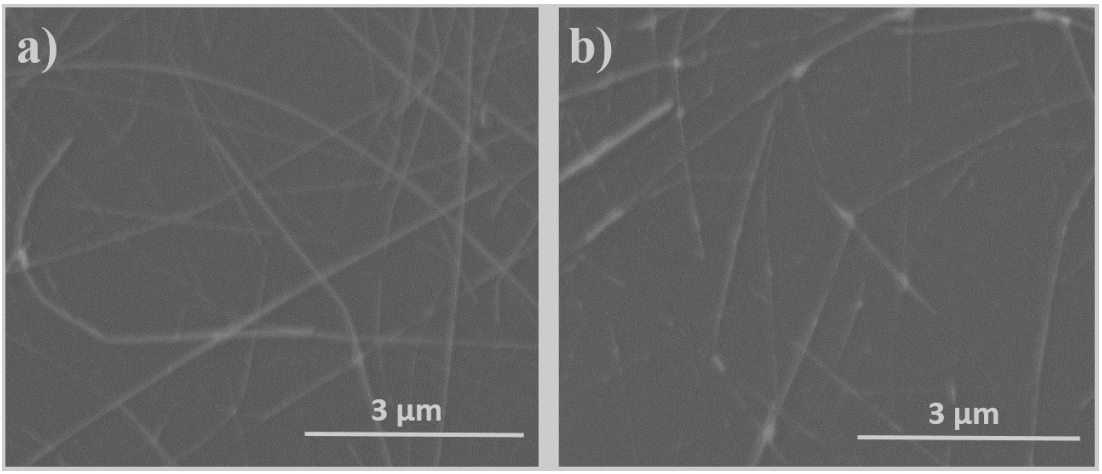


**Figure 4. 32** SEM images of PEDOT: PSS deposited (a) BTA passivated and (b) bare Cu NW networks after 4 months.

Cu NW/PEDOT: PSS sample's SEM image showed that the structural integrity of the network was lost with severe etching of the NWs. Due to acidic nature of PEDOT:PSS (pH ~ 3) bare Cu NWs were dissolved and ruptured within this polymeric media and the overall electrical percolation of network was destroyed. This finding confirms the sheet resistance measurements. On the other hand, Cu NW/BTA/PEDOT: PSS samples showed remarkable resistance against chemical corrosion when compared to the poor performance of Cu NW/PEDOT: PSS samples. No morphology change was observed for the Cu NW/BTA/PEDOT: PSS samples. So, BTA passivated samples showed better resistance against corrosion, confirming that BTA layer also significantly slows down the acidic corrosion rate of Cu NWs. This result is in agreement with the previously reported studies in which it was shown that BTA treatment decrease acidic corrosion rate of bulk Cu [138].

# CHAPTER 5

## CONCLUSIONS AND FUTURE RECOMMENDATION

### 5.1. Conclusions

This thesis is focused on the most challenging issue related with Cu NWs, which is the improvement of their oxidation stability. Considerable number of studies have been proposed to improve the stability of Cu NWs under various aggressive environments [4][107][119][125][128][139]. However, this work offered a novel method for the protection of Cu NWs against corrosion and to the best of our knowledge, this is the first study enhancing the corrosion stability of Cu NWs using a typical, effective bulk Cu corrosion inhibitor, BTA.

In the first part of this thesis, Cu NWs were reproducibly synthesized via a facile and environmentally benign hydrothermal method. Obtained Cu NWs were efficiently purified and dispersed in an alcoholic solution to further use them in subsequent network fabrication steps. Then characterizations to reveal uniformity, morphology, dimensions, purity and crystallinity were performed. Pure and crystalline Cu NWs synthesized in this work had an average diameter of 45.4 ± 17.4 nm and length of 49.3 ± 19.9 μm.

Then, transparent and conducting Cu NW networks were fabricated via simple, cost-effective and scalable spray deposition process. To improve optoelectronic performance, the effect of network density on transmittance and sheet resistance of the networks was studied in detail. It was shown that an increase in the network density (amount of NWs per unit area) linearly decreases the transmittance. On the other hand, a power law relation between network density and sheet resistance was observed. Moreover, the effect of annealing temperature and time were investigated.

Optimum temperature and time for annealing was determined as 200°C and 20 minutes to improve the performance of Cu NW networks

In the final part, a novel, simple, solution based and highly effective method to improve the resistance of Cu NW networks against oxidation was demonstrated. In this method, bulk Cu corrosion inhibitor benzotriazole (BTA) was used for the passivation of Cu NW networks. The stability of BTA passivated samples under various environments were studied by monitoring the change in their sheet resistance values. BTA passivation was found to provide an outstanding stability under ambient conditions as well as high humidity conditions. Sheet resistance of BTA passivated Cu NW networks remained nearly constant ($R/R_0 < 1.1$) upon exposure to atmosphere while bare Cu NW networks became non-conducting in 12 days. BTA also maintained its corrosion inhibition efficiency under 75 and 90% RH conditions. Initial sheet resistances of BTA passivated networks were maintained up to 10 days under 75% RH condition, while it is maintained for 7 days under 90% RH. Only very slight increase in sheet resistance after 7 days were observed for networks stored under 90% RH environment so that normalized sheet resistance was only 1.7 at the end of 10 days. In sharp contrast, high humidity conditions severely affected bare Cu NW networks, it took only 2 days and a day to lose their conductivity completely under 75 and 90% RH environments, respectively. Moreover, thermal stability of BTA passivated networks at temperatures of 75, 125 and 150°C were investigated. ATR-IR was used to monitor the thermal stability of BTA for the protection of Cu NW networks and BTA was found to be thermally stable up to 125 °C. Lastly, chemical corrosion stability of both bare and passivated networks were investigated by depositing acidic PEDOT: PSS conductive polymer on top of these networks. BTA also improved the resistance against acidic corrosion, so that sheet resistance of passivated networks increased only by a factor of 5, while the sheet resistance of bare networks increased by a factor of 500.

## 5.2. Future Recommendations

A perfect passivation layer proposed to protect random networks of metallic nanowires should satisfy some critical features as; *(i)* highly efficient corrosion protection, *(ii)* no detrimental effect on optoelectronic performance of the network (particularly sheet resistance and transmittance), *(iii)* easy and scalable application over electrodes with large areas. In terms of these features, BTA exhibited outstanding performance to improve the stability of Cu NWs without deteriorating the optoelectronic performance of Cu NW networks. In addition, it is demonstrated that BTA deposition onto Cu NWs is a simple, cheap and solution based method. Therefore, it will be very important to demonstrate the integration of BTA passivated Cu NW networks as a transparent electrode into various optoelectronic devices such as organic photovoltaics and organic light emitting diodes. Moreover, BTA passivated electrodes' roughness can be compared with bare electrodes since the roughness issue is of great interest for the utilization of metal NW networks as TCEs in optoelectronic devices. Although, optoelectronic performance of Cu NW networks did not get significantly altered with BTA deposition, more effective rinsing procedures should be developed to get rid of excess BTA from the electrodes and thus 2% decrease in transmittance can also be recovered.

Another future study may involve direct solution based synthesis of Cu NWs with BTA to make them corrosion resistant in one step. This will eliminate the need for additional procedures as reported here for passivation.

Lastly, dispersion of Cu NW networks using polymers with azole groups or deposition of azole group containing semiconducting polymers onto already deposited Cu NW networks instead of BTA will be also very valuable to investigate. This will facilitate the integration of Cu NW networks into optoelectronic devices.

## REFERENCES


[1] S. Ye, A. R. Rathmell, Z. Chen, I. E. Stewart, and B. J. Wiley, "Metal nanowire networks: The next generation of transparent conductors," *Adv. Mater.*, vol. 26, no. 39, pp. 6670–6687, 2014.

[2] S. Bhanushali, P. Ghosh, A. Ganesh, and W. Cheng, "1D Copper Nanostructures: Progress, Challenges and Opportunities," *Small*, vol. 11, no. 11, pp. 1232–1252, 2015.

[3] Y. Won, A. Kim, D. Lee, W. Yang, "Annealing-free fabrication of highly oxidation-resistive copper nanowire composite conductors for photovoltaics," *NPG Asia Mater.*, vol. 6, no. 6, pp. e105-9, 2014.

[4] J. Chen, W. Zhou, Y. Fan, Z. Zhang, "Solution-processed copper nanowire flexible transparent electrodes with PEDOT:PSS as binder, protector and oxide-layer scavenger for polymer solar cells," *Nano Res.*, vol. 8, no. 3, pp. 1017–1025, 2015.

[5] H. G. Im, S. Jung, J. Hin, D. Lee, "Flexible transparent conducting hybrid film using a surface-embedded copper nanowire network: A highly oxidation-resistant copper nanowire electrode for flexible optoelectronics," *ACS Nano*, vol. 8, no. 10, pp. 10973–10979, 2014.

[6] J. Jiu and K. Suganuma, "Metallic nanowires and their application," *IEEE Trans. Components, Packag. Manuf. Technol.*, vol. 6, no. 12, pp. 1733–1751, 2016.

[7] H. Shang, G. Cao "Template-based synthesis of nanorod or nanowire arrays," pp. 169–186.

[8] S. N. Mohammad, "Analysis of the Vapor – Liquid – Solid Mechanism for Nanowire Growth and a Model for this Mechanism," *Nano Lett.*, vol. 8, no. 5, pp. 1532–1538, 2008.

[9] S. N. Mohammad, “Self-catalysis: A contamination-free, substrate-free growth mechanism for single-crystal nanowire and nanotube growth by chemical vapor deposition,” *J. Chem. Phys.*, vol. 125, no. 9, 2006.

[10] S. Vaddiraju, H. Chandrasekaran, and M. K. Sunkara, “Vapor phase synthesis of tungsten nanowires,” *J. Am. Chem. Soc.*, vol. 125, no. 36, pp. 10792–10793, 2003.

[11] P. Mohanty, I. Yoon, T. Kang, K. Seo, “Simple vapor-phase synthesis of single-crystalline Ag nanowires and single-nanowire surface-enhanced raman scattering,” *J. Am. Chem. Soc.*, vol. 129, no. 31, pp. 9576–9577, 2007.

[12] G. Glaspell, V. Abdelsayed, K. M. Saoud, and M. S. El-Shall, “Vapor-phase synthesis of metallic and intermetallic nanoparticles and nanowires: Magnetic and catalytic properties,” *Pure Appl. Chem.*, vol. 78, no. 9, pp. 1667–1689, 2006.

[13] Y. Xia, P. Yang, Y. Sun, Y. Wu, B. Mayers “One-Dimensional Nanostructures: Synthesis, Characterization, and Applications,” *Adv. Mater.*, vol. 15, no. 5, pp. 353–389, 2003.

[14] R. S. Wagner and W. C. Ellis, “Vapor-liquid-solid mechanism of single crystal growth,” *Appl. Phys. Lett.*, vol. 4, no. 5, pp. 89–90, 1964.

[15] H. Choi, *Semiconductor Nanostructures for Optoelectronic Devices*. 2012.

[16] H. Choi and S. H. Park, “Seedless growth of free-standing copper nanowires by chemical vapor deposition,” *J. Am. Chem. Soc.*, vol. 126, no. 20, pp. 6248–6249, 2004.

[17] C. Kim, W. Gu, M. Briceno, I. M. Robertson, H. Choi, and K. Kim, “Copper nanowires with a five-twinned structure grown by chemical vapor deposition,” *Adv. Mater.*, vol. 20, no. 10, pp. 1859–1863, 2008.

[18] H. T. Tung, J. M. Song, T. Y. Dong, W. S. Hwang, and I. G. Chen, “Synthesis

of surfactant-free aligned single crystal copper nanowires by thermal-assisted photoreduction," *Cryst. Growth Des.*, vol. 8, no. 9, pp. 3415–3419, 2008.

[19] D. Haase, S. Hampel, A. Leonhardt, J. Thomas, N. Mattern, and B. Büchner, "Facile one-step-synthesis of carbon wrapped copper nanowires by thermal decomposition of Copper(II)-acetylacetonate," *Surf. Coatings Technol.*, vol. 201, no. 22–23 SPEC. ISS., pp. 9184–9188, 2007.

[20] Z. Liu and Y. Bando, "A novel method for preparing copper nanorods and nanowires," *Adv. Mater.*, vol. 15, no. 4, pp. 303–305, 2003.

[21] R. Tsukamoto, M. Muraoka, M. Seki, H. Tabata, and I. Yamashita, "Synthesis of CoPt and FePt3 nanowires using the central channel of tobacco mosaic virus as a biotemplate," *Chem. Mater.*, vol. 19, no. 10, pp. 2389–2391, 2007.

[22] G. A. Gelves, Z. T. M. Murakami, M. J. Krantz, and J. A. Haber, "Multigram synthesis of copper nanowires using ac electrodeposition into porous aluminium oxide templates," *J. Mater. Chem.*, vol. 16, no. 30, pp. 3075–3083, 2006.

[23] J. Richter, M. Mertig, W. Pompe, I. Mönch, and H. K. Schackert, "Construction of highly conductive nanowires on a DNA template," *Appl. Phys. Lett.*, vol. 78, no. 4, pp. 536–538, 2001.

[24] H. Cao, L. Wang, Y. Qiu, and L. Zhang, "Synthesis and I-V properties of aligned copper nanowires," *Nanotechnology*, vol. 17, no. 6, pp. 1736–1739, 2006.

[25] M. E. Toimil Molares, J. Brötz, V. Buschmann, "Etched heavy ion tracks in polycarbonate as template for copper nanowires," *Nucl. Instruments Methods Phys. Res. Sect. B Beam Interact. with Mater. Atoms*, vol. 185, no. 1–4, pp. 192–197, 2001.

[26] S. Shin, B. S. Kim, K. M. Kim, B. H. Kong, H. K. Cho, and H. H. Cho, "Tuning the morphology of copper nanowires by controlling the growth

processes in electrodeposition," *J. Mater. Chem.*, vol. 21, no. 44, pp. 17967–17971, 2011.

[27] I. Enculescu, Z. Siwy, D. Dobrev, C. Trautmann, M. E. Toimil Molares, "Copper nanowires electrodeposited in etched single-ion track templates," *Appl. Phys. A Mater. Sci. Process.*, vol. 77, no. 6, pp. 751–755, 2003.

[28] T. Gao, G. Meng, Y. Wang, S. Sun, and L. Zhang, "Electrochemical synthesis of copper nanowires," *J. Phys. Condens. Matter*, vol. 14, no. 3, pp. 355–363, 2001.

[29] Y. Chang, M. L. Lye, and H. C. Zeng, "Large-scale synthesis of high-quality ultralong copper nanowires," *Langmuir*, vol. 21, no. 9, pp. 3746–3748, 2005.

[30] A. R. Rathmell, S. M. Bergin, Y. L. Hua, Z. Y. Li, and B. J. Wiley, "The growth mechanism of copper nanowires and their properties in flexible, transparent conducting films," *Adv. Mater.*, vol. 22, no. 32, pp. 3558–3563, 2010.

[31] S. Ye, A. R. Rathmell, I. E. Stewart, Y. Ha, C. Wilson, "A rapid synthesis of high aspect ratio copper nanowires for high-performance transparent conducting films," *Chem. Commun.*, vol. 50, no. 20, pp. 2562–2564, 2014.

[32] Y. Shi, H. Li, L. Chen, and X. Huang, "Obtaining ultra-long copper nanowires via a hydrothermal process," *Sci. Technol. Adv. Mater.*, vol. 6, no. 7, pp. 761–765, 2005.

[33] M. Mohl, M. Pusztai, P. Kukovecz, "Low-temperature large-scale synthesis and electrical testing of ultralong copper nanowires," *Langmuir*, vol. 26, no. 21, pp. 16496–16502, 2010.

[34] M. Jin, G. He, H. Zhang, J. Zeng, Z. Xie, and Y. Xia, "Shape-controlled synthesis of copper nanocrystals in an aqueous solution with glucose as a reducing agent and hexadecylamine as a capping agent," *Angew. Chemie - Int. Ed.*, vol. 50, no. 45, pp. 10560–10564, 2011.

[35] U. S. Shenoy and A. N. Shetty, “Simple glucose reduction route for one-step synthesis of copper nanofluids,” *Appl. Nanosci.*, vol. 4, no. 1, pp. 47–54, 2014.

[36] B. Wiley, T. Herricks, Y. Sun, and Y. Xia, “Polyol synthesis of silver nanoparticles: Use of chloride and oxygen to promote the formation of single-crystal, truncated cubes and tetrahedrons,” *Nano Lett.*, vol. 4, no. 9, pp. 1733–1739, 2004.

[37] F. Qian, P. C. Lan, T. Olson, C. Zhu, E. B. Duoss, “Multiphase separation of copper nanowires,” *Chem. Commun.*, vol. 52, no. 78, pp. 11627–11630, 2016.

[38] T. Sannicolo, M. Lagrange, A. Cabos, C. Celle, J. P. Simonato, and D. Bellet, “Metallic Nanowire-Based Transparent Electrodes for Next Generation Flexible Devices: a Review,” *Small*, vol. 12, no. 44, pp. 6052–6075, 2016.

[39] A. Kumar and C. Zhou, “The Race To Replace Tin-Doped Indium,” *ACS Nano*, vol. 4, no. 1, pp. 11–14, 2010.

[40] R. G. Gordon, “C riteria for Choosing Transparent Conductors,” *History*, no. August, pp. 52–57, 2000.

[41] A. R. Schlatmann, D. W. Floet, A. Hilberer, “Indium contamination from the indium-tin-oxide electrode in polymer light-emitting diodes,” *Appl. Phys. Lett.*, vol. 69, no. 12, pp. 1764–1766, 1996.

[42] A. I. Hofmann, E. Cloutet, and G. Hadziioannou, “Materials for Transparent Electrodes: From Metal Oxides to Organic Alternatives,” *Adv. Electron. Mater.*, 2018.

[43] G. Fanchini, H. E. Unalan, and M. Chhowalla, “Optoelectronic properties of transparent and conducting single-wall carbon nanotube thin films,” *Appl. Phys. Lett.*, vol. 88, no. 19, pp. 19–21, 2006.

[44] R. Yuksel, Z. Sarioba, A. Cirpan, P. Hiralal, and H. E. Unalan, “Transparent and Flexible Supercapacitors with Single Walled Carbon Nanotube Thin Film

Electrodes," *ACS Appl. Mater. Interfaces*, vol. 6, no. 17, pp. 15434–15439, 2014.

[45] A. Du Pasquier, H. E. Unalan, A. Kanwal, S. Miller, and M. Chhowalla, "Conducting and transparent single-wall carbon nanotube electrodes for polymer-fullerene solar cells," *Appl. Phys. Lett.*, vol. 87, no. 20, pp. 1–3, 2005.

[46] D. S. Hecht, A. M. Heintz, R. Lee, L. Hu, "High conductivity transparent carbon nanotube films deposited from superacid," vol. 075201, 2011.

[47] Y. Zhou and R. Azumi, "Carbon nanotube based transparent conductive films: progress, challenges, and perspectives," *Sci. Technol. Adv. Mater.*, vol. 17, no. 1, pp. 493–516, 2016.

[48] F. Zhang, M. Johansson, M. R. Andersson, J. C. Hummelen, and O. Inganäs, "Polymer Photovoltaic Cells With Conducting Polymer Anodes," *Adv. Funct. Mater.*, vol. 14, no. 9, pp. 662–664, 2002.

[49] Y. Xia and J. Ouyang, "Significant conductivity enhancement of conductive poly(3,4- ethylenedioxythiophene): Poly(styrenesulfonate) films through a treatment with organic carboxylic acids and inorganic acids," *ACS Appl. Mater. Interfaces*, vol. 2, no. 2, pp. 474–483, 2010.

[50] Y. Wen and J. Xu, "Scientific Importance of Water-Processable PEDOT–PSS and Preparation, Challenge and New Application in Sensors of Its Film Electrode: A Review," *J. Polym. Sci. Part A Polym. Chem.*, vol. 55, no. 7, pp. 1121–1150, 2017.

[51] B. L. Groenendaal, F. Jonas, D. Freitag, H. Pielartzik, and J. R. Reynolds, "Its Derivatives : Past , Present , and Future **," no. January 2000, pp. 481–494, 2018.

[52] K. S. Novoselov, A. K. Geim, S. V. Morozov, D. Jiang, Y. Zhang, "Electric Field Effect in Atomically Thin Carbon Films," *Science (80-. ).*, vol. 306, no.

5696, pp. 666–669, 2004.

[53] Y. Wang, Y.. Zheng, X. Xu, E. Dubuisson, Q. Bao, J. Lu, "Electrochemical delamination of CVD-grown graphene film: Toward the recyclable use of copper catalyst," *ACS Nano*, vol. 5, no. 12, pp. 9927–9933, 2011.

[54] S. Bae, H. Kim, Y. Lee, X. Xu, J. S. Park, Y. Zheng, "Roll-to-roll production of 30-inch graphene films for transparent electrodes," *Nat. Nanotechnol.*, vol. 5, no. 8, pp. 574–578, 2010.

[55] D. Zhang, K. Ryu, X. Liu, E. Polikarpov, J. Ly, "Transparent, conductive, and flexible carbon nanotube films and their application in organic light-emitting diodes," *Nano Lett.*, vol. 6, no. 9, pp. 1880–1886, 2006.

[56] J. Zou, H. L. Yip, S. K. Hau, and A. K. Y. Jen, "Metal grid/conducting polymer hybrid transparent electrode for inverted polymer solar cells," *Appl. Phys. Lett.*, vol. 96, no. 20, pp. 2008–2011, 2010.

[57] Y. Jang, J. Kim, and D. Byun, "Invisible metal-grid transparent electrode prepared by electrohydrodynamic (EHD) jet printing," *J. Phys. D. Appl. Phys.*, vol. 46, no. 15, 2013.

[58] J. Van De Groep, P. Spinelli, and A. Polman, "Transparent conducting silver nanowire networks," *Nano Lett.*, vol. 12, no. 6, pp. 3138–3144, 2012.

[59] Q. Tang, L. Fang, Y. Wang, M. Zou, and W. Guo, "Anisotropic flexible transparent films from remaining wood microstructures for screen protection and AgNW conductive substrate," *Nanoscale*, vol. 10, no. 9, pp. 4344–4353, 2018.

[60] O. Ergun, S. Coskun, Y. Yusufoglu, and H. E. Unalan, "High-performance, bare silver nanowire network transparent heaters," *Nanotechnology*, vol. 27, no. 44, 2016.

[61] S. Coskun, E. Selen Ates, and H. Emrah Unalan, "Optimization of silver

nanowire networks for polymer light emitting diode electrodes," *Nanotechnology*, vol. 24, no. 12, 2013.

[62] L. Gonzalez-Garcia, J. H. M. Maurer, B. Reiser, I. Kanelidis, and T. Kraus, "Ultrathin Gold Nanowires for Transparent Electronics: Breaking Barriers," *Procedia Eng.*, vol. 141, pp. 152–156, 2016.

[63] S. Gong, Y. Zhao, Q. Shi, Y. Wang, L. W. Yap, and W. Cheng, "Self-assembled Ultrathin Gold Nanowires as Highly Transparent, Conductive and Stretchable Supercapacitor," *Electroanalysis*, vol. 28, no. 6, pp. 1298–1304, 2016.

[64] D. Zhang, R. Wang, M. Wen, D. Weng, X. Cui, "Synthesis of ultralong copper nanowires for high-performance transparent electrodes," *J. Am. Chem. Soc.*, vol. 134, no. 35, pp. 14283–14286, 2012.

[65] H. Guo, N. Lin, Y. Chen, Z Wang, Q. Xie, T. Zheng, "Copper nanowires as fully transparent conductive electrodes," *Sci. Rep.*, vol. 3, 2013.

[66] T.-H. Duong and H.-C. Kim, "An extremely simple and rapid fabrication of flexible transparent electrodes using ultralong copper nanowires," *Ind. Eng. Chem. Res.*, p. acs.iecr.7b04709, 2018.

[67] A. R. Rathmell and B. J. Wiley, "The synthesis and coating of long, thin copper nanowires to make flexible, transparent conducting films on plastic substrates," *Adv. Mater.*, vol. 23, no. 41, pp. 4798–4803, 2011.

[68] Q. Huang, C. M. Lilley, M. Bode, and R. Divan, "Surface and size effects on the electrical properties of Cu nanowires," *J. Appl. Phys.*, vol. 104, no. 2, 2008.

[69] Y. Zhao, Y. Zhang, Y. Li, Z. He, and Z. Yan, "Rapid and large-scale synthesis of Cu nanowires via a continuous flow solvothermal process and its application in dye-sensitized solar cells (DSSCs)," *RSC Adv.*, vol. 2, no. 30, pp. 11544–11551, 2012.

[70] Z. Chen, A. R. Rathmell, S. Ye, A. R. Wilson, and B. J. Wiley, "Optically transparent water oxidation catalysts based on copper nanowires," *Angew. Chemie - Int. Ed.*, vol. 52, no. 51, pp. 13708–13711, 2013.

[71] Y. Tang, S. Gong, Y. Chen, L. W. Yap, and W. Cheng, "Manufacturable conducting rubber ambers and stretchable conductors from copper nanowire aerogel monoliths," *ACS Nano*, vol. 8, no. 6, pp. 5707–5714, 2014.

[72] H. C. Chu, Y. C. Chang, Y. Lin, S. H. Chang, W. C. Chang, "Spray-Deposited Large-Area Copper Nanowire Transparent Conductive Electrodes and Their Uses for Touch Screen Applications," *ACS Appl. Mater. Interfaces*, vol. 8, no. 20, pp. 13009–13017, 2016.

[73] C. Bao, J. Yang, H. Gao, F. Li, Y. Yao, H. Yang, "In Situ fabrication of highly conductive metal nanowire networks with high transmittance from deep-ultraviolet to near-infrared," *ACS Nano*, vol. 9, no. 3, pp. 2502–2509, 2015.

[74] J. Song, J. Li, J. Xu, and H. Zeng, "Superstable transparent conductive Cu@Cu4Ni nanowire elastomer composites against oxidation, bending, stretching, and twisting for flexible and stretchable optoelectronics," *Nano Lett.*, vol. 14, no. 11, pp. 6298–6305, 2014.

[75] I. E. Stewart, A. R. Rathmell, L. Yan, S. Ye, P. F. Flowers,"Solution-processed copper-nickel nanowire anodes for organic solar cells," *Nanoscale*, vol. 6, no. 11, pp. 5980–5988, 2014.

[76] S. Coskun, H. E. Unalan "Synthesis of Silver Nanowires Through Polyol Process," 2012.

[77] S.-T. Oh, T. Sekino, and K. Niihara, "Fabrication and mechanical properties of 5 vol% copper dispersed alumina nanocomposite," *J. Eur. Ceram. Soc.*, vol. 18, no. 1, pp. 31–37, 1998.

[78] S. P. A. Gill, "Controlling the Rayleigh instability of nanowires," *Appl. Phys. Lett.*, vol. 102, no. 14, pp. 0–4, 2013.

[79] G. R. Patel, N. A. Thakar, and T. C. Pandya, “Size and shape dependent melting temperature and thermal expansivity of metallic and semiconductor nanoparticles,” *AIP Conf. Proc.*, vol. 1731, pp. 1–4, 2016.

[80] M. Hasegawa, M. Watabe, and K. Hoshino, “A theory of melting in metallic small particles,” *J. Phys. F Met. Phys.*, vol. 10, no. 4, pp. 619–635, 1980.

[81] J. Wang, X. Chen, G. Wang, B. Wang, W. Lu, and J. Zhao, “Melting behavior in ultrathin metallic nanowires,” *Phys. Rev. B - Condens. Matter Mater. Phys.*, vol. 66, no. 8, pp. 1–5, 2002.

[82] J. Chang and E. Johnson, “Surface and bulk melting of small metal clusters,” *Philos. Mag.*, vol. 85, no. 30, pp. 3617–3627, 2005.

[83] Z. Liu, X. Sui, K. Kang, and S. Qin, “Logarithmic size-dependent melting temperature of nanoparticles,” *J. Phys. Chem. C*, vol. 119, no. 21, pp. 11929–11933, 2015.

[84] M. Lagrange, D. P. Langley, G. Giusti, C. Jiménez, Y. Bréchet, and D. Bellet, “Optimization of silver nanowire-based transparent electrodes: Effects of density, size and thermal annealing,” *Nanoscale*, vol. 7, no. 41, pp. 17410–17423, 2015.

[85] S. Leroy, *Aluminum Alloys: New Trends in Fabrication and Applications*. 2016.

[86] F. Clarelli, B. De Filippo, and R. Natalini, “Mathematical model of copper corrosion,” *Appl. Math. Model.*, vol. 38, no. 19–20, pp. 4804–4816, 2014.

[87] A. Fateh, M. Aliofkhazraei, and A. R. Rezvanian, “Review of corrosive environments for copper and its corrosion inhibitors,” *Arab. J. Chem.*, 2017.

[88] V. Brusic, “Copper Corrosion With and Without Inhibitors,” *J. Electrochem. Soc.*, vol. 138, no. 8, p. 2253, 1991.

[89] F. Zucchi, G. Trabanelli, and M. Fonsati, “Tetrazole derivatives as corrosion

inhibitors for copper in chloride solutions," *Corros. Sci.*, vol. 38, no. 11, pp. 2019–2029, 1996.

[90] R. B. Faltermeier, "A Corrosion Inhibitor Test for Copper-Based Artifacts," *Stud. Conserv.*, vol. 44, no. 2, pp. 121–128, 1998.

[91] N. R. T. Bharucha and Baker, "Working With Copper: Benzotriazole: An effective corrosion inhibitor for copper alloys 2 Working With Copper: Benzotriazole: An effective corrosion inhibitor for copper alloys 3," *Copp. Dev. Assoc. Int. Copp. Res. Assoc.*, vol. 104409, no. 5, pp. 696–697, 1964.

[92] N. K. Allam, A. A. Nazeer, and E. A. Ashour, "A review of the effects of benzotriazole on the corrosion of copper and copper alloys in clean and polluted environments," *J. Appl. Electrochem.*, vol. 39, no. 7, pp. 961–969, 2009.

[93] S. Ramesh and S. Rajeswari, "Evaluation of inhibitors and biocide on the corrosion control of copper in neutral aqueous environment," *Corros. Sci.*, vol. 47, no. 1, pp. 151–169, 2005.

[94] J. B. Cotton and I. R. Scholes, "Benzotriazole and Related ' Compounds As," *Brit. Corros. J.*, vol. 2, pp. 1–5, 1967.

[95] G. Xue and J. Ding, "Chemisorption of a compact polymeric coating on copper surfaces from a benzotriazole solution," *Appl. Surf. Sci.*, vol. 40, no. 4, pp. 327–332, 1990.

[96] D. Chadwick and T. Hashemi, "Adsorbed corrosion inhibitors studied by electron spectroscopy: Benzotriazole on copper and copper alloys," *Corros. Sci.*, vol. 18, no. 1, pp. 39–51, 1978.

[97] L. À, H., Quõâmica, I. De, Saäo, U. De, Av, P., Lineu, P., "Use of a rotating cylinder electrode in corrosion studies of a 90 / 10 Cu ± Ni alloy in," *J. Appl. Electrochem.*, pp. 981–985, 2000.

[98] T. M. Christensen and N. R. Sorensen, “Thermal stability of benzotriazole on copper during atmospheric corrosion,” *Surf. Interface Anal.*, vol. 17, no. 1, pp. 3–6, 1991.

[99] O. F. Copper, “Queensland University of Technology School of Physical Sciences the Inhibition of Copper Corrosion in Aqueous Environments With,” no. February, 2004.

[100] C. Guozhong, *Nanostructures and Nanomaterials: synthesis, properteid and applications*. World Scientific, 2004.

[101] L. Cadamartiriti, G. A. Ozin, J. Lehn, “Concepts of Nanochemistry,” pp. 3409–3410, 2010.

[102] Z. Liu and Y. Bando, “Oxidation behaviour of copper nanorods,” *Chem. Phys. Lett.*, vol. 378, no. 1–2, pp. 85–88, 2003.

[103] X. Liu and Y. Zhou, “Electrochemical synthesis and room temperature oxidation behavior of Cu nanowires,” *J. Mater. Res.*, vol. 20, no. 9, pp. 2371–2378, 2005.

[104] X. Luo, U. Sundararaj, and J. L. Luo, “Oxidation kinetics of copper nanowires synthesized by AC electrodeposition of copper into porous aluminum oxide templates,” *J. Mater. Res.*, vol. 27, no. 13, pp. 1755–1762, 2012.

[105] L. Xu, Y. Yang, Z. W. Hu, and S. H. Yu, “Comparison Study on the Stability of Copper Nanowires and Their Oxidation Kinetics in Gas and Liquid,” *ACS Nano*, vol. 10, no. 3, pp. 3823–3834, 2016.

[106] C. Mayousse, C. Celle, A. Fraczkiewicz, and J. P. Simonato, “Stability of silver nanowire based electrodes under environmental and electrical stresses,” *Nanoscale*, vol. 7, no. 5, pp. 2107–2115, 2015.

[107] I. E. Stewart, S. Ye, Z. Chen, P. F. Flowers, and B. J. Wiley, “Synthesis of Cu-Ag, Cu-Au, and Cu-Pt Core-Shell Nanowires and Their Use in Transparent

Conducting Films," *Chem. Mater.*, vol. 27, no. 22, pp. 7788–7794, 2015.

[108] Y. Wei, S. Chen, Y. Lin, Z. Yang, and L. Liu, "Cu-Ag core-shell nanowires for electronic skin with a petal molded microstructure," *J. Mater. Chem. C*, vol. 3, no. 37, pp. 9594–9602, 2015.

[109] S. M. Alia, K. Jensen, C. Contreras, F. Garzon, B. Pivovar, and Y. Yan, "Platinum coated copper nanowires and platinum nanotubes as oxygen reduction electrocatalysts," *ACS Catal.*, vol. 3, no. 3, pp. 358–362, 2013.

[110] Z. Niu, F. Cui, Y. Yu, N. Becknell, Y. Sun, P. Yang, "Ultrathin Epitaxial Cu@Au Core-Shell Nanowires for Stable Transparent Conductors," *J. Am. Chem. Soc.*, vol. 139, no. 21, pp. 7348–7354, 2017.

[111] B. D. Anderson, J. B. Tracy, B. D. Anderson, and J. B. Tracy, "Nanoparticle conversion chemistry: Kirkendall effect, galvanic exchange, and anion exchange," vol. 6, no. 21, 2014.

[112] T. Uchikoshi, Y. Sakka, M. Yoshitake, and K. Yoshihara, "A study of the passivating oxide layer on fine nickel particles," *Nanostructured Mater.*, vol. 4, no. 2, pp. 199–206, 1994.

[113] L. A. Meier, A. E. Alvarez, S. G. García, and M. C. del Barrio, "Formation of Cu and Ni Nanowires by Electrodeposition," *Procedia Mater. Sci.*, vol. 8, pp. 617–622, 2015.

[114] A. R. Rathmell, M. Nguyen, M. Chi, and B. J. Wiley, "Synthesis of oxidation-resistant cupronickel nanowires for transparent conducting nanowire networks," *Nano Lett.*, vol. 12, no. 6, pp. 3193–3199, 2012.

[115] S. Ye, I. E. Stewart, Z. Chen, B. Li, A. R. Rathmell, and B. J. Wiley, "How Copper Nanowires Grow and How To Control Their Properties," *Acc. Chem. Res.*, vol. 49, no. 3, pp. 442–451, Mar. 2016.

[116] Y. Sun, B. Mayers, and Y. Xia, "Metal Nanostructures with Hollow Interiors,"

*Adv. Mater.*, vol. 15, no. 78, pp. 641–646, 2003.

[117] F. K. Shan and Y. S. Yu, "Band gap energy of pure and Al-doped ZnO thin films," vol. 24, pp. 1869–1872, 2004.

[118] P. C. Hsu, H. Wu, T. J. Carney, M. T. Mcdowell, "Passivation coating on electrospun copper nanofibers for stable transparent electrodes," *ACS Nano*, vol. 6, no. 6, pp. 5150–5156, 2012.

[119] Z. Chen, S. Ye, I. E. Stewart, B. J. Wiley, and C. E. T. Al, "Copper Nanowire Networks with Transparent Oxide Shells That Prevent Oxidation without Reducing Transmittance," no. 9, pp. 9673–9679, 2014.

[120] T. Ackermann, S. Sahakalkan, Y. Zhang, A. Mettenborger, S. Mathur, "Improved performance of transparent silver nanowire electrodes by adding carbon nanotubes," *9th IEEE Int. Conf. Nano/Micro Eng. Mol. Syst. IEEE-NEMS 2014*, pp. 81–85, 2014.

[121] C. S. Lee, J. E. Yoo, K. Shin, C. O. Park, and J. Bae, "Carbon nanotube-silver nanowire composite networks on flexible substrates: High reliability and application for supercapacitor electrodes," *Phys. Status Solidi Appl. Mater. Sci.*, vol. 211, no. 12, pp. 2890–2897, 2014.

[122] C. Nanowires, K. Yan, Q. Xue, D. Xia, "The Core / Shell Composite Nanowires," vol. 3, no. 8, pp. 2235–2240, 2009.

[123] B. Deng, A. W. Xu, G. Y. Chen, R. Q. Song, and L. Chen, "Synthesis of copper-core/carbon-sheath nanocables by a surfactant-assisted hydrothermal reduction/carbonization process," *J. Phys. Chem. B*, vol. 110, no. 24, pp. 11711–11716, 2006.

[124] L. Shi, R. Wang, H. Zhai, Y. Liu, L. Gao, and J. Sun, "A long-term oxidation barrier for copper nanowires : graphene says yes," pp. 4231–4236, 2015.

[125] A. Aliprandi, T. Moreira, C. Anichini, M Stoeckel, "Hybrid Copper-Nanowire

– Reduced-Graphene-Oxide Coatings : A ‘ Green Solution ’ Toward Highly Transparent , Highly Conductive , and Flexible Electrodes for ( Opto ) Electronics,” vol. 1703225, pp. 1–6, 2017.

[126] F. Alotaibi, T. T. Tung, J. Nine, C. J. Coghlan, and D. Losic, “Silver Nanowires with Pristine Graphene Oxidation Barriers for Stable and High Performance Transparent Conductive Films,” *ACS Appl. Nano Mater.*, vol. 1, pp. 2249–2260, 2018.

[127] K. Naito, R. Inuzuka, N. Yoshinaga, and W. Mei, “Transparent conducting fi lms composed of graphene oxide / Ag nanowire / graphene oxide / PET,” *Synth. Met.*, vol. 237, no. December 2017, pp. 50–55, 2018.

[128] S. C. Reduced- and G. C. S. Nanowire, “Solution-Processed Copper/Reduced-Graphene-Oxide Core/Shell Nanowire Transparent Conductors,” 2016.

[129] F. Zhou, Z. Li, G. J. Shenoy, L. Li, and H. Liu, “Enhanced room-temperature corrosion of copper in the presence of graphene,” *ACS Nano*, vol. 7, no. 8, pp. 6939–6947, 2013.

[130] S. Zhao, F. Han, J. Li, X. Meng, W. Huang, “Advancements in Copper Nanowires: Synthesis, Purification, Assemblies, Surface Modification, and Applications,” *Small*, vol. 1800047, pp. 1–30, 2018.

[131] Y. Ahn, D. Lee, Y. Jeong, H. Lee, and Y. Lee, “Flexible metal nanowire-parylene C transparent electrodes for next generation optoelectronic devices,” *J. Mater. Chem. C*, vol. 5, no. 9, pp. 2425–2431, 2017.

[132] J. F. Young, “Humidity control in the laboratory using salt solutions-a review,” *J. Appl. Chem.*, vol. 17, no. 9, pp. 241–245, 2007.

[133] A. Wexler and S. Hasegawa, “Relative humidity-temperature relationships of some saturated salt solutions in the temperature range 0 degree to 50 degrees C,” *J. Res. Natl. Bur. Stand. (1934).*, vol. 53, no. 1, p. 19, 1954.

[134] S. Poulston, P. M. Parlett, P. Stone, and M. Bowker, “Surface oxidation and reduction of CuO and Cu2O studied using XPS and XAES,” *Surf. Interface Anal.*, vol. 24, no. 12, pp. 811–820, 1996.

[135] R. Hajimammadov, M. Mohl, and K. Kordas, “Native oxide formation on pentagonal copper nanowires: A TEM study,” *Surf. Sci.*, vol. 672–673, no. March, pp. 19–22, 2018.

[136] G. O. Lloyd, “Atmospheric Corrosion,” pp. 1–8.

[137] H. H. Khaligh and I. A. Goldthorpe, “Failure of silver nanowire transparent electrodes under current flow,” *Nanoscale Res. Lett.*, vol. 8, no. 1, p. 235, 2013.

[138] S. Ullah, A. M. Shariff, M. A. Bustam, M. Nadeem, M. Y. Naz, and M. Ayoub, “Study on effect of benzotriazole and surfactants on corrosion inhibition of copper alloys in sulphuric acid,” *Int. J. Electrochem. Sci.*, vol. 10, no. 11, pp. 9443–9455, 2015.

[139] X. Lu, J. Chen, S. E. Skrabalak, and Y. Xia, “Galvanic replacement reaction: A simple and powerful route to hollow and porous metal nanostructures,” *Proc. Inst. Mech. Eng. Part N J. Nanoeng. Nanosyst.*, vol. 221, no. 1, pp. 1–16, 2007.

## APPENDIX A: Matlab Code For Amd Calculation

```
A = imread('Directory of the .tif file'); % uploads image
B= rgb2gray(A); % converts image into gray scale
C=B( 1:870,1:1000); % crops image so that scale bar section excluded
figure;
imshow(C); % shows the cropped image
C = im2double(C); % unit conversion
J = imadjust(C,[90/255, 140/255],[0 1]); % adjusts contrast
figure;
imshow(J); % shows image with adjusted contrast
K=sum(sum(J)); % calculates the number of white pixels
K=K/(870*1000); % calculates the fraction of number of white pixels
to the total number of pixels
K % shows the calculated result
```